RÉPUBLIQUE DU CAMEROUN
Paix-Travail-Patrie
****
UNIVERSITÉ DE YAOUNDÉ I
****
FACULTÉ DES SCIENCES
****
CENTRE DE RECHERCHE ET DE FORMATION DOCTORALE EN SCIENCES TECHNOLOGIE ET GÉOSCIENCES
****
UNITÉ DE RECHERCHE ET DE FORMATION DOCTORALE EN PHYSIQUE ET APPLICATIONS
****
DÉPARTEMENT DE PHYSIQUE
BP: 812 Yaoundé
Email: crfd@uy1.uninet.cm

REPUBLIC OF CAMEROON
Peace-Work-Fatherland
****
UNIVERSITY OF YAOUNDE I
****
FACULTY OF SCIENCE
****
POSTGRADUATE SCHOOL OF SCIENCE TECHNOLOGY AND GEOSCIENCES
****
RESEARCH AND POSTGRADUATE TRAINING UNIT FOR PHYSICS AND APPLICATIONS
****
DEPARTMENT OF PHYSICS
P.O. Box: 812 Yaounde
Web Site: www.uy1researchstg.cm

Laboratory of Earth's Environment Physics

African Easterly Jets Dynamics over Central Africa.

A thesis defended publicly for the degree of Doctor of Philosophy in Physics.

Option: Atmospheric Sciences

by

KUETE GOUANDJO Giresse

Registration number: 12W0802

Master degree in Physics

Under the supervision of

POKAM MBA Wilfried
Senior Lecturer
University of Yaounde 1

Richard WASHINGTON
Professor
University of Oxford

Year 2023

UNIVERSITE DE YAOUNDE I
UNIVERSITY OF YAOUNDE I

FACULTE DES SCIENCES
FACULTY OF SCIENCE

DEPARTEMENT DE PHYSIQUE
DEPARTMENT OF PHYSICS

ATTESTATION DE CORRECTION DE LA THESE DE DOCTORAT/Ph.D

Nous, Professeur, **Appolinaire VONDOU DERBETINI ,** et Professeur **NOUAYOU Robert** respectivement Examinateur et Président du Jury de la thèse de Doctorat/Ph.D de Monsieur **KUETE GOUANDJO Giresse** Matricule **12W0802**, préparée sous la direction de **Wilfried POKAM MBA**, Chargé de Cours Université de Yaoundé1 et **Richard WASHINGTON**, Professeur Université de Oxford, intitulée : « **African Easterly Jets Dynamics over Central Africa** », soutenue le **Mercredi 18 Octobre 2023**, en vue de l'obtention du grade de Docteur/PhD en Physique, Spécialité **Physique de l'Environnement Terrestre,** option **Sciences de l'Atmosphère,** attestons que toutes les corrections demandées par le Jury de soutenance ont été effectuées.

En foi de quoi, la présente attestation lui est délivrée pour servir et valoir ce que de droit.

Fait à Yaoundé le ..27..NOV..2023.....

Examinateur

Pr VONDOU Appolinaire

Le Président du Jury

Pr NOUAYOU Robert

UNIVERSITE DE YAOUNDE I
FACULTE DES SCIENCES
Le Chef de Département
DEPARTEMENT DE PHYSIQUE

Le Chef de Département de Physique

Jean-Marie Bienvenu
Professeur

African Easterly Jets Dynamics over Central Africa

Giresse KUETE GOUANDJO

A thesis defended publicly for the degree of Doctor of Philosophy

November 22, 2023

Dedication

I dedicate this work, which I did with a lot of love and passion, to my dearest mother Christina Tiwa and my elder sister Stephanie Leomine.

Acknowledgements

I thank God Almighty, because not anything is impossible for him.

My thanks go first of all to my director, Wilfried Pokam. Thank you for taking the risk of welcoming me into your research team as one of your first students. It was not an easy choice for you because you knew your expectations. During this degree, I have benefited enormously from your advice, vision and enthusiasm. You have provided me with unique opportunities, through collaborations, travel and fieldwork, which have been the highlights of my PhD. These experiences have given me perspectives on climate science and academia that I could not have gained anywhere else.

Secondly, my deepest gratitude goes to my supervisor Pr Richard Washington for the opportunity to work with him. I am extremely grateful for your invaluable advice, continuous support, and patience during my PhD study. Your immense knowledge and plentiful experience have encouraged me in all the time of my academic research. You have also provided me with unique opportunities, through collaborations and travel grant. You also made me part of the great Oxford research team and I learned a lot from them, especially Dr Rachel James, Dr Ellen Dyer, Dr Neil Hart, Dr Emma Howard, Dr Callum Munday. Thank you.

I am also grateful to Pr Vondou Derbetini Appolinaire who has often provided me with valuable help, attentive support and encouragement. Always available to provide advice, but also to encourage me. I also want to salute his human qualities.

I am deeply grateful to Dr Kamsu for his help. He took more than a year to discuss with me and help me in my work without even knowing who I am and without even seeing me physically. I say thank you for your time, your expertise and especially the help you have given me in the field of programming.

Words cannot express my gratitude to all LEMAP teachers. I also could not have undertaken this journey without you all, who generously provided knowledge and expertise.

I am also very grateful to all the teachers in the Physics Department of the University of Yaounde 1.

It was a real pleasure to work with the LaunchPAD team. Thank you for being a supportive, cohesive and fun research group. Having a friendly research group to share ideas with has been invaluable in building my confidence as a scientist. Thank you for the many explanations of your collective deep understanding of the African climate system. Special thanks to Dr Rachel James and Dr Ellen Dyer.

Thank you to my dearest parents whom I love very much and to all my family, my brothers and sisters, especially my sister Stephanie Leomine. No words will suffice to say how grateful I am to you. Having a big sister like you is the greatest blessing!

Thank you to my extended family for all you have done for me and for all you are still doing.

I want to take this little message to express all my gratitude to my academic elders from LEMAP with whom I had a great time, we discussed a lot about science and especially about everyday life. A special thanks to Dr Tamoffo, Dr Taguela and Moihamette, with whom I discuss science every day. Thanks to Dr Fotso Nguemo, Dr Nonki, Dr Dommo, Dr Kamga, Dr Njouenwet and Dr Kemgang with whom I had a great time.

I also want to thank all my classmates since Master 2, especially Iden-Flore and Moihamette.

Thank you to all the students of LEMAP without exception.

Thanks to all my friends without exception.

Contents

List of figures

List of tables

Acronyms

AEJ:	African Easterly Jet
AEJ-N:	African Easterly Jet North
AEJ-S:	African Easterly Jet South
TEJ:	Tropical Easterly Jet
CA:	Central Africa
CB:	Congo Basin
CAB:	Congo Air Boundary
CMIP:	Coupled Model Intercomparison Project
CORDEX:	COordinated Regional climate Downscaling EXperiment
SON:	September-October-November
MAM:	March-April-May
RCM:	Regional Climate Model
GCM:	Global Climate Model
NCEP:	National Center for Environmental Prediction
WEA:	West Equatorial Africa
LLW:	Low Level Westerly
MERRA:	Modern-Era Retrospective analysis for Research and Applications
ITCZ:	Inter-Tropical Convergence Zone
SST:	Sea Surface Temperature
MCS:	Meso-scale Convective Systems
TRMM:	Tropical Rainfall Measuring Mission
AV:	Added Value
ERAINT:	ERA-Interim
GPCP:	Global Precipitation Climatology Project
EOF:	Empirical Orthogonal Function
PC:	Principal Component
IOD:	Idian Ocean Dipole
PPEs:	Perturbed Physical Ensembles
RCPs:	Representative Concentration Pathways
RCA4:	Rossby Centre Regional Atmospheric Climate Model

Abstract

This thesis characterized the representation of two regional atmospheric climate features, AEJ-N and AEJ-S, in reanalysis data sets and climate model outputs. It has shown that the dynamics of these systems are fundamental to the climate distribution and simulation of rainfall over central Africa. The AEJ-S in particular is an important feature of the central African mid-level circulation and has been identified as a key contributor to convection over the region, but yet less is known about its dynamic and structure. By examining AEJ-S mechanisms, this thesis will improves the foundation of new mechanisms that help to identify suitable metrics for the evaluation of Global models over the Central Africa region. As climate models are vital to the assessment of the impacts of climate change, establishing how well models reproduce key processes is important to our confidence in these tools. In the first part of the results in this thesis, we used reanalysis data to establish mechanisms related to AEJ-S dynamics. Results demonstrate that AEJ-S is dominated by rotational circulation and is maintained by a mid-level high that forms over the Kalahari region from September to November. At the core of this high, anticyclonic circulation is induced and maintains AEJ-S located at the northern flank of the high. A link between AEJ-S dynamics and southern subtropical westerly waves is also revealed. It is shown that, when waves amplify over southern subtropics, they modify lower tropospheric heating. Depending on the phase of the wave, this modifies the latitude temperature gradient throughout equatorial regions, therefore modulating the intensity of the jet. At the intraseasonal scale, we describe the meteorological characteristics directly associated with the upper wave flow such as wave structure and periodicity. Results show that the eastward propagation of the wave takes about 10 days to reach the west coast of South Africa and its passage over the Continent takes about 06 days. Its impact on the warming of the atmosphere and on the mid-level circulation is associated with phases, structure and wave periodicity when it crosses the sub-continent. By clarifying mechanisms that govern the AEJ-S, this research work contributes to insight into central Africa climate dynamics and suggests a link

between central Africa and southern Africa climate systems.
We examine in the second part the model representation of the SON characteristics, such as location and intensity, of the AEJ north and south. The analysis evolves to assess key drivers of the AEJ from energetic interactions, the characteristics of mid-level highs and thermal heat lows and the nature of surface thermal heating. In general, the spread of simulated AEJ locations around reanalyses is larger for the CMIP5 sample compared to CMIP6 equivalent models, indicating improvement from CMIP5 to CMIP6. However, this improvement in some CMIP6 models (e.g. GISS-E2-1-G and MIROC6) is not related to a maximum surface meridional gradient in temperature. Most CMIP5 and CMIP6 models underestimate the surface temperature gradient over the AEJ-N region. As a first-order diagnostic of the jet's acceleration, most coupled models better simulate the atmospheric energetic interactions over the AEJ-N region which leads to its strong contribution to AEJ-N maintenance compared to AEJ-S. This study strengthens our understanding of the mid-level circulation over Central Africa by detecting gaps in the mechanisms maintaining the AEJ in coupled models and highlights processes that should be improved in future ensembles.

Key words: AEJ. Heat low. Southern Subtropical Waves. Anticyclonc circulation. Models. Central Africa. Southern Africa.

Résumé

Cette thèse examine la représentation de deux caractéristiques climatiques régionales: AEJ-N et AEJ-S, avec les données de réanalyse et les sorties de modèles climatiques. Nous avons montré que la dynamique de ces systèmes est fondamentale pour la distribution climatique et la simulation des précipitations en Afrique centrale. L'AEJ-S en particulier est une caractéristique importante de la circulation en moyenne troposphère en Afrique centrale et a été identifiée comme un contributeur clé à la convection sur la région. Cependant, sa dynamique et sa structure sont encore très peu connues. Dans la première partie des résultats, nous avons utilisé les données de réanalyse pour établir les mécanismes liés à la dynamique de l'AEJ-S. Les résultats montrent que l'AEJ-S est dominée par une circulation rotationnelle et, est maintenue par un système anticyclonique de la moyenne troposphère qui se forme sur la région du Kalahari de Septembre à Novembre. Au cœur de ce système de haute pression, une circulation anticyclonique est induite et maintient l'AEJ-S située sur son flanc nord. Un lien entre la dynamique de l'AEJ-S et les ondes d'Ouest subtropicales du Sud est également montré à l'échelle saisonnière.

Il est établi que, lorsque les ondes s'amplifient, elles modifient le réchauffement de surface. Selon la phase de l'onde, cela modifie le gradient de température vers les régions équatoriales, modulant ainsi l'intensité du jet. Par contre à l'échelle intra-saisonnière, nous décrivons les caractéristiques météorologiques directement associées à l'onde telles que sa structure et sa périodicité. Les résultats montrent que l'onde prend environ 10 jours pour s'installer et que son activité met environ 06 jours sur le continent après son installation. Son impact sur le réchauffement de l'atmosphère et sur la circulation de la moyenne troposphère est associé aux phases, à la structure et à la périodicité de l'onde lorsqu'elle traverse le sous-continent. En clarifiant les mécanismes qui contrôlent l'AEJ-S, ce travail de recherche contribue à la compréhension de la dynamique climatique de l'Afrique centrale et suggère un lien entre les systèmes climatiques d'Afrique centrale et australe. Ce travail améliore également la recherche de nouveaux mécanismes qui aident à identifier des métriques appro-

priées pour l'évaluation des modèles. Ces modèles étant essentiels à l'évaluation des impacts du changement climatique, il est important de déterminer comment ils reproduisent les processus clés tels que les systèmes AEJ.

Ainsi, dans la deuxième partie, nous examinons la représentation par les modèles des caractéristiques telles que la localisation et l'intensité de l'AEJ-N et l'AEJ-S à partir des interactions énergétiques, des caractéristiques des anticyclones de moyenne troposphère et des dépressions thermiques de surface. En général, la dispersion des localisations simulées de l'AEJ autour des réanalyses est plus importante dans CMIP5 par rapport aux modèles équivalents CMIP6, montrant une amélioration entre CMIP5 et CMIP6. Cependant, cette amélioration dans certains modèles CMIP6 (par exemple GISS-E2-1-G et MIROC6) n'est pas liée à un gradient maximal de température de surface. La plupart des modèles CMIP5 et CMIP6 sous-estiment le gradient de température de surface sur la région AEJ-N et simulent mieux les interactions énergétiques atmosphériques. Entraînant sa forte contribution à la maintenance de l'AEJ-N par rapport à l'AEJ-S. Cette étude renforce notre compréhension de la circulation de la moyenne troposphère en détectant les lacunes dans les mécanismes de maintennance de l'AEJ dans les modèles et met en évidence les processus qui devraient être améliorés dans les projections futures.

Mots clés: AEJ. Dépression thermique. Ondes subtropicales. Circulation anticyclonique. Modèles. Afrique centrale. Afrique australe.

General Introduction

The economic growth of Central Africa (CA) is inextricably related to climate. The slow progress of the economy of this region may be attributed to the low productivity of agricultural resources and its high population growth (Piabuo and Tieguhong, 2020). Here agriculture is still mainly rainfed (Fotso-Nguemo et al., 2018) therefore strongly controlled by climate variability. According to climate models, CA is projected to exhibit a continuous and significant increase in global temperature (King and Harrington, 2018). Such future drying trends are likely to impact the wet season, where rainfall is projected to increase (Dunning et al., 2018). This recent study shows that the combination of an increase in rainfall per rainy day over CA with a small change in the number of rainy days increases total seasonal rainfall. Whilst response to global warming over CA may not have a significant impact on total seasonal rainfall, high intense rainfall events are projected to increase rather than their frequency (Sonkoué et al., 2019). Climate change is already being felt across the region, climate-resilient development is very crucial and urgent adaptation action needed to avert the worst impacts.

The most significant limitation factor of climate research in the Congo Basin (CB) is the lack of observational data, mainly the result of the extreme size and access ratio of the region, worsened by the political instability of recent decades. Historical data sets have been compiled for the region (Aguilar et al., 2009; Nicholson et al., 2012), but the number of maintained rain gauges has been in rapid decline since the 1980s (Harris et al., 2014). Only some few (03 in 2013) meteorological stations in the Democratic Republic of the Congo have been reported, this compared to over 3000 stations which report to the Met Office in the UK alone (an area 40 times smaller). However, the Congo's significance is increasingly being recognized in scientific literature, not least because anthropogenic-induced climatic changes have been brought to the forefront of African environmental policy (James and Washington,

2013). Because of the scarity of observational data, understanding of the dynamical mean state climatology in the CB is primarily based on reanalysis products.

The large and rapid increase in climate stress associated with population growth raises environmental concerns that may have considerable impacts on the carbon storage, climate and biodiversity of the CA rainforest (Jiang et al., 2019). For a region where the economic growth is highly dependent on water resources (Hua et al., 2018; Pereira, 2017) and its climate variability is still poorly explored (Creese and Washington, 2016; Washington et al., 2013), the understanding of its fundamental regional climate dynamics must be improved. Henceforth understanding how the climate of this region varies is of vital importance.

The Central African climate is of particular importance to the global climate and a crucial element of the large-scale global circulation, yet it is vastly understudied (e.g. Nicholson, 2018). The region remains very sensitive to climate variability and change as the whole of Africa (Joshi et al., 2011; Lennard et al., 2018). This is typically true for the climatology regional system, which is conditioned by numerous climate processes operating on different temporal and spatial scales. The components of the local atmospheric dynamics, which operate essentially on a synoptic time scale, mainly control the regional characteristics of the climatology, and are critical for realistic simulation of the regional climate system (Tamoffo et al., 2019). Therefore, they must be well understood.

One of the greatest challenges in the study of the climate system in Africa, and CA in particular, is to improve the understanding of the processes that influence its climate. However, significant progress has been made recently in this sense (Pokam et al., 2014; Hua et al., 2018; Kuete et al., 2019; Raghavendra et al., 2020; Howard and Washington, 2020; Longandjo and Rouault, 2020a; Alber et al., 2021), even for understanding drivers of climate projections (James et al., 2018; Tamoffo et al., 2019; Creese et al., 2019). These projections of future change are subject to a high degree of uncertainty, not least because climate models struggle to represent the mean state of the Central African Atmosphere (Creese and Washington, 2016; Tamoffo et al., 2019; Taguela et al., 2022; Crowhurst et al., 2020, 2021). For these reasons, the elucidation of the climate dynamics of CA is in itself an interesting contribution to climate science.

To contribute to the understanding of the fundamental dynamics of the atmo-

sphere of this region in order to characterize the climatological expression of its climate, this thesis focuses on mid-level circulation. In doing so, a set of critical elements that influence climate systems that can be well simulated by climate models will be studied. The focus will be on reinforcing our limited understanding of the drivers of the mid-level circulation by sensing the shortcomings of the African Easterly Jet (AEJ) maintenance mechanisms. The AEJ systems have been chosen based on the following criteria:

-They play a role in producing the intense convection and high frequency of lightning that characterise the climate of CA;

-They may also help to explain a paradox in which, despite the extreme intensity of convection, equatorial rainfall in this region is low;

-The strong active phase of the AEJ system over equatorial CA coincided with the maximum rainfall season over the region;

-It is associated with the interannual variability of rainfall over the region and ;

-The fact that it is relatively unstudied to date in climate models.

The main objective of this research is to explain the variability and dynamics of the climate of CA from a climatological point of view. In pursuit of this objective, this work will present the climatology, maintenance mechanisms and variability of the AEJ system and its influence on rainfall variability. This thesis will also focus on the historical representation of the AEJ system through global models to determine whether the models' reproduction of key processes is important to the confidence we attach to these tools. The remainder of this thesis proceeds as follows. Chapter one presents the literature review that introduces the current understanding of the climate of CA. We focus first on the observed climatological basic state, second on the local climate dynamics of the region, third on observed interannual variability, and finally describe the overarching goals and aims of the thesis and further ask research questions. In chapter 2, the first section describes the observational data used, and followed, the climate models that will be considered in this thesis are introduced, and the process-based approach is placed within the context of these models. The last section of chapter 2 precisely defines the region of interest within CA. Chapter 3 presents the results of our work with related discussions and also reviews the ability of climate models to simulate the Central African climate. After that we summarize our results and suggest future work.

Chapter 1

Literature review and Research questions

The following sections provide a literature review that describes the current understanding of the climate in CA. First, the main atmospheric characteristics of the climatological mean state are presented. As much of the understanding of this mean state is derived from reanalyses products rather than direct observations, the extent to which reanalyses products agree over CA is then examined. Although the literature review is robust, gaps are identified with respect to the structure and dynamics of these weather systems. Third, this section examines a brief history of the latest climate modelling science and various kind of modelling tools (climate models) are also discussed, and then a description of the modelling procedure. Finally, the main mechanisms of interannual precipitation variability are examined.

1.1 Climatological mean state

Figure 1 shows the main climatological atmospheric features of CA. These features will be defined and the literature on their dynamics will be discussed.

1.1.1 Tropical rain belt

The African Tropical rain Belt is a large region of high humidity and convective precipitation that has a north-south meridional movement over the African continent during the year (Dunning et al., 2016). This annual movement (Figure 2) is analogous to that of the Intertropical Convection Zone (ITCZ) although the association of the latitudinal migration of the ITCZ with equatorial rainy seasons has recently been questioned by (Nicholson, 2018). Instead, this author showed that the latitudinal migration of precipitation does not coincide with the region of strong surface

convergence. Future changes in rainfall seasonality over Africa are associated with continental thermal lows (Dunning et al., 2018). As increases in carbon emissions create changing heating conditions for rain clouds, these future changes will affect the tropical rain belt and have a significant impact on food security in many countries across Africa. In West Africa, the rain belt moves rapidly northwards, forming the West African monsoon in late June (Sultan et al., 2003). In Eastern and CA, the southward and northward passage of the tropical precipitation band during the September-November (SON) and March-April-May (MAM) seasons are responsible for short and long rains respectively. According to a study by researchers at the University of California, the future climate will shift the tropical rain belt northward over East Africa and the Indian Ocean, resulting in increased drought stress in Southeast Africa and Madagascar. The African tropical rain belt shifts progressively towards the Southern Hemisphere during the October-December season, reaching its southernmost location between January and February marking the rainy season in this part, before retreating towards equatorial CA between March and May.

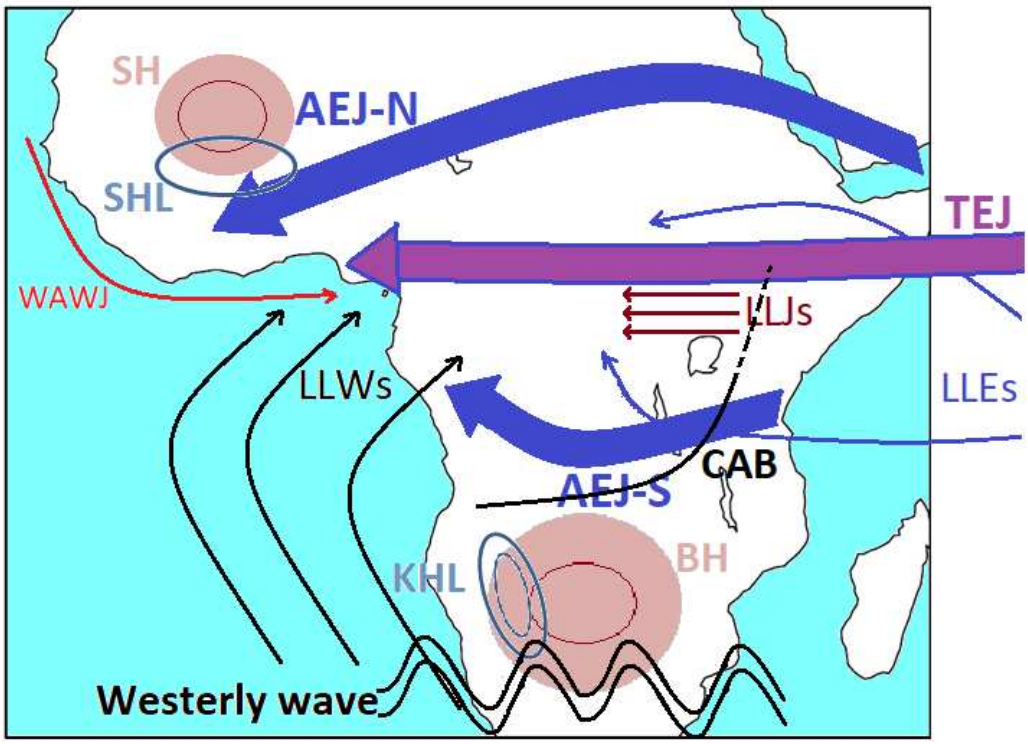

Figure 1: *Schematic of key mean-state features of the Central African atmosphere during September-November. Saharan High (SH); Saharan Heat Low (SHL); African Easterly Jet North (AEJ-N); African Easterly Jet South (AEJ-S); Tropical Easterly Jet (TEJ); Low Level Westerlies (LLWs); Kalahari Heat Low (KHL); Botswana High (BH); Congo Air Boundary (CAB); Low Level Easterlies (LLEs); Low Level Jet (LLJs); West African Westerly Jet (WAWJ).*

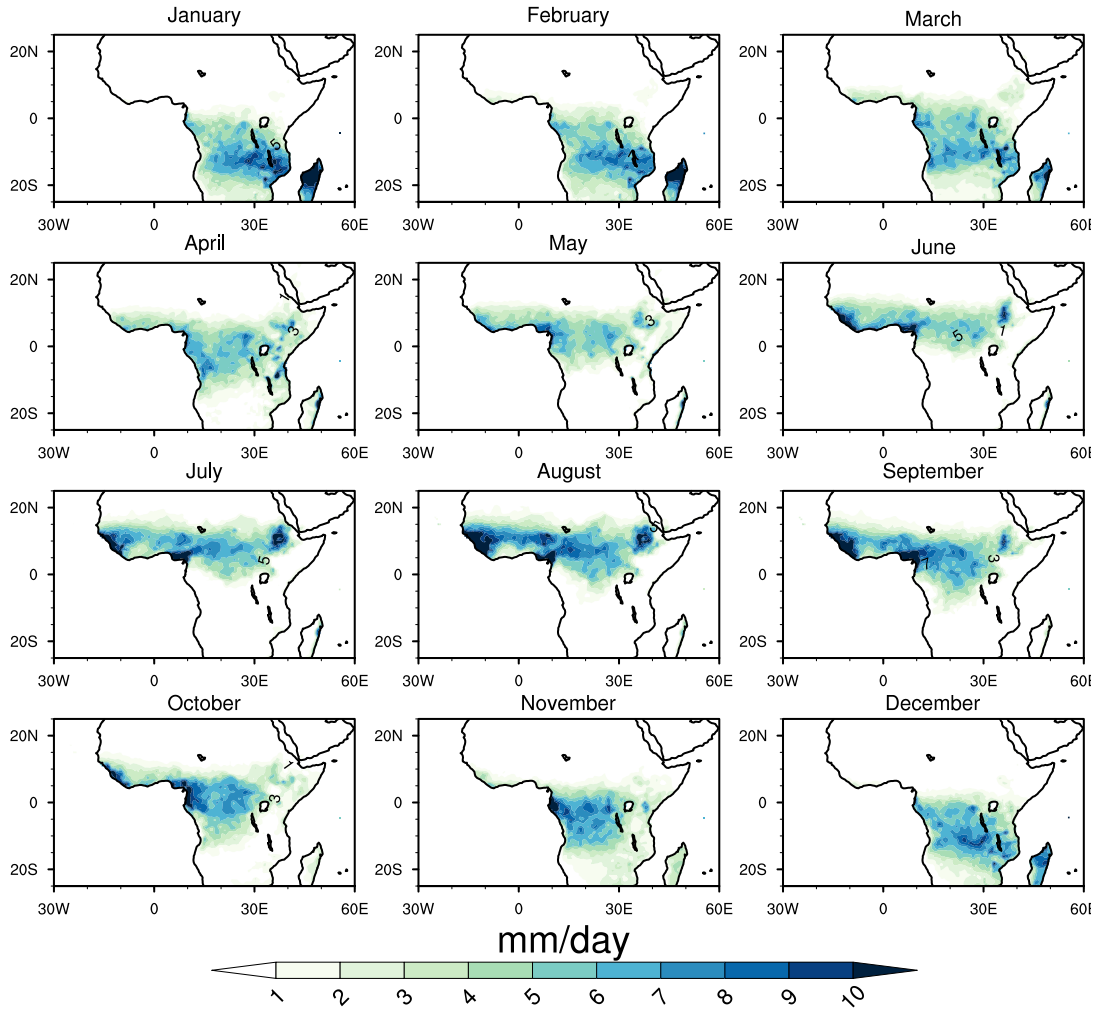

Figure 2: *Long term mean (1985-2015) annuall cycle of rainfall (mm day^{-1}) from the GPCP dataset. This also shows the seasonality of the location and strength of tropical rainbelt.*

The Central African rainy seasons bear differences from the low-level convergence associated with the ITCZ. However, Nicholson (2018) shows that low-level winds are divergent, on average, over much of the region during these seasons. Thus, the observed wind patterns further contradict the ITCZ paradigm to explain the seasonal cycle in Africa's equatorial latitudes. Although arguably the most important climatic feature of tropical Africa, many questions remain unanswered about the tropical rainbelt (Nicholson, 2018), including questions about its equatorial edge. While the seasonal shift of the rain belt is clearly in phase with the annual cycle, the precise dynamics of this oscillation over equatorial Africa, which results in surface convergence leading directly to ascent and hence precipitation, are unclear. The obvious question is what produces the seasonal cycle over equatorial Africa, a region of extraordinarily intense thunderstorms and convective activity. The characteristics and dynamics of the equatorial margin of the rain belt determine the climatology,

variability and change of rainfall in the equatorial rim region. It is therefore important that these dynamics are better understood. This thesis will answer these questions in Chapter 3 by analysing the dynamics of the AEJ which has been identified as an important feature of convection over equatorial Africa.

1.1.2 Low-level Circulation

The annual cycle of the horizontal wind structure is illustrated in Figure 3. In the lower troposphere, the dynamics of the atmospheric circulation, namely the low-level westerlies (LLWs), are both dominated by inflows (outflows) from the Atlantic and Indian Oceans (from the continent to the oceans). These features of the lower tropospheric circulation were first examined by (Fontaine and Janicot, 1992). It is a persistent feature of the region's climate (Dezfuli and Nicholson, 2013; Nicholson and Dezfuli, 2013; Pokam et al., 2014) that occurs in all months of the year with varying strength, and is particularly active during the SON wet season, while it is weaker during MAM (Pokam et al., 2012; Van der Ent et al., 2013; Pokam et al., 2014). Atlantic Ocean advection is the most studied (Van der Ent et al., 2010, 2013; Pokam et al., 2014; Dyer et al., 2017).

LLWs owe their existence to the pressure and temperature gradients between the relatively cool ocean and the superheated Saharan desert Fontaine and Janicot (1992). The circulation of moist air from the Atlantic Ocean, called Low-Level Equatorial Westerlies (Nicholson and Grist, 2003), is the result of southeasterly trade winds on the northeastern side of the St. Helena High (South Atlantic), which become westerly winds under Coriolis effect after crossing the equator (Figure 1.3). As clearly demonstrated by Nicholson and Grist (2003), this situation is well defined throughout the year, and quite pronounced from July to September. Pokam et al. (2014) used four reanalysis datasets to investigate and characterise the control mechanisms of LLWs over Western Equatorial Africa (WEA). The results of their study contradict the conventional view that Atlantic Ocean LLWs are modulated by the strength of the South Atlantic High, but suggest that LLWs are instead driven by differential heating between the Atlantic and the Congo Basin, with the former serving as a heat sink due to subsidence and the latter as a heat source due to the strong latent heat release. Dezfuli and Nicholson (2013) showed that dry years are characterised by weak near-surface westerlies and wet years by a core of westerly flow near

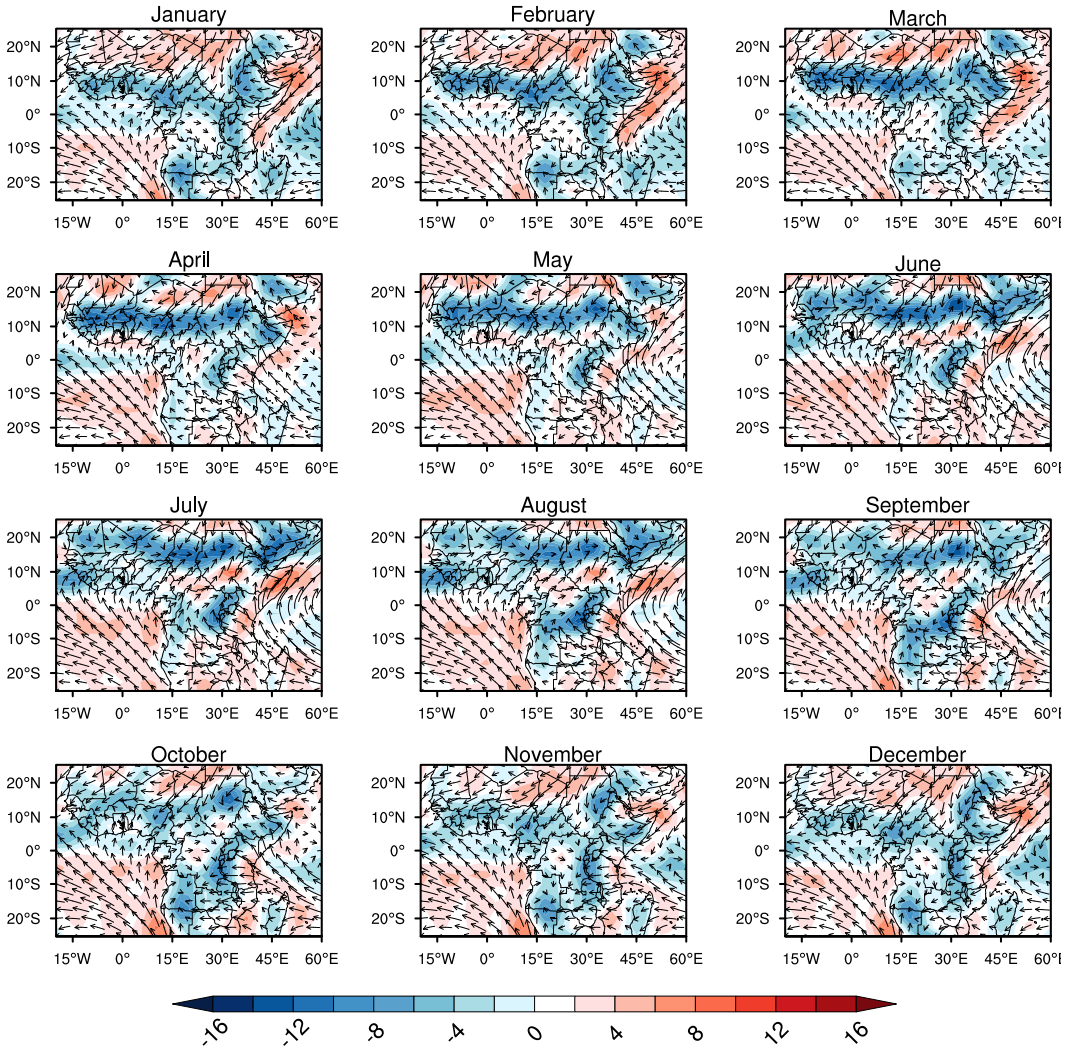

Figure 3: *Monthly means (1985-2015) of the total horizontal circulation and divergence at 925 hPa from ERA5.*

850 hPa over West Africa and WEA. The important role of low-level easterlies has been highlighted by Van der Ent et al. (2010). Similarly, Dyer et al. (2017) showed that during MAM and SON rainy seasons, the mixing between westerly inflow from the Atlantic Ocean and easterly inflow from the Indian Ocean conditions the area of increased precipitation, associated with the movement of the low-level convergence. McCollum et al. (2000) reported that the LLW jet over the Atlantic Ocean supplied moisture to CA inland, and Vigaud et al. (2009) outlined the important role played by this LLW jet to deepen convection.

1.1.3 African Easterly Jets

One key process that is known to have a central influence on rainfall formation across the central African region is the African Easterly Jet (AEJ). The AEJ is a prominent feature of the mid-tropospheric zonal wind that forms over CA. The jet is considered

to play a crucial role in rainfall development over the CA region from September to November (Nicholson and Grist, 2003). The jet presents two components. A northern component is known as the African Easterly Jet North (AEJ-N) of the northern hemisphere, and a southern component is known as the African Easterly Jet South (AEJ-S) of the southern hemisphere. Nicholson and Grist (2003) were the first authors to use this appellation for these two mid-level jets to distinguish them. The climatological AEJ-N is identifiable throughout the year (Figure 4) from January when it lies at its southernmost location (3^0N) and moves northward to its most northern location in August (13^0N) with maximum wind speeds reaching 13 m.s^{-1} in September, as it begins shifting southward towards the equator (Nicholson and Grist, 2003). Characteristics of the southern component were also described by these authors, they state that AEJ-S is well defined from September to November and its core location lies between 5^0S and 10^0S with a mean core speed reaching 8 m.s^{-1}.

While some studies have used reanalysis data to understand the dominant processes of climate variability in CA by highlighting the important role of AEJ-N (Pokam et al., 2012; Dezfuli and Nicholson, 2013; Nicholson and Dezfuli, 2013) and AEJ-S (Jackson et al., 2009; Adebiyi and Zuidema, 2016; Kuete et al., 2019), some studies on model process-based evaluation have shown that model rainfall biases are mainly related to bias in terms of location and intensity of AEJs in models (Creese and Washington, 2018; Tamoffo et al., 2019).

1.1.3.1 African Easterly Jets Origin

Several studies (Burpee, 1972; Cook, 1999; Thorncroft and Blackburn, 1999; Nicholson and Grist, 2003; Parker et al., 2005; Wu et al., 2009) have stated that AEJ-N is a response to strong surface heating. It is shown that the AEJ is set up in association with two diabatically forced meridional circulations. One associated with surface sensible heat flux and dry convection in the Saharan thermal heat low region and another associated with deep moist convection in the intertropical convergence zone located at the equator of this zone. The heating of thermal lows, which reaches the height of the AEJ around 700 mb, is particularly important in maintaining the AEJ and its associated surface meridional gradients in temperature. Cook (1999) studied the generation of the African easterly jet using GCM simulations and comparison

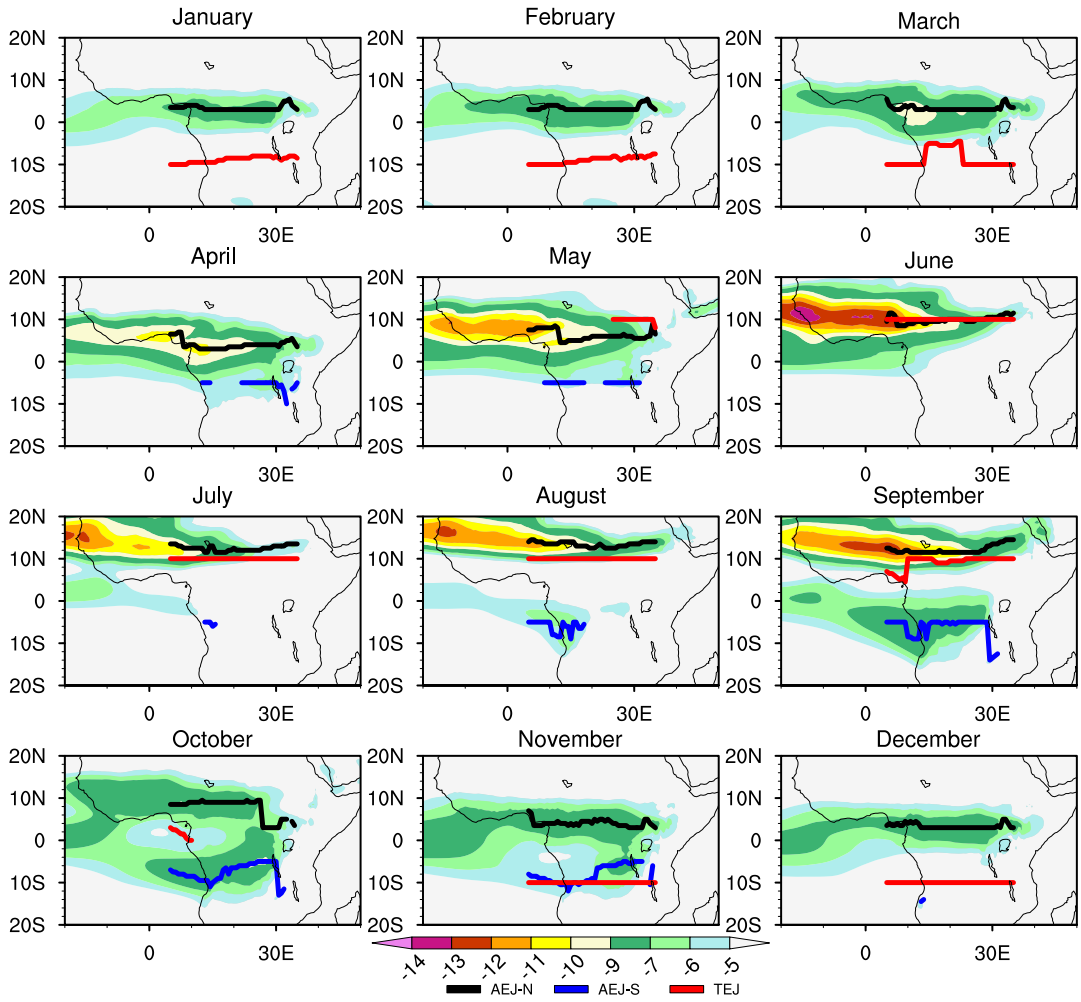

Figure 4: *Spatial and temporal variability from ERA5 of TEJ axes (red solid lines), AEJ-N axes (black solid lines) and AEJ-S axes (blue solid lines) cores. Shaded colors areas (U-winds speeds > 6 $m.s^{-1}$) indicates the local mean positions of the AEJ jets. The core speeds of these jets are localised over CA on the longitudes 10^0E-30^0E for all jets, and on the latitudes 10^0S-10^0N for the TEJ, 3^0N-20^0N for the AEJ-N and 5^0S-20^0S for the AEJ-S.*

with NCEP reanalysis and states that AEJ-N is established by the presence of a positive surface temperature gradient, which, by thermal wind relation and geostrophic circulation, induces zonal wind shear in mid-troposphere. Nicholson and Grist (2003) also found that AEJ-N results from a positive surface temperature gradient between the hot Sahara and humid congo basin.

AEJ-S also owes its existence to a meridional surface temperature gradient, but this time, thermal contrast is between the hot and dry subtropical Namib-Kalahari region that is associated with dry convection (Adebiyi and Zuidema, 2016; Munday and Washington, 2017; Howard and Washington, 2018; Kuete et al., 2019) and sub-humid region of Congo basin associated with deep tropospheric moist convection dominated by Mesoscale Convective System (Nicholson and Grist, 2003; Jackson

et al., 2009). Very few studies have attempted to understand the origin and maintenance of the AEJ-S possibly because early studies of the mid tropospheric circulation focused on months when the jet was not present (e.g. Newell and Kidson, 1984). The main characteristics of the observed AEJ-S were described and also the major role this Jet plays in rainfall development over CA in SON was also pointed out. Early studies also found tha the AEJ-S is a thermal wind and is confined between two regions of differing convective characteristics.

1.1.3.2 African Easterly Jets dynamics

Climate models and reanalysis data have highlighted the vital role of both African easterly jet components in the dynamics of central and west Africa climate. Particularly during the September to November rainy season, the two jets are key features for the CA convective regime and mid-tropospheric circulation (Nicholson and Grist, 2003; Jackson et al., 2009; Haensler et al., 2013) and are prominent for rainfall variability (Pokam et al., 2012; Dezfuli and Nicholson, 2013; Nicholson and Dezfuli, 2013; Maidment et al., 2015; Dyer et al., 2017; Nicholson et al., 2018; Hua et al., 2019). It is shown that AEJ is maintained in association with surface heating and dry convection. In the Saharan region, the heat low heating is important in accelerating the AEJ-N (Chen, 2004). Following studies from Munday and Washington, (2017) and Howard and Washington, (2018) on Angola Heat low dynamic in CMIP5 models, Kuete et al., (2019) put in evidence for the crucial role of the Kalahari heat low and southern westerly waves in maintaining the AEJ-S.

Kuete et al., (2019) in their study showed that, depending on the phase of the wave, this modifies the state of the atmosphere and consequently modifies surface heating including heat low and therefore surface gradient towards equatorial regions that settle AEJ-S. Future changes in the strength of Sahara and Kalahari heat lows have been assessed by Dunning et al., (2018). Simulations indicate an increase in the strength of the Saharan heat low. The Angola heat low also experienced a similar increase but with a lower magnitude. As these features significantly contribute to climate variability over CA through modulation of the AEJ components, such future changes are likely to impact the region's climate. Other maintenance processes that contribute to accelerating the jets are divergence circulation deflected by Coriolis acceleration and mid-tropospheric highs over Sahara and Kalahari.

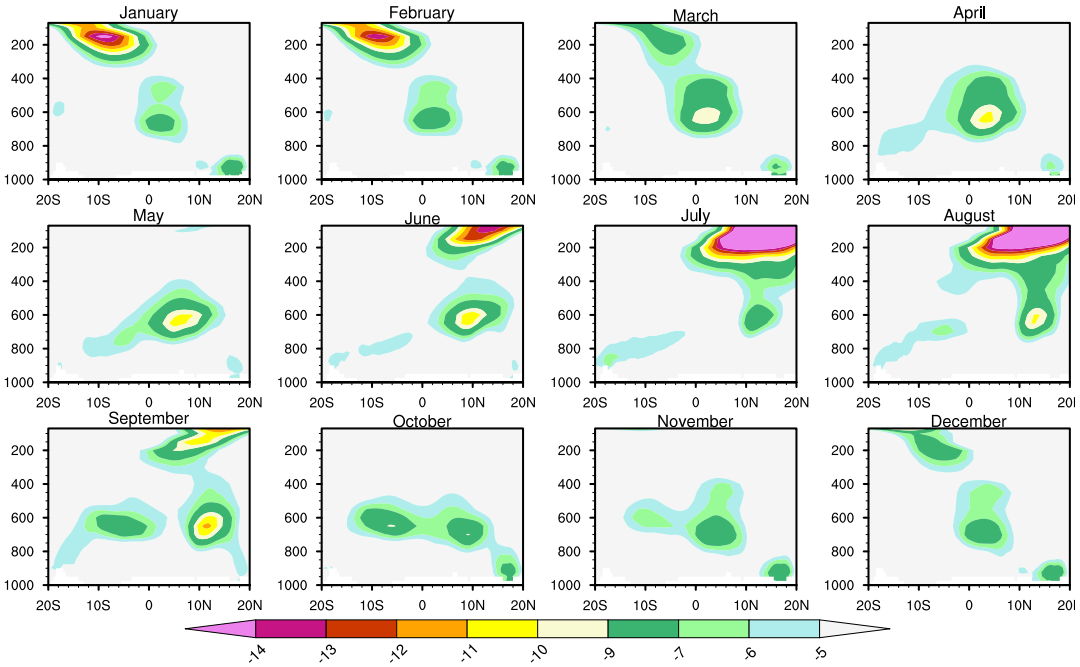

Figure 5: *Monthly means (1985-2015) latitude–height cross section of zonal wind from ERA5 averaged across 12^0E-28^0E longitudes showing vertical locations and intensities of AEJ (U-winds > 6 m.s^{-1}) at mid-level and TEJ (U-winds > 6 m.s^{-1}) at 200 mb.*

Chen (2004) studied maintenance mechanisms of the AEJ-N and showed that AEJ-N is maintained by the Coriolis acceleration associated with meridional divergence circulation.The contribution of the Saharan high to the maintenance of the AEJ-N had been examined by Cook (1999) and Chen (2004). They showed that AEJ-N located south of the high pressure is accelerated through an anticyclonic circulation that is induced at its core. Spinks et al. (2015) analysed AEJ-N during August and identified a maximum core wind speed located in East Africa south of the Arabian High. Much like the Western core located south of the Saharan high, the east maximum wind is maintained by an anticyclonic circulation associated with maximum geopotential gradient at the core of the Saharan and Arabian Highs, which causes the jet to be geostrophic. Following studies from Chen (2004), Kuete et al., (2019) showed that a mid-level high over the Kalahari region accelerates AEJ-S located at the northern flank of the high through an anticyclonic that is induced at the core of the high. Despite this progress in the dynamics of the AEJ components, very little is known about how models reproduce their control and maintenance mechanisms.

1.1.3.3 Process-Based assessment of African Easterly Jets

A new methodology for model evaluation is a process-based evaluation. This method is of particular importance for the assessment of local climate because it advances in understanding the functioning of local climate and also how it is represented in models through the assessment of processes governing the climate of the region (James et al., 2018). Process-based assessments have advanced in southern Africa (Dieppois et al., 2015; Lazenby et al., 2016; Munday and Washington, 2017), East Africa (Tierney et al., 2015; Yang et al., 2015; Hirons and Turner, 2018), Sahel (Cook and Vizy, 2006; Biasutti et al., 2009; James et al., 2015) and central Africa (Creese and Washington, 2018; Creese et al., 2019; Tamoffo et al., 2019, 2020, 2022; Crowhurst et al., 2021; Taguela et al., 2022).

Creese and Washington (2018) assessed dynamical processes related to model wetness over the eastern Congo basin. Results of their study showed that wet models have a weaker AEJ-N in terms of intensity with the mean core located more poleward, while on the contrary, stronger and more equatorward AEJ-N in dry models contributes to the suppression of precipitation in this part of the basin. Using process-based assessment with special emphasis on the climatological characteristic of moisture flux convergence, Tamoffo et al. (2019) established that, dryness biases of Congo basin rains are associated with stronger outflows of moisture divergence driven by a strong AEJ at the western boundary, and weaker inflows at the eastern boundary driven by a weak AEJ. These previous findings on rainfall model biases over CA are associated with the representation of the strength and location of AEJs in the models. This, therefore, suggests that there is no clear relationship yet between a model's ability to simulate observed rainfall and the associated AEJs dynamics. The only mechanism that is commonly explored in models to understand bias in location and strength of AEJs is the surface temperature gradient to which AEJ owes its origin. Here, we take a step forward not only in showing the link between AEJs and the surface temperature gradient but also in understanding their associated dynamics. This could be important to scientists to improve their simulation and help understand the model's rainfall biases.

1.1.4 Tropical Easterly Jet

The Tropical Easterly Jet (TEJ) is one of the most visible features of the upper-tropospheric circulation in the Northern Hemisphere. In the upper troposphere, this Jet extends from Indochina to the west coast of Africa and has its maximum speed at about 25 m.s^{-1} near latitude 5^0S-10^0S over the Arabian Sea (Krishnamurti, 1971). It develops in response to the temperatue gradient between the Himalayan Plateau and Indian Ocean between November-March and June-September, extending westward into Africa (Dezfuli, 2017; Nicholson and Klotter, 2021). The TEJ is an important parameter in the study of the West and Central African climate. The annual cycle of the spatial and vertical evolution of the TEJ are shown in Figures 4 and 5. Over the southern part of the CB, the annual cycle and magnitude of the TEJ shows a double maximum in wind speed. During its first maximum in February, it is located in the Southern Hemisphere between 5^0S to 10^0S, and its central speed is about 13 m.s^{-1}. This corresponds to its southernmost latitude, over the southern part of the CB. From February onwards, the TEJ moves northwards. As it crosses the equator, its magnitude decreases to about 6 m.s^{-1}(Figure 5). It reaches 7^0N in May and its first minimum core velocity is 9 m.s^{-1} (Nicholson and Grist, 2003). In the same study, the results also show that, at its northernmost position in July, the maximum intensity of the second wind is about 19 m.s^{-1}.

The TEJ tends to be stronger in wet years over the Sahel, in opposition to the AEJ-N which tends to be weaker and more poleward (Creese and Washington, 2018; Nicholson and Grist, 2003). Upper-level easterly flow is evident throughout the year, and there is a weak secondary maximum south of the equator during January and February. However, this is not usually referred to as the TEJ and is much weaker than the upper-level flow. The TEJ appears to both modulate, and be modulated by, convective rainfall; studies suggest that upper-level divergence in the exit region of the jet over West CA may promote convection at the surface (Dezfuli and Nicholson, 2013; Nicholson and Dezfuli, 2013), whilst Thorncroft and Blackburn (1999) suggest the TEJ forms partially in response to convection over the continent.

1.1.5 The Congo Air Boundary

The Congo Air Boundary (CAB), also known as the Zaire Air Boundary, is traditionally defined as the place where LLW winds, which originate as recirculated Atlantic southeasterly winds, meet the easterly trade winds of the Indian Ocean at the surface (Taljaard, 1972; Torrance, 1979). The CAB is also a dry line because the converging air masses differ strongly in moisture, with the LLW being close to saturation after their journey over the Congo rainforest, and the easterly currents having been "continentalized" and dried over the Great Escarpment (Torrance, 1979; Leroux, 2001). Taljaard (1986) and Heerden and Taljaard (1998) describe the CAB as the mean location of the core of a broad zone where active weather dominates, and discuss tropical lows that travel westward along the CAB. In the Austral summer, the CAB extends from Angola eastwards through Zambia, and then turns northward to extend up through east Africa. In winter, it retreats northwards to the Congo basin.

Studies of the CAB have primarily focussed on synoptic charts and drawn heavily on the individual forecasting experience of expert meteorologists in the pre-satellite era (Taljaard, 1972; Torrance, 1979). In the intervening decades, the CAB disappeared from mainstream climate science, though it remained well- known in the weather forecasting and paleoclimate communities (Tierney et al., 2011). In an effort to understand the regional circulation complexities, a novel algorithm is developed by Howard and Washington (2019) to identify the CAB in ERA-5. It is established that either a dryline CAB or KD is present in southern Africa for over 95% of days between August and December, crossing the second and main rainy season in the CB. In this study, links were established with the Angola and Kalahari thermal lows, showing the possible link between the CAB and the AEJ-S, whose intensity is closely impacted by the Kalahari thermal low, and which could play a major role in the precipitation climatology in CA. In southern Africa, models from phase 5 of the Coupled Model Intercomparison Project (CMIP5) predict robust future drying associated with a delayed rainy-season onset. Howard and Washington (2020) relate these rainfall changes to dynamical shifts in two classes of weather systems: the CAB and tropical lows. Their study established that the climatological locations and frequencies of these systems are reasonably well represented in the CMIP5 models.

1.1.6 The Congo Basin Cell

The seasonnality of rainfall over CA is primarily dominated by large-scale circulations including the Hadley and Walker cells. Pokam et al. (2012) argued that the recycling of precipitation over CA is regulated by both low-level moisture flux direction and strength at seasonal time scales, with the seasonal migration of the rainfall-maximum position controlled by the vertical moist instability. Longandjo and Rouault (2020b) show that another viewpoint is to consider this low-level westerly jet as the lower branch of the Walker-like cell over CA.

Indeed, some studies (Bayr et al., 2014; Thorsten and Richter, 2014; Pokam et al., 2014; Cook and Vizy, 2016; Neupane, 2016) have recently suggested the presence of a walker-type cell over CA. Flohn and Fleer (1975) depicted a dominant asymmetric overturning circulation over AC, with low-level westerlies supplying water vapour from the eastern Atlantic as a lower branch. On the other hand, Webster (1983) found symmetrical overturning cells, with convergent branches at low levels, with moist air flowing from surrounding oceans into the Central African landmass. Aloft, the uplifts diverges into what are considered the two return branches, before sinking over the eastern Atlantic and western Indian Ocean respectively, thus closing the circulation. Depending on the season, the ascending branch is located either over eastern Africa or over the eastern Atlantic (Atlantic coastal region). This inconsistency indicates that the regional scale atmospheric dynamics over CA has not yet been studied and remains largely undocumented. Furthermore, at low levels, Pokam et al. (2014) found that the Walker-like circulation is driven by divergent circulation over CEA, with the low-level branch (LLW), controlled by the differential adiabatic heating between CA and the eastern Atlantic Ocean. Hua et al. (2018) suggested that the better the equatorial Walker circulation is reproduced, then the better the drought over CA is captured.

This zonal overturning circulation over CA (Figure 6) occurs when the sea surface temperature (SST) of the Atlantic cold tongue matures to set up favourable atmospheric conditions for its development (Cook and Vizy, 2016), and Neupane (2016) suggested that the LLW is controlled by the land-ocean thermal contrast between CA and the eastern Atlantic Ocean. However, Cook and Vizy (2016) suggest that the variation in equatorial Atlantic SSTs is not associated with interannual variability in the strength of this shallow overturning circulation. It is not yet entirely clear what

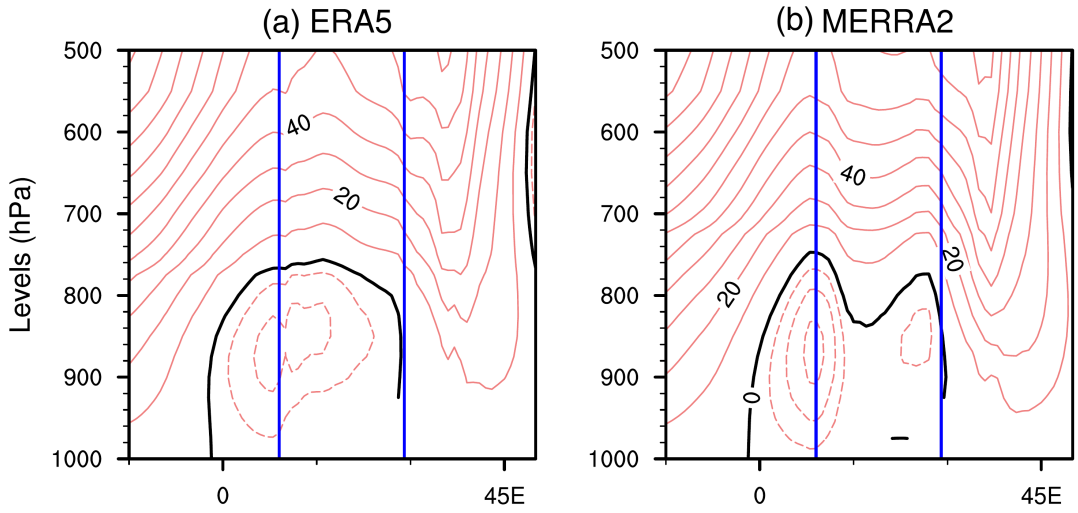

Figure 6: *September–November climatological mean of the zonal mass-weighted stream function (contours: $10^{11} kg.s^{-1}$) computed with 5^0S–5^0N averaged zonal wind for (a and b) ERA5 and MERRA2. Solid and dashed contours represent positive and negative values of mass-weighted stream functions respectively, seperated with the zero value of mass-weighted stream (thicker contour). Contour intervals are 10 between positive contours and 4 between negative contours. The vertical lines are the zonal boundaries of the Central African region.*

the physical mechanisms are that are responsible for the development and maintenance of this low-level zonal overturning circulation over CA. In addition, this zonal overturning circulation over CA is timed out of phase with Central African rainfall. Complementing previous work on the low-level zonal overturning circulation, Longandjo and Rouault (2020b) have explained the physical processes responsible for the formation, seasonal evolution and variability of the low-level zonal overturning circulation. They considered this low-level zonal overturning circulation as the CB cell. Their study also provided comprehensive insight into the connection between this zonal overturning circulation and local rainfall and results show that, this CB cell persists year round, with maximum intensity and width in August/September and minimum intensity and width in May. Furthermore, the efficiency of the Congo basin cell determines seasonality over CA. Investigating process biases in precipitation in three versions of the Met Office Unified Model over CA with coupled and atmospheric formulations for each version; Taguela et al. (2022) show that the models describe a wet (dry) bias over the eastern (west coast) CA during the SON season, with the wet (dry) bias being stronger in the coupled (atmosphere only) models. The overestimation of the simulated sinking branch of the Atlantic-Congo zonal overturning cell is associated with a strong near-surface temperature and pressure gradient between CA and the eastern Atlantic Ocean. This leads to strong LLWs which dry

the coastal western CA and strengthen the intensity of the Congo basin cell.

1.1.7 Convection and Mesoscale Convective Systems

In equatorial Africa, most of the cloud cover is convective in origin and organised in aggregates called Mesoscale Convective Systems (MCSs) (Nicholson and Grist, 2003). MCSs produce a large proportion of the world's precipitation, especially in the CB, they account for 70-80% of rainfall and are of major importance from a climatological point of view. They are also essential for the energy balance of the planet, as they are mainly responsible for the vertical transport of the energy surplus of the tropics from the lower to the upper layers (Fiolleau and Roca, 2013). Moreover, the MCSs materialise the link between rainfall and the large-scale circulation (Mathon and Laurent, 2001). MCSs are collections of cumulonimbus clouds that organise into a large, contiguous rainfall-producing system, with the resulting rainfall covering areas in the order of 100 km or moreat least one direction (Dezfuli, 2017).

With the advent of space weather satellites, the last decades have seen significant advances in the documentation of precipitation, convective systems, water vapour and radiation at the top of the atmosphere (Fiolleau and Roca, 2013). MCSs in particular have the advantage of being observable with good spatial and temporal resolution by satellite and have been the subject of several studies. These include Nesbitt and Zipser (2003) and Jackson et al. 2009, who used data from the Tropical Rainfall Measurement Mission (TRMM), and (Vondou et al., 2010), who used data from Meteosat 7. Common to all these studies was an understanding of the mechanisms associated with the occurrence of MCSs in the CA region, and their links to local variabilities in the diurnal rainfall cycle. In tropical Africa, there are four regions of MCS maxima; over local orographic maxima (Ethiopian Highlands, Mount Cameroon), over Lake Victoria, and across a large region in the central-west CB near the equator (Jackson et al., 2009).

In the east CB, MCSs preferentially form on the western slopes of the Rift Valley mountains, and propagate westward at a rate of between 8 and 20 $m.s^{-1}$. High MCS activity in the Cameroonian Highlands contributes to some of the world's highest rainfall totals; at the Debundscha station in Cameroon, mean annual rainfall often exceeds 10 m (Jackson et al., 2009). These authors attributed the seasonal differences over the CB in the amount and location of rainfall to MCS activity.

Their study also showed that there are more MCSs during SON, particularly over the Ethiopian Highlands and Mount Cameroon, which are not significant regions of MCS activity during MAM. Conversely, maximum MCS activity over Lake Victoria occurs during MAM. The high occurrence of MCSs in CB may also explain why the region experiences the highest frequency of lightning strikes in the world (Albrecht et al., 2016). Despite this, the CB receives less annual precipitation than the convective hotspots of the Amazon and the maritime continent. In addition, the CB experiences higher levels of aerosols than other tropical land areas, which can influence convective activity by reducing the radius of cloud droplets and thus reducing the effectiveness of precipitation (McCollum et al., 2000).

1.1.8 Moisture flux and transport

An important factor in the spatial seasonnal variability of precipitation in a region is the availability, transport and content of moisture flux in the atmosphere. The moisture necessary for precipitation has three main sources: moisture already in the atmosphere, advection and convergence of moisture from outside the region, and recycling of precipitation through evaporation. The importance of each of these sources is crucial for precipitation over the CB and their main characteristics are still under studied. Pokam et al. (2012) suggest that there are two maxima of moisture convergence: the first during the MAM wet season, resulting from moisture flux near 700 hPa and embedded in the northerly component of the African easterly jet (AEJ-N), and the second during SON at lower levels (850–1000 hPa), dominated by advection from the Atlantic. Washington et al. (2013) indicate that assessment of moisture transport into the CB could help constrain coupled model outputs. In this sense, Creese and Washington (2016) fill the research gap in the CB by using qflux (convergence of moisture flux) in the CMIP5 ensemble to estimate the magnitude and distribution of modeled precipitation. The results show that qflux (which is assumed to be better constrained than parameterized rainfall) has a strong relationship with precipitation. The strongest correlations occur at 700 hPa in March-May ($r = 0.70$) and at 850 hPa in June-August, September-November and December-February ($r = 0.66$, $r = 0.71$ and $r = 0.81$). Analysis of moisture transport pathways indicates that modeled rainfall is sensitive to the amount of moisture entering the basin. Tamoffo et al. (2019) show that RCA4 modelled dry biases in the CB are associated with

dry upper-tropospheric layers, resulting from a western outflow stronger than the eastern inflow and related to the northern component of African Easterly Jet.

Using a water tagging scheme in the Community Earth System Model, Dyer et al. (2017) find that along with recycling from the basin itself, advection from the Indian Ocean is a major source of moisture for the region. The magnitude and location of moisture flux convergence has also been linked to rainfall amounts in the Congo Basin. Pokam et al. (2012) find that total column moisture flux (qflux) convergence is stronger in wet years than dry years, and dominated by convergence at low-levels. Other studies have indicated that the interannual variability of rainfall is more strongly associated with moisture convergence in the region than moisture already in the atmosphere, as the latter does not change significantly between extremely wet and dry years (Dezfuli and Nicholson, 2013; Cook and Vizy, 2016)

1.2 Representation of CA atmosphere in reanlaysis data

Because of the scarity of observational data, understanding of the dynamical mean state climatology in the CB described above is primarily based on reanalysis products. This section examines the extent to which our view the central African mean state depends on reanalysis data and the degree to which reanalysis products vary.

Cook and Vizy (2016) investigated the existence, seasonality, and variability of a CB Walker circulation in reanalyses and connections with rainfall. Results indicate that the ERAI and JRA-55 reanalysis produce very similar representation of the CB Walker circulation, with a broad region of upward motion between 15°E and 30°E, and subsidence to the west. The region of rising motion is somewhat broader in the lower-resolution ERA40 and NCEP2 reanalyses, but similarly located. The center of the circulation in the ERA40 and JRA-55 reanalyses is a little lower, at 800 hPa, than in the ERAI and NCEP2 climatologies. Even with these differences, it is clear that the Walker circulation is similar in each reanalysis, as is the vertical velocity field. Longandjo and Rouault (2020b) also analysed mechanisms of a CB cell using reanalyses (ERA-Interim, NCEP-2, and JRA-55). Their results show that, this shallow cell path is larger in NCEP-2 and JRA-55 than in ERA-Interim. There is also a good degree of consistency in the variability of the CB cell intensity between ERA-Interim and JRA-55, but NCEP-2 seems to not reproduce realistically the in-

terannual variability of the CB cell. Pokam et al. (2014) described seasonal means and the interannual variability of the low-level circulation over west equatorial Africa in some detail using NCEP-1, NCEP-2, Era-Interim and MERRA. A focus is made on the contribution of divergent and nondivergent circulation to the total flow. The increased resolutions of ERA-Interim and MERRA provide a clear depiction of two distinct cells of LLW north and south of 6°N. The northern cell is related to the development of the zonal circulation driven by the heat low.

Hua et al. (2019) comprehensively evaluate available reanalysis datasets based on quality-controlled radiosonde observations and a new gauge-based rainfall dataset (called NIC131) to identify the best datasets for understanding climate, patterns and variability of rainfall in the understudied central African region. They found that, while the reanalyses (i.e., 20CR, CFSR, ERA-Interim, JRA-55, MERRA2, NCEP-1 and NCEP-2) could reproduce major features such as the seasonal cycle, they exhibit considerable spread in rainfall magnitude and spatiotemporal characteristics. MERRA2 is closest to NIC131 for the mean climatology and inter-annual variability, whereas ERA-Interim is too wet across all months and has more rainfall over equatorial Africa. The rainfall produced in the reanalyses is strongly dependent on the model's hydrologic cycle and is also affected by model biases. To attribute the distinct differences in the CA rainfall among the seven reanalyses, they also examine the large-scale atmospheric circulation characteristics and results show that the differences in the lower and mid-tropospheric circulation reasonably explain these in the rainfall climatology among the reanalyses. Kuete et al. (2019) examined the formation and maintenance mechanisms of the AEJ-S, and its links with southern sub-tropical waves using reanalysis data sets of ERA-Interim, NCEP-2 and MERRA2. Results show a very good agreement across reanalyzes (ERA-Interim and MERRA-2) on changes in the strength of AEJ-S and precipitation responses over central Africa. NCEP-2 did not feature a clear relation between rainfall anomalies and AEJ-S strength. In contrast, the spatial pattern of rainfall anomalies is more complex with positive rainfall anomalies over southern Africa and west Africa while negative anomalies are in evidence over East Africa and the western part of the CB.

Overall, there is sufficient agreement between the reanalysis products to suggest that the circulation characteristics of the Central African mid-state presented are plausible. However, it is advisable to present results from several reanalysis datasets,

in order to check the behavior of the reanalysis models. Furthermore, the disagreement between spatial rainfall (Hua et al., 2019) is a result of the fact that reanalysis models, like climate models, need to parameterize rainfall processes.

1.3 Historical simulated climate of Central Africa in global and regional models: Process-Based Evaluation

Climate models are vital to the assessment of the impacts of climate change in the Central African regions. Establishing how well models reproduce key processes is important to the confidence we attach to these tools. In this section, CMIP simulations of the climate of CA are reviewed. The historical simulations are first examined, with particular attention to the current understanding of the sources of the actual rainfall bias. Next, the literature on the drying trend over CA and the variability in climate model projections is presented.

Process-based assessment methods establish whether models better reproduce reference data (with 'realism'), using a set of physically credible processes (James et al., 2018). The purpose of this assessment is two fold. The first is to improve scientific understanding of the annual cycle of the CB climate. If some models simulate the climate realistically against reference data, this would enhance the reliability of the model's representation of the physical parameters, and then provide information on why the annual cycle has the characteristics it does. The second objective is to identify methods to improve the way in which CB climate is generated in GCMs and RCMs.

CMIP model experiments are the main tool used to predict and diagnose future climate change due to anthropogenic warming. However, a realistic representation of the actual climate is considered a largely necessary (but not sufficient) condition for these projections to be plausible. This includes an examination of climate processes and historical wet or dry conditions. Where model biases in rainfall exist, an understanding of the model processes that may be causing them can help to justify the doubt about the plausibility of biases in rainfall change signals. A large number of literature has recently been compiled to assess the biases in rainfall and circulation over CA in the historical CMIP and RCM simulations (e.g.,Washington et al., 2013, Aloysius et al., 2016; Creese and Washington 2016, 2018; Fotso-Kamga et al.,2019;

Sonkoué et al.,2019; Taguela et al.,2020, 2022; Tamoffo et al.,2019, 2020).

Washington et al. (2013) were the first to identify the wide dispersion of raimfall amount and distribution in the CB wet seasons in CMIP5 models. Based on this, Creese and Washington (2016) suggested that an observational campaign at key CB boundaries could help constrain model rainfall dispersion. In addition, Creese and Washington (2018) argued that wet models west of the CB tend to have a stronger warm SST bias in the eastern tropical Atlantic than dry models. This leads to more ocean evaporation, enhanced local convection and higher rainfall in the western CB during SON. On the other hand, model wetness in the eastern basin is not related to the strenth of the Atlantic SST warm biases and appears to be more related to dynamical processes such as stronger LLWs that contribute to greater moisture advection into and uplift over the eastern CB, and also have a weaker and more polar AEJ-N. Using CMIP5 global models, Aloysius et al. (2016) reveal that skills of simulated temperature is better than those of rainfall. There is an important discrepancy in the climatology of rainfall appearing in the seasonality, spatial patterns, and magnitude of rainfall. Taguela et al. (2022) investigate processes leading to precipitation biases over CA in different versions of the MetUM model. Results show that in all versions and formulations (coupled and atmospheric only), the models depict a dipole bias over the region with a wet bias at the eastern CA and a dry bias over the coastal western CA. The wet (dry) bias is stronger in the coupled (atmospheric) models and is linked to a misrepresentation of the Atlantic-Congo zonal overturning cell, leading to a strong near-surface temperature and pressure gradient between CA and the eastern Atlantic Ocean.

There is a well-established difference in CB SON rainfall which varies by up to a factor of 3 among CMIP5 models. This encrease doubt on the credibility of global coupled models that are very wet in the west of the CB and have a large Atlantic SST bias or dry in the east of CB and associated to a stronger and more equatorward AEJ. This suggest that, downscaling could be showned beneficial for the region and improve the results of global models. By employing a process-based analysis approach, Tamoffo et al. (2020) intercompare abilities of RCMs to those of driving GCMs to investigate added value (AV) in rainfall and its some drivers over CA. Results indicate that simulations with highest AVs in the rainfall climatology also show improvements in the representation of the moisture flux and AEJs. In addition, a

comprehensive evaluation of RCA4 responses to eight CMIP5 forcings in the CB has been presented by Tamoffo et al. (2019b). Their work shows that, in the historical climate framework, although RCA4 models have dry biases, they well capture the observed features of the actual climate, including seasonal and intraseasonal variability of model rainfall, more consistent in the dry season. Furthermore, by comparing the climatological characteristics of individual experiments with those of the evaluation experiment and the RCM ensemble model, their study shows similar features, thus confirming the hypothesis of systematic biases as the main sources of model errors. Recently, Creese and Washington (2016) argued that the CMIP5 ensemble model is not appropriate for modelling Congo rainfall due to divergent climatological characteristics between the models. Thus, the results of Tamoffo et al. (2019) show that downscaling using a common RCM is a plausible option to overcome this problem, in case the RCM has a good ability to reproduce the real climate.

Creese and Washington (2018) show that there are two possible approaches to improving the representation of CB climate in models given the scarcity of observations. The first is to improve the availability and use of climate data in the region. This will greatly contribute to improving our understanding of the climate in this region, as well as providing better quality data for the evaluation of climate models. The second approach is to develop ways of evaluating climate models in the absence of observed data. This is the dominant approach adopted in future work in the region, and is intended to be complementary to the data rescue projects that are underway in the region.

1.4 Interannual rainfall variability

Monitoring climate variability remains a critical issue for the scientific community. CA, for example, is a hotspot for inter-annual rainfall variability, and rainfall is very sensitive to local climate variables, resulting in high variability. This high interannual variability, coupled with a high dependence on rainfall for food, energy and water needs, makes the region highly vulnerable to droughts and floods events.

The interannual variability of CA remains complex, mainly because it is linked to multiple interrelated sources of variability from other parts of the continent, not all of which are well understood in the Central African region. The main source of

interannual variability is the AEJ, which is linked to Central African rainfall through mid-level convection. Most regions of equatorial Africa experience two rainy seasons during the course of the year. One is during MAM and the second and main rainy season is during SON. Mechanisms controlling the year-to-year variability of rainfall over equatorial Africa were examined by Nicholson and Dezfuli (2013) and Dezfuli and Nicholson (2013) respectively. Nicholson and Dezfuli (2013) showed that during the April–June rainy season, interannual variability in this coastal sector shows a strong link to changes in local sea surface temperatures (SSTs) and the South Atlantic subtropical high. To understand potential causal mechanisms of this link, various atmospheric parameters were evaluated for wet and dry composites. Their results suggest that in the tropics, a crucial control on rainfall variability is the intensity of the zonal circulation so as a La Niña (El Niño) type signal is apparent in association with wet (dry) composites. Anomalies in the local zonal circulations show that the wet (dry) composite is associated with an intensification (weakening) of the TEJ and LLWs, but a weakening (intensification) of the mid-level AEJs. On the other hand, during the second rainy season, Dezfuli and Nicholson (2013) show that the wet (dry) conditions in the eastern Congo basin are associated with El Nino (La Nina)–like phases.

Another factor that modulates the interannual variability of rainfall in the CA region is the Indian Ocean Dipole (IOD). Recently, Moihamette et al. (2022) examined the influence of extreme IOD events on CA rainfall from September to December over the period 1980-2016. Their results show that during extreme positive IOD events, CA experiences increased moisture inflow from the Indian Ocean leading to increased rainfall, while the opposite process is recorded during negative IOD events, with the magnitude of anomalies in positive IOD events being stronger than that in negative IOD events. A similar relationship is identified by Dezfuli and Nicholson (2013) between positive IOD years and enhanced rainfall in the east CB during SON, while the opposite pattern (negative IOD in wet years) is observed in the west of the basin at the Angola coast. Investigation of the large-scale factors has demonstrated that climate variability in Africa can be influenced by forcing from adjacent (Atlantic and Indian) and remote (tropical Pacific) oceans, where variability in SSTs can influence moisture availability and advection (Pokam et al., 2012, 2014; Yang et al., 2015; Dyer et al., 2017). Pressure gradients between the Atlantic and Indian Oceans

have also been found to be related to zonal differences in rainfall in the CB. (Dezfuli et al., 2015) showed that in wet years, the strong contrast between high pressure in the equatorial Atlantic and low pressure in the southwestern Indian Ocean leads to increased westerly winds in the CB, which converge over the East African highlands. This leads to high rainfall in the eastern part of the basin and drying in the western part of the basin, as a subsiding branch forms in response to the increased uplift in the east.

1.5 Aims and Reseach questions

Based on the above literature review, we identify an important feature of the regional climatology of CA, which can be used to characterize future changes over the region, namely the AEJ in the middle troposphere. The overarching goal of this thesis is to contribute to a deep understanding of convection over CA, by providing insights into the expression of the climatological structure of the AEJ components and dynamics using reanalyses (as these jets have been identified as key contributors to convection over the region), then assessing model behaviours of these jets in the historical periods using the two latest versions of global coupled models (CMIP5 and CMIP6). Given the limited scientific attention given to the climate of the Congo Basin, and even more so to model assessment in this region, we will assess model behaviour over the historical period using a new model assessment methodology; process-based approaches. Applying these approaches can provide insights into the plausibility of climate change in the Congo Basin, a convective core of the African continent and one of the three wettest places on Earth, alongside the Amazon Basin and Maritime Continent.

Although it is established that both components of the AEJ play an important role in rainfall variability in the Congo Basin, both in seasonal climatology and in inter-annual variability as indicated in the literature review above, their maintenance mechanisms are still poorly studied, especially the southern component, which is present during the second and main rainy season over the region from September to November. The northern component is active all year round and stronger. In order to express the climatology and variability of rainfall over the Central African region from an AEJ perspective, the following objectives need to be achieved.

Aim 1 : To develop a flexible method for identifying the intensity and location of the AEJ core in daily and monthly reanalysis data and model outputs over a range of spatial resolutions;

Aim 2 : To characterize the climatological structure of the AEJ in the reanalyses, and examine the behaviour and spatial distribution of the AEJ in the models;

Aim 3 : To investigate the dynamics that drives maintenance of the AEJ in reanalyses, and determine how the variability pattern in the strength of the AEJ in models is related to the mechanisms identified;

Aim 4 : To establish the role of westerly waves over southern Africa in modulating the southern component of the AEJ intensity (AEJ-S); and

Aim 5 : Characterise the periodicity and intensity of the wave signal on daily timescales.

Through investigations of the control and maintenance processes of the AEJ, we hope to enhance the understanding of the physical mechanisms that regulate the mid-level atmospheric circulation over CA and improve the basis for new mechanisms that help to identify appropriate metrics for the evaluation of global and regional models over CA, representing opportunities for process-based assessment, with the aim of better characterizing future changes and assessing their plausibility.

1.6 Conclusion

This chapter have summarised main component of the Congo Basin climate system, including key features of the climate regime such as low-level circulation, mid-level circulation, upper tropospheric circulation and the regional convective system. New characteristics of the basin's rainfall regime are also presented, such as the Congo basin Cell and the Congo Air Boundary. A brief summary of the moisture availability and transport in the region is also shown. Finally, a review of models' assessment approaches in the CB is likewise presented.

Chapter 2

Study Area, Data and Methods

This chapter starts with the location and description of the study area. It then outlines the datasets and methodologies that have been used in this thesis. The first part of the analysis presented in Chapter 3 is based primarily upon reanalysis datasets and gridded precipitation products, while the second part studies the CMIP5 CMIP6 climate model database. These three types of data are described below.

2.1 Key Study area

This thesis takes into account the meteorology and climate variability of the Central African sub-region. It straddles the Equator and is drained largely by the Congo River system. It comprises, according to common historical ties many countries, being part of French Equatorial Africa. Some countries like Rwanda and Burundi, although they are located east of the East African Rift System, which forms the eastern divide of the Congo basin, are also often considered part of the region because of their long administrative connections. This region is characterized by hot and wet climates on both sides of the Equator. The equatorial strip that extends from the Atlantic Ocean to the Western Rift Valley is influenced throughout the year by large and local scales features resulting in rainfall seasonality and variability. Annual rainfall exceeds 2,000 mm in coastal regions in the West, in the centre of the Congo Basin, and on the mountain summits bordering the Western Rift Valley.

The study area for this thesis is determined by taking the following considerations into account. Firstly, it is one of the three global convective hotspots (Webster, 1983), experiencing the highest frequency of lightning strikes on the planet (Jackson et al., 2009) and dominates global rainfall totals during the transition seasons (Xie et al.,

2003). Second, the rainforest is a globally important carbon sink and therefore a crucial component of the global climate system via the carbon cycle (Williams et al., 2007). Thirdly, the region's population is heavily dependent on rain-fed agriculture and has already experienced severe land degradation due to drought in recent years. Climate forecasting is therefore crucial for these populations, as rainfall is expected to increase (Dunning et al., 2018).

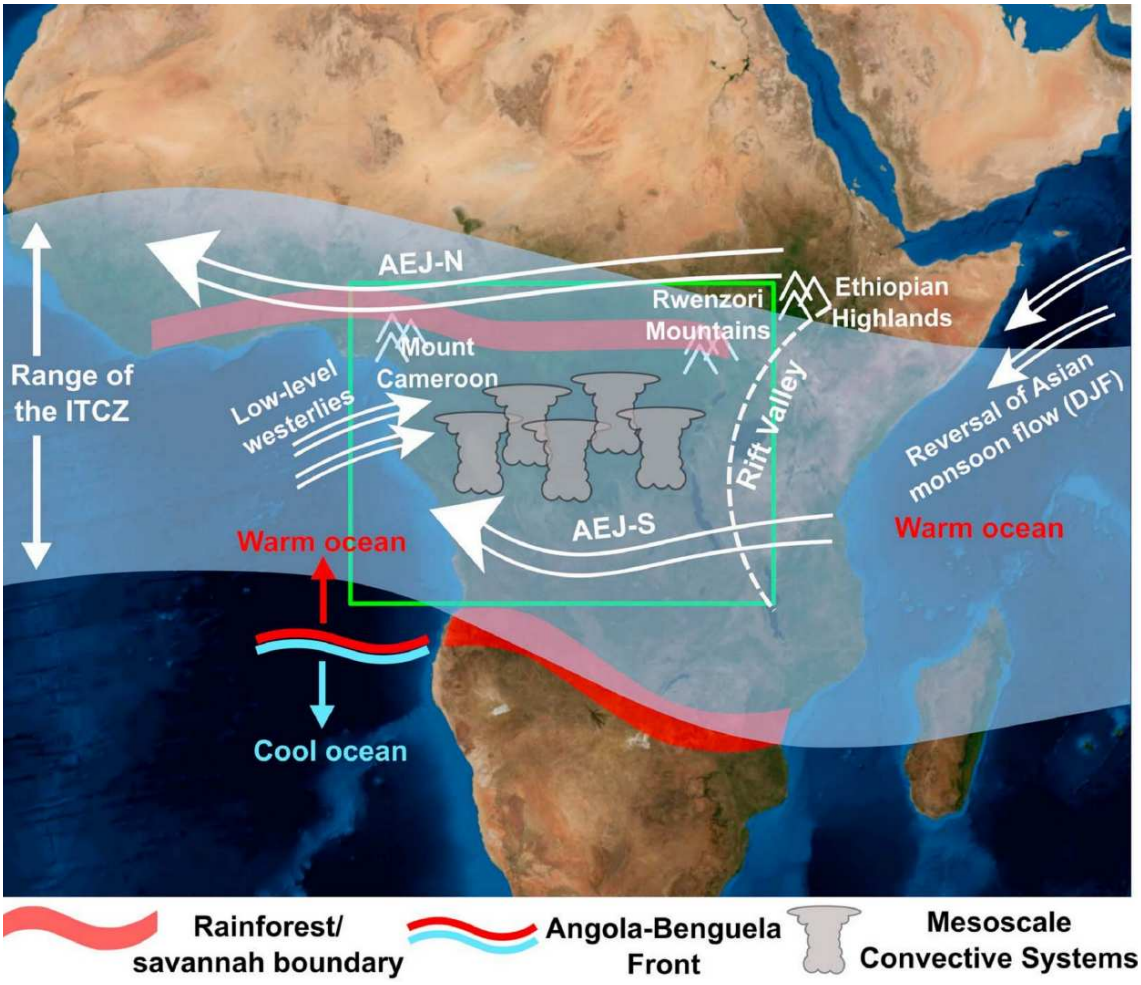

Figure 7: *Region of interest shown by the green box with schematic showing two main key features of the Congo Basin climate study in this thesis: AEJ-N = African easterly jet, north and AEJ-S = African easterly jet, south. Locations are approximate.Background image: NASA Visible Earth yes.*

Figure 7 shows the study area and the two main features of the mid-tropospheric atmospheric circulation investigated in this thesis, namely the northern and southern components of the African Easterly Jet, details of which will be given in Chapter 3. This figure also shows that the northern component of the jet is more present and stronger than the southern component. The two jets are generally considered to form due to strong meridional surface temperature gradients between the equator and the subtropics. This indicates the importance of the land surface characteristics

of the Congo rainforest for this study, especially does driving moisture circulation patterns.

The approach of this thesis intends to focus on mid-level atmospheric features that have received some attention previously. Therefore, the central region of attention is the margin of the equatorial tropical rain belt. Since a process-based approach is adopted, emphasis is also placed on the semi-arid tropical regions further south and north, where climatologists have already built up a comprehensive literature base, particularly with regard to tropical thermal lows (Sahara and Kalahari thermal lows) and subtropical highs (Sahara and Botswana highs).

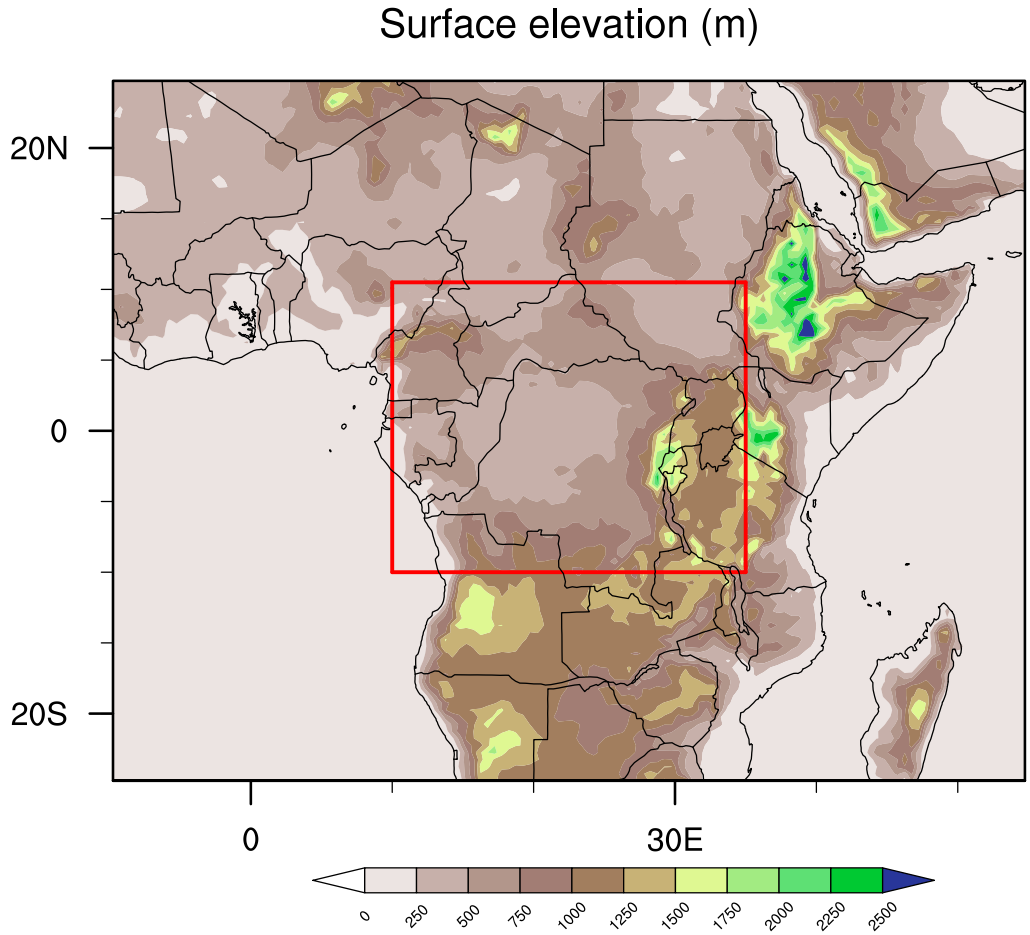

Figure 8: *Land surface height (m) over the central Africa domain (red box) and surrounding regions. Data is from the USGS GTOPO30 digital elevation model.*

This region is characterised by complex topography and dense hydrographic network which is the dominant source of electricity production in the region. The land surface height in the Congo Basin region is shown in Figure 8, and the average elevation of the basin is over 750 m. The figure also indicates that there is a difference of approximately 2000 m in surface elevations between the eastern and western boundaries of CB. The African Rift Valley highlands seperate the region at the eastern

sector and the presence of this high terrain is likely to influence the climate, including influencing the amount of moisture than can reach the basin from the Indian Ocean (Moihamette et al., 2022) and have also been identified as a preferential location for convection in the region (Jackson et al; 2009; Dezfuli et al; 2015). To the west, the CB borders the Atlantic Ocean, and to the northwest of the region, are the highlands of Mount Cameroon.

Vegetation is also significant for this region. Its link to evaporation makes it a crucial driver of CB climate. Zhou et al. (2014) showed that a high rate of vegetation cover characterizes CB, and due to population growth and climate change, this cover is decreasing (Malhi, 2018). Crowhurst et al; 2020 perform an exploratory process-based assessment of CB evaporation in 11 CMIP5 models and show that models with realistic precipitation simulate higher precipitation in November, the peak of the second wet season than in March, the peak of the first. This is important for controlling surface temperature variations in the region and thus the impact on the surface temperature gradients that control the AEJ.

2.2 Datasets

2.2.1 Reanalysis Products

Reanalysis datasets are the result of a series of atmospheric forecast models that assimilate meteorological measurements from around the world. They can be considered as a consistent approximation of the state of the global atmosphere at sub-daily and monthly resolution, and decadal time scales. The accuracy of the reanalysis data is limited by the availability of measurements for assimilation. In regions where measurements are abundant, confidence in the reanalysis is higher than in places where measurements are scarce. CA falls into the latter category, where reanalysis is more model-based than observation-based. Despite this, the dynamic aspects of the circulation are trusted when using reanalysis data. Reanalysis products are used for three purposes in this thesis. Firstly, they are studied on a monthly time scale to identify the AEJ. Second, the reanalyses are used to characterize the climatological structure, pattern and spatial distributions, variability and dynamics of the AEJ system. Thirdly, reanalyses are used to compare the historical representation of AEJ in the CMIP5 and CMIP6 models with that of the reanalysis products.

The main parameter used to identify the AEJ is the zonal component of the horizontal wind. Other atmospheric parameters such as air temperature, vorticity, geopotential height, air humidity and divergence are used to analyse AEJ composites. Reanalysis-derived rainfall estimates are also used in this thesis, although they are generally avoided due to their dependence on unresolved convection. Also, gridded rainfall products derived from satellite and gauge data are used. Three reanalysis products are used in this study: ERA-Interim, ERA-5 and MERRA2. By using this range of reanalysis products, some of the uncertainties in the estimated atmospheric state are captured and trusted.

2.2.1.1 ERA-Interim

ERA-Interim was released in 2011 by Dee et al. (2011) at a spectral resolution of approximately 75 km at the equator with 60 vertical levels. The assimilation scheme used in this thesis is a 4D-Var scheme at a temporal resolution of 1 month and a horizontal resolution of approximately 0.75 degrees in the north-south direction, and 0.625 in the east-west direction. ERA-Interim is the focus of Chapter 3 and it is analysed from 1980 to 2015.

2.2.1.2 ERA-5

ERA-5 is an updated ECMWF reanalysis with superior resolution and an updated version of the Integrated Forecasting System (IFS) as compared to ERA-Interim (Copernicus Climate Change Service (C3S), 2017; Hersbach et al. (2020)). ERA-5 is at a temporal resolution of 1 month and a spectral resolution of approximately 31 km at the equator, equivalent to a horizontal resolution of approximately 0.25 degrees in the north-south direction, and 0.25 in the east-west direction. The version is 10 years more modern than ERA-Interim. ERA-5 also uses a monthly 4D variational analysis in this thesis. ERA-5 is used in Chapter 3 and it is also used for validation of AEJ in CMIP5 and CMIP6 models.

2.2.1.3 MERRA-2

MERRA-2 is a retrospective reanalysis product produced by NASA's Global Modelling and Assimilation Office <gelaro2017modern. MERRA-2 uses the GEOS atmospheric forecast model, which has a finite volume dynamical core. It has 72

vertical levels stretching up to 0.01 hPa, 1 month temporal resolution and a horizontal resolution of approximately 0.5 degrees in the north-south direction, and 0.625 in the east-west direction. The horizontal grid geometry is based on a cubed sphere. MERRA-2 is available from 1980 through to the near-present. This dataset is used to cross-check the AEJ analysis of Chapter 3, and has a larger role in validating the historical representation of AEJ in CMIP5 and CMIP6 models.

2.2.2 Gridded Rainfall Datasets

Gridded rainfall datasets are important to assess the degree to which the inter-annual variability of the identified AEJ systems controls the inter-annual variability of rainfall over CA.

The rainfall datasets all combine rainfall station data with satellite imagery and are chosen to optimise the length of data that overlaps with the reanalyses period considered (1979 - 2015). Due to a shortage of observational data over the African continent (Washington and Preston (2006)), gridded rainfall datasets tend to be undesirably dependent on the algorithms used to construct rainfall estimates from the input data (Awange et al. (2016)). For this reason, several rainfall datasets are generally considered, and key results must be robust across multiple datasets. In this thesis, we have used only GPCP data, which better represents the seasonality of rainfall in CA. It is detailed below.

2.2.2.1 GPCP

Version 2.3 of the Global Precipitation Climatology Project (GPCP) monthly dataset is described in detail by Adler et al. (2018). This product comprises data from rain gauge stations, satellites, and sounding observations have been merged to estimate monthly rainfall on a 2.5-degree global grid from 1979 to the present. The careful combination of satellite-based rainfall estimates provides the most complete analysis of rainfall available to date over the global oceans, and adds necessary spatial detail to the rainfall analyses over land. In addition to the combination of these data sets, estimates of the uncertainties in the rainfall analysis are provided as a part of the GPCP products.

2.2.3 Coupled Model Intercomparison Projects: phases 5 and 6

The CMIP5 and CMIP6 datasets are a collection of coordinated GCM experiments run by many climate modelling groups around the world. This study is based on monthly mean outputs from sixteen historical experiments of GCMs: 8 simulations from CMIP5 (Taylor et al. (2012)) and 8 simulations from the newly developed CMIP Phase-6 (CMIP6) (Eyring et al. (2016)). Historical simulations are analysed over the period 1980-2005 for CMIP5 and 1980-2010 for CMIP6, with a focus on SON. Table 1 provides details of the CMIP5 and CMIP6 models included in this study. Models have been selected because they have been frequently used in the literature and therefore will be of interest for comparison with previous work. In particular some CMIP5 models have been identified as representing the region well in previous literature, or showing an unusual representation or interesting biases to be explored. In addition, a comparison of all CMIP5 and CMIP6 models from a process-based perspective is not plausible, at least not in this thesis only. It is made clear in the conclusions that the results apply to a subset of models from the CMIP ensembles. To assess the capabilities of CMIP models, two reanalysis data are used, ERA-5 (Hersbach et al. 2020) and MERRA-2 (NASA, 2016).

2.3 Methods

The overall methodological approach of this thesis is to identify and analyse the dynamics and characteristics of two dominant features of the regional atmospheric circulation over Africa, namely: the AEJ-N and the AEJ-S, with a focus on the less studied AEJ-S. These dynamics and features are then used to evaluate processes in climate models. In this section, we present the same algorithm used to identify these two jets. The methodology used to characterise the behaviour, spatial distributions, dynamics and impact on the interannual variability of rainfall are the same for both jets are therefore described in situ in Chapter 3.

2.3.1 Estimation of the Surface Meridional Gradient in Temperature

It has been shown that AEJ results from thermal contrast and located slightly equatorward of the lower tropospheric meridional temperature gradient. The mid-level AEJ components develop because the warming of the thermal low regions of the

Table 1: Name and description of CMIP5 and CMIP6 models and reanalysis data used in this study.

Acronym expansions are available online at http://www.ametsoc.org/PubsAcronymList.				
Model Name	Institutions	Atmospheric Horizontal Resolutions	Vertical Levels	References
CMIP5				
CMIP6				
BCC_CSM1.1(m)	BCC	1.120 X 1.120	26	Wu et al. (2014)
BCC-CSM2-MR	BCC	1.120 X 1.120	26	Wu et al. (2019)
CNRM-CM5	CMCC	1.120 X 1.120	31	Voldoire et al. (2013)
CNRM-CM6-1	CMCC	1.120 X 1.120	31	Voldoire et al. (2018)
HadGEM2-CC	MOHC	1.250 X 1.80	38	Jones et al. (2011)
UKESM1	MOHC	1.250 X 1.80	38	Sellar et al. (2019)
HadGEM2-ES	MOHC	1.250 X 1.80	38	Jones et al. (2011)
HadGEM3-GC31-LL	MOHC	1.250 X 1.80	38	Malcolm (2017)
MIROC5	MIROC	1.40 X 1.40	40	Watanabe et al. (2010)
MIROC6	MIROC	1.40 X 1.40	40	Watanabe et al. (2018)
MRI-ESM1	MRI	1.10X1.10	48	Yukimoto et al. (2012)
MRI-ESM2-0	MRI	1.10X1.10	48	Yukimoto et al. (2019)
GISS-E2-R	NASA GISS	2.00X2.50	40	Kim et al. (2012)
GISS-E2-1-G	NASA GISS	2.00X2.50	40	NASA (2018)
GFDL CM3	NOAA/GFDL	2.00X2.50	48	Donner et al. (2011)
GFDL CM4	NOAA/GFDL	1.00X1.250	48	Huan et al. (2018)

Sahara and Kalahari creates a surface temperature and thermal gradients with the equatorial regions of CB. The Atmosphere responds by generating vertical wind shear to maintain the thermal wind balance. We quantified low-level potential temperature according to:

$$\theta = T * (\frac{P_s}{P})^{0.286}, \tag{2.1}$$

P_s and P are surface pressure (1013 hPa) and pressure at 850 hPa respectively. T is air temperature at 850 hPa. We then perform a centered finite difference operation on the Yth dimension representing latitude coordinates (yi) to obtain meridional potential temperature gradient as follows.

$$\frac{\partial \theta}{\partial Y} = \frac{\theta_(yi+1) - \theta_(yi-1)}{Y_(yi+1) - Y_(yi-1)}, \tag{2.2}$$

2.3.2 African Easterly Jets Track Algorithm

This algorithm is used to detect the locations and intensities of AEJs in Chapter 3. The thresholds and parameters defined in the algorithm are based on the literature

review. A set of criteria are applied as follows to extract AEJs:

(1) : Load model or reanalysis monthly zonal winds over the domain (20°S-20°N, 10°E-30°E) and select 700 and 600 hPa pressure levels. As the two jets (northern and southern) components are located in differents domains, to represent locations and intensities of the two components, we have to extract AEJ-N (northern component) and AEJ-S (southern component) from the monthly zonal winds of our domain.

(2) : Create variable *Un* which represent AEJ-N in the latitudinal range (3°N-20°N) create variable *Us* which represent AEJ-S in the latitudinal range (5°S-20°S).

(3) : Now calculate Un monthly mean climatology and average over the longitude range (12°E-24°E) between 700 and 600 hPa levels (AEJ-N is located at 700 hPa from January to August and at 600 hPa from September to December). Also calculate *Us* monthly mean climatology and average over the longitude range (12°E-24°E) and select 600 hPa pressure level (AEJ-S is only present at 600 hPa).

(4) : Calculate for all months and for all latitude points minimum value for *Un* and *Us*. As noted in Chapter 1 on the AEJ overview, AEJs are defined as monthly-mean easterly winds with values exceeding -6 $m.s^{-1}$. The Minus sign stands here for winds that are easterlies since the jets are easterly winds.

(5) : Extraction of core mean locations and intensities of each component :

- Location and intensity of AEJ-N: If for each latitude point and for each month and for the two levels 700 and 600 hPa, the value of *Un* is equal to the minimum value and minimum value of *Un* is lower or equals to -6 (-6 is the threshold) then retain the latitude and intensity corresponding.
- Location and intensity of AEJ-S : if for each latitude point and for each month and for level 600 hPa level, the value of *Us* is equal to a minimum value of *Us* and minimum value of *Us* is lower or equals to -6 (-6 is the threshold) then retain the latitude point and intensity corresponding.

2.3.3 African Easterly Jets as Geostrophic wind

Cook (1999) showed that AEJ is essentially geostrophic and is associated with a meridional temperature gradients below the level of the jet maximum. As a first step in understanding the generation of the AEJ, we investigate the degree to which the jet is geostrophic. Here, geostrophy is defined as a balance between the pressure gradient and the local Coriolis accelerations according to :

$$f.v = (\frac{1}{\rho})\frac{\partial P}{\partial x}, \tag{2.3}$$

$$f.u = -(\frac{1}{\rho})\frac{\partial P}{\partial y}, \tag{2.4}$$

in which f is the Coriolis parameter, u and v the zonal and meridional components of velocity, x and y the zonal and meridional coordinates, P the pressure, and ρ the density. By substituting using the hydrostatic limits, we have:

$$f.v = -g\frac{\partial P}{\partial x}.\frac{\partial Z}{\partial P} = g\frac{\partial Z}{\partial x}, \tag{2.5}$$

$$f.u = g\frac{\partial P}{\partial y}.\frac{\partial Z}{\partial P} = -g\frac{\partial Z}{\partial y}, \tag{2.6}$$

with Z the height of the constant pressure surface (geopotential height). This leads us to the following result for the geostrophic wind components (u_g, v_g):

$$u_g = -\frac{g}{f}\frac{\partial Z}{\partial y}, \tag{2.7}$$

$$v_g = \frac{g}{f}\frac{\partial Z}{\partial x}, \tag{2.8}$$

Previous work has associated the AEJ with meridional temperature gradients. The temperature gradient results in the mid-tropospheric AEJ through the thermal wind relation:

$$U \simeq -\frac{R_d}{f}\frac{\partial < \theta_v >}{\partial y} ln(\frac{P_s}{P}), \tag{2.9}$$

U is the zonal wind at the level of the jet and $< \theta_v >$ is the mean virtual potential temperature below the jet. R_d , f , P_s and P are the dry gas constant, Coriolis parameter, surface and mid-level pressure, respectively.

The easterly wind maximum at mid-level (700-600 mb) is "a response to the surface baroclinic zone and the reversal of the temperature gradient in the middle troposphere," referring to the reestablishing of a negative meridional temperature gradient above the jet maximum. The atmospheric moisture budget complicates the relationship between the geostrophic wind shear and the temperature gradient according to:

$$\frac{\partial \phi}{\partial y} \simeq -\frac{\partial \theta_v}{\partial y} = -(1 + 0.6q)\frac{\partial \theta}{\partial y} + 0.6\theta\frac{\partial q}{\partial y} \tag{2.10}$$

where θ_v is virtual potential temperature and q is specific humidity.

2.3.4 Estimation of the Atmospheric kinetic energy

To analyse the maintenance processes that contribute to the acceleration of the AEJ, focus is on contribution from the divergent circulation deflected by Coriolis acceleration and mid tropospheric highs. Following Nielsen and Chen (1993), Chen (2004) state equations of kinetic energy of divergent (V_D) and rotational (V_R) flows as follow :

$$\frac{\partial k_D}{\partial t} \simeq \nabla.(V_D k) - (\zeta + f)(u_D v_R - u_R v_D) - V_D.\nabla\phi, \tag{2.11}$$

$$\frac{\partial k_R}{\partial t} \simeq \nabla.(V_R k) - (\zeta + f)(u_D v_R - u_R v_D) - V_R.\nabla\phi, \tag{2.12}$$

where $k_D = (u_D + v_D)^2/2$, $k_R = (u_R + v_R)^2/2$, $V_D = (u_D,v_D)$ is divergent wind, $V_R = (u_R,v_R)$ is rotational wind, ζ is relative vorticity and f is the Coriolis force.

The deflection of divergent meridional circulation into rotational zonal flow by Coriolis acceleration leads to establishment of the conversion between divergent kinetic energy into rotational kinetic energy. This conversion named $C(k_D, k_R)$ is expressed as follow :

$$C(k_D, k_R) = -(\zeta + f)(u_D v_R - u_R v_D) \tag{2.13}$$

To compute the components of divergent and rotational wind, we used decompisition of total horizontal velocity according to Helmholtz theorem as follow:

$$\vec{V} = \vec{V}_\psi + \vec{V}_\chi \tag{2.14}$$

where

$$\vec{V_\psi} = \vec{k} \times \vec{\nabla}_\psi \tag{2.15}$$

and

$$\vec{V_\chi} = \vec{\nabla}\chi \tag{2.16}$$

V_ψ is rotational wind, ψ is the stream function, V_χ is divergent wind, χ is the velocity potential, $\vec{k}$ is the unit vector in the vertical direction, and $\vec{\nabla}$ is the horizontal gradient. To obtain velocity potential (χ) which represents divergent circulation, and stream function, we solved the folowwing Poisson equations

$$D = \vec{\nabla}^2\chi \tag{2.17}$$

$$\zeta = \vec{\nabla}^2\psi \tag{2.18}$$

where D is the wind divergence and ζ is the relative vorticity in (2.9 and 2.10). We then obtained divergent wind components (u_D, v_D) and the rotational wind components (u_R, v_R) using equations (2.17) and (1.18) bellow respectively.

$$(u_D, v_D) = (\frac{\partial\chi}{\partial x}, \frac{\partial\chi}{\partial y}) \tag{2.19}$$

$$(u_R, v_R) = (-\frac{\partial\psi}{\partial y}, \frac{\partial\psi}{\partial x}) \tag{2.20}$$

.

The deflection of divergent meridional circulation by Coriolis force close to the jet core leads to the conversion of divergent kinetic energy into rotational kinetic energy and accelerates the jet (Chen 2004). This mechanism is described in more detail in Sect. 1 of Chapter 3. In the first section of Chapter 3 that a link between AEJ-S dynamics and southern subtropical westerly waves is also revealed. It is shown that, when waves amplify over southern subtropics, they modify lower tropospheric heating. Depending on the phase of the wave, this modifies the cross latitude temperature gradient throughout equatorial regions, therefore modulating the intensity of the jet.

To investigate the connection between AEJ-S and subtropical westerly waves, we used geopotential height to locate upper level troughs and ridges and 850 hPa air temperature to assess modulation of the heating regime at an altitude important to the AEJ-S. This connection is assessed through composite analysis during months

of strong and weak AEJ-S, where strong AEJ-S is defined as a jet core with values exceeding 8 m.s^{-1} and weak AEJ-S corresponds to a jet core with values between 6 and 2 m.s^{-1}. Table.2 presents all possible strong and weak months individual in the reanalysis. Strong composite anomalies are defined as mean of strong AEJ-S minus climatology, whereas the weak composite anomaly is computed as mean of weak AEJ-S minus climatology. All computations are for September-October-November months.

Table 2: September-October-November months when the AEJ-S is strong and weak in reanalysis

Strong months			Weak months		
MERAA-2	ERAINT	NCEP-2	MERARA-2	ERAINT	NCEP-2
Sept1983	Sept1983	Sept1983	Nov1988	Nov1983	Sept1986
Oct1983	Sept1984	Oct1983	Nov1989	Nov1984	Sept1987
Sept1984	Sept1988	Sept1984	Nov1991	Nov1985	Sept1992
Oct1984	Sept1989	Sept1985	Nov1992	Oct1986	Sept1993
Oct1987	Sept1991	Oct1985	Sept1993	Nov1986	Nov1993
Sept1988	Sept1995	Nov1985	Nov1993	Oct1987	Sept1994
Sept1989	Sept1996	Nov1986	Nov1996	Nov1987	Oct1994
Oct1990	Oct1996	Oct1987	Nov1997	Nov1988	Nov1994
Nov1990	Sept1997	Nov1987	Nov1998	Nov1989	Sept1995
Sept1991	Oct1998	Oct1989	Nov1999	Oct1991	Oct1995
Oct1992	Sept2000	Oct1990	Nov2000	Nov1991	Nov1995
Oct1993	Oct2000	Nov1990	Nov2001	Nov1992	Sept1996
Oct1994	Sept2001	Oct1993		Nov1993	Oct1996
Oct1995	Sept2003			Nov1994	Nov1996
Oct1996				Nov1995	Sept1997
Oct1998				Nov1996	Oct1997
Sept2000				Nov1998	Sept1998
Oct2000				Nov1999	Oct1998
Sept2001				Nov2000	Nov1998
Oct2002				Nov2001	Sept1999
Nov2002				Nov2002	Oct1999
Oct2003					Nov1999
					Nov2000
					Nov2001

Calculating anomalies

Most of the tools we will present in wave analysis are based specifically on the calculation of the anomalies of the parameters necessary to describe the characteristics of the wave. The interest in the anomaly field is important, as it allows us to focus on extreme sequences with respect to the mean state. The general idea in

climate variability is to calculate deviations from the seasonal cycle. Considering that a time series X_t can be put in the form $X_{y,d}$ (y and d denote the year and the day of the year, respectively), we will proceed as follows:

(1) We calculate the mean seasonal cycle :

$$\bar{X_d} = \frac{1}{N_y} \sum_y X_{y,d} \tag{2.21}$$

With N_y being the number of years in the data set.

(2) The intraseasonal anomaly is calculated by subtracting the mean seasonal cycle from the initial $X_{y,d}$ field as follow:

$$X'_{y,d} = X_{y,d} - \bar{X_d} \tag{2.22}$$

2.3.5 The Empirical Orthogonal Function Analysis (EOF)

Having identified southern subtropical westerlies, we showed that this wave activity, as it crosses the subcontinent, has the potential to modulate the strength of the AEJ-S through its impact on the modulation of the intensity of the Kalahari thermal heat low since the jet is a thermal wind. This opens up an approach to the impact of the wavy flow on intraseasonal variability of precipitation through modulation of the AEJ-S, as many studies conducted on the jet have so far been based on seasonal and interannual variability. Thus, it is important to describe the meteorological characteristics directly associated with these westerly waves such as wave signature and periodicity.

To explore and understand the main modes of variability, spatial and temporal patterns of the wave signal, the first four components of the EOF analysis were applied to daily geopotential height anomalies. The EOF is a useful statistical tool for identifying and for classifying main patterns that explains the largest fraction of the total variance of a field. In this thesis, the classical EOF has been applied. Its premise is based on the temporal variance-covariance matrix $\sum$. We consider a spatio-temporal matrix of geopotential height at 300 mb in space and time $Z(x, y, t)$ where x is the number of longitudes, y latitudes and t time ($t = 1, ..., n$). n is the length of the matrix on the temporal serie. Diagonal elements of Z represent the variance of the domain's grid points whereas non-diagonal elements define the covariance of all pairs of points in this domain. The covariance matrix is defined by:

$$\sum = \frac{1}{n-1} Z Z^T \tag{2.23}$$

As $\sum$ is symmetrical and hence diagonalisable, it can be following written:

$$\sum = A\lambda^2 A^T \tag{2.24}$$

with A the orthogonal matrix of $\sum$ eigenvectors and λ^2 the orthogonal matrix including eigenvalue associated to A. It's these eigenvalues that are expressed as a percentage of variance (Var in %) according to the following equation:

$$Var(\lambda_i) = \frac{100\lambda_i}{\sum_{i=1}^{n} \lambda_i} \tag{2.25}$$

Finally, the temporal series of the principal component (PC_i) is reconstructed in projecting the initial spatio-temporal matrix Z on each of the eigenvectors A_i as mentioned in equation (2.16),

$$PC_i = ZA_i \tag{2.26}$$

the weight of each being function of the amount of the corresponding variance (eigenvalues).

In Chapter 3, process based metrics are used to investigate the skill of CMIP models to capture the dynamics associated with the AEJ. This involves investigating how the intense surface heating associated with the subcontinental thermal heat low drives the meridional surface temperature gradient and results in the mid-level AEJ. As the whole AEJ system is supported by a mid-tropospheric thermal circulation, we then show in sections 5 and 6 how dry thermal convection over the Namib-Kalahari and Sahara dryland thermal lows supports strong rising motion forming mid-level highs associated with anticycloninc circulation and divergent centres. This process approach is important for the maintenance of the AEJ. Analyses in this study also focus on surface heat flux such as downward solar radiation, sensible heat flux, latent heat flux, and surface upward long-wave radiation.

Chapter 3

Results

The AEJ is a key feature of the central African wet season atmosphere which influences rainfall across the continent. Highest rainfall amounts occur over CA during the SON rainy season during which both the northern (AEJ-N) and southern (AEJ-S) components of the AEJ are active. Although both components of AEJ are prominent for rainfall variability over CA, few studies have attempted to understand the dynamics of the southern component possibly because early studies of the mid tropospheric circulation over southern Africa focused on months when the jet was not present.

The first part of thesis describes characteristics of the AEJ-S using reanalyses and points out the major role this Jet plays in rainfall development over CA in SON. The second part examines model representation of the September to November characteristics, such as location and intensity, of the AEJ north and south in a sample of 16 commonly evaluated CMIP5 and CMIP6 models and in two reanalyses (ERA5 and MERRA2). The analysis evolves to assess key drivers of the AEJ from energetic interactions, the characteristics of mid-level highs and thermal lows and the nature of surface thermal heating. By clarifying mechanisms that govern the AEJ-S, this research work contributes to insight into CA climate mechanisms and suggests a link between CA and Southern Africa climate systems. This research work also improves the foundation of new mechanisms that help to identify suitable metrics for the evaluation of Global models over the Central Africa region. This study strengthens our understanding of the mid-level circulation over Central Africa by detecting gaps in the mechanisms maintaining the AEJ in coupled models and highlights processes that should be improved in future ensembles.

3.1 African Easterly Jet South Dynamics

3.1.1 Foreword

The African Easterly Jet South (AEJ-S) is an important feature of the CAn mid tropospheric circulation and has been identified as a key contributor to convection over the region. During SON, a mid-tropospheric (600 hPa) maximum easterly wind occurs over Africa between 5°S-20°S where monthly easterly wind speed exceeds 6 $m.s^{-1}$ (Nicholson and Grist 2003; Adebiyi and Zuidema, 2016; Kuete et al., 2019). These studies also found that the AEJ-S is a thermal wind and is confined between two regions of differing convective characteristics. To the south of the jet, is the Kalahari heat low associated with strong, dry convection (Munday and Washington 2017; Howard and Washington, 2018), while to the north, is the humid Congo Basin associated with deep tropospheric moist convection dominated by Mesoscale Convective System (Jackson et al., 2009).

However, while this advanced understanding of the AEJ-S, it does not explain how the jet is maintained (e.g Thorncroft and Blackburn, 1999) which is an important gap in understanding the functioning of central and southern Africa climate systems. Meanwhile understanding of maintenance mechanisms of AEJ-N (Thorncroft and Blackburn 1999; Chen, 2004; Wu et al., 2009) has contributed to a fuller understanding of its dynamics and in turn those of the West African monsoon system (Cook, 2015). In light of this, an improved understanding of the mechanisms that maintain the AEJ-S therefore has the potential to unlock the understanding of jet dynamics, and, in turn, the climate system over both Central and Southern Africa.

It is well established that westerly waves play an important role in modulating the weather and climate over southern Africa, including the September to November season when the poleward temperature gradient in the southern African subtropics is enhanced by radiative heating over the landmass (evidenced by the development of the Angolan heat low) and the cold Southern Ocean which is slow to respond to Spring heating (Taljaard et al. (1961); Taljaard and Van Loon (1962))

Processions of westerly waves evident in a surface pressure spectral peak near 6 days (Preston-Whyte and Tyson (1973)), cross the subcontinent bringing cold tropospheric conditions and displacement and even removal of the heat low in the trough of the wave and warm conditions aided by adiabatic heating and strong development

of the heat low when the ridge of the wave overlies the subcontinent. Such wave activity therefore has the potential to modulate the strength of the AEJ-S given that the jet is a thermal wind driven by cross-latitude temperature gradients. Historically, the central and southern African climate systems have been treated as two independent systems. Data gaps over Angola and the southern Democratic Republic of Congo have arguably solidified the separation of the two regions such that there is scant evidence of interaction between them. One isolated example is the pattern of continental inter-decadal rainfall modulation identified by Nicholson (1986) where enhanced (decreased) rainfall over CA is accompanied by reduced (increased) rainfall over southern Africa. This section has two key aims:

1) To contribute to understanding the formation and maintenance mechanisms of the AEJ-S where the formation mechanism is defined as a process to which the jet owes its existence whereas the maintenance mechanism is that which contributes to the acceleration of the jet subsequent to formation. Maintenance mechanisms include mid-level highs and anticyclonic circulation over southern Africa.

2) To establish the role of westerly waves over southern Africa in modulating the AEJ-S intensity.

3.1.2 African Easterly Jet South and rainfall in Central Africa

The annual distribution of rainfall over CA is characterized by two maxima seasons (Nicholson et al., 2018) ; in MAM and SON. SON is the wetter of the two seasons and coincides with the strongest moisture inflow (Pokam et al., 2012). The SON season is also marked by strong convective activity over the region during which the AEJ-S has a significant contribution (Jackson et al., 2009). Before investigating the association between AEJ-S strength and rainfall distribution over CA, we first present composite analyses of strong and weak AEJ-S using ERA-Interim, NCEP-2 and MERRA-2 reanalyzes (Fig. 9).

For the strong composite, AEJ-S is about 2.5 $m.s^{-1}$ stronger in NCEP-2 and ERA-Interim than climatology while MERRA-2 is about 1.5 $m.s^{-1}$ stronger. The anomalous jet structure in the strong composites is more extensive in the case of NCEP-2, covering 5-14°S and through a depth of the atmosphere from 850 to 400 hPa whereas in ERA-Interim the strengthening is further equatorward between 2-9°S and confined to a more shallow layer above 700 hPa. MERRA-2 AEJ-S structure

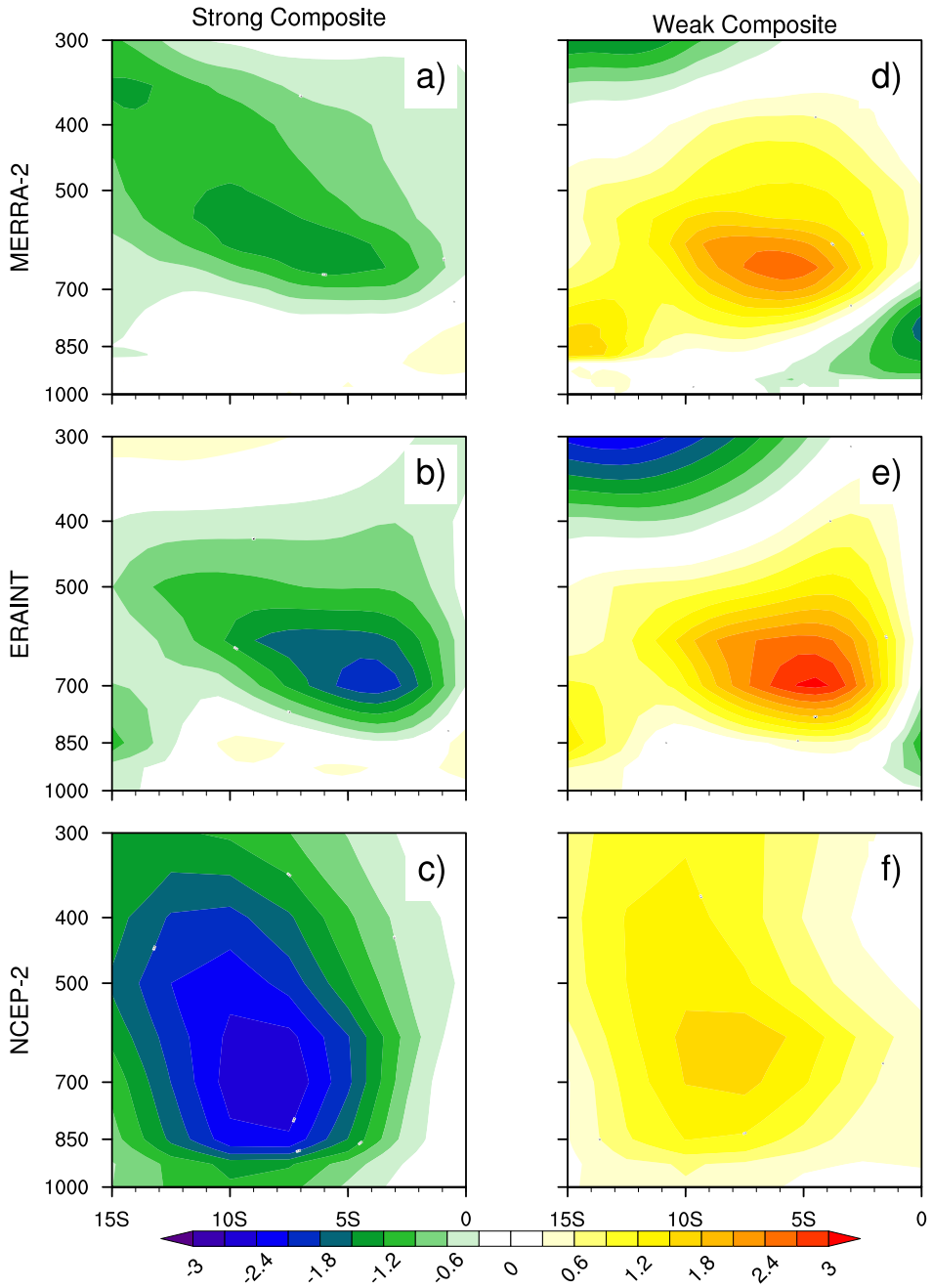

Figure 9: *Latitude/height cross-sections of African Easterly Jet South (U m.s^{-1}) composite anomalies for Bottom-Top NCEP-2, ERAINT, MERRA-2. Strong composite is the mean of strongest months minus climatology (left column) and weak composite is the mean of weakest months minus climatology (right column).*

is a blend of the other two reanalyses. During months of weak AEJ-S, NCEP-2 was about 2 m.s^{-1} weaker than climatology with the anomalous jet core at around 700 hPa. In MERRA-2 and ERA-Interim, the jet was about 3 m.s^{-1} weaker than climatology.

Composite anomalies of spatial rainfall distribution were calculated based on composites of strong and weak AEJ-S (Fig.10). Figure 10 shows that rainfall over southern CA from 5°N extending to southern Africa (20°S) and AEJ-S strength are in phase opposition. During months of strong AEJ-S, less rainfall occurs. Strong AEJ-

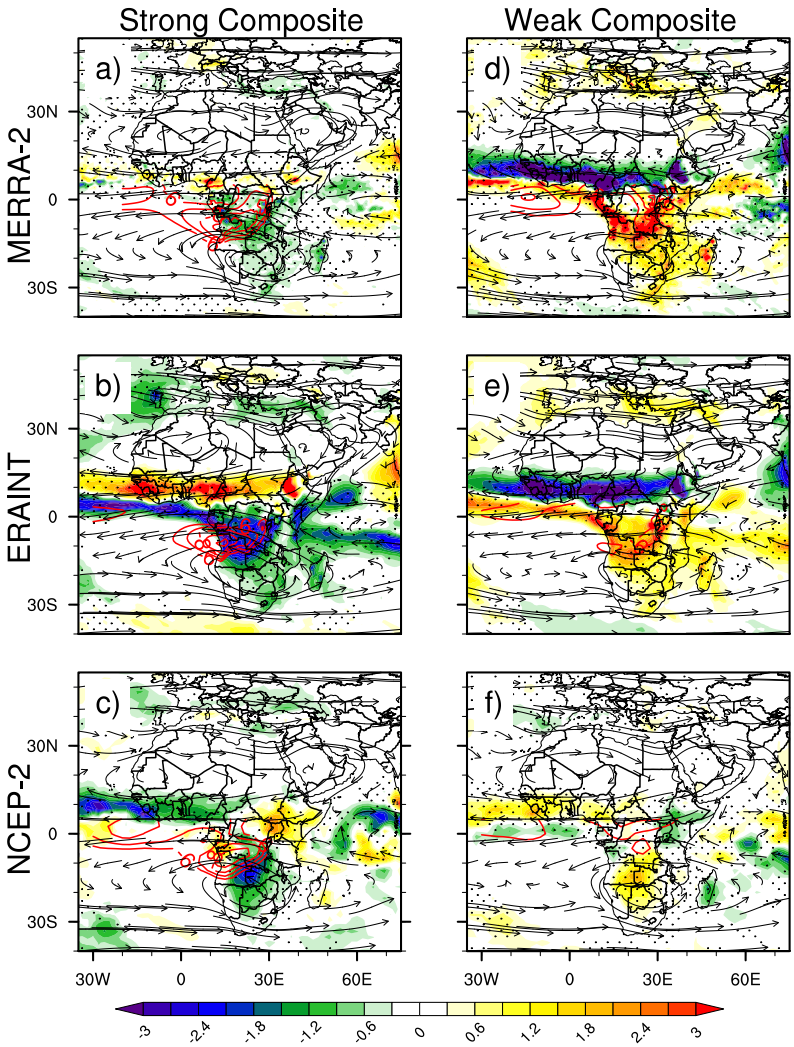

Figure 10: *Long term mean SON rainfall (mm day^{-1}) composite anomalies. Strong composite (a, b and c) and weak composite (d, e, f). Red solid lines for each plot represent zonal wind intensity at 600 hPa for the respectively composites. Stipples represent area where rainfall anomalies are significant at 0.05 level and vectors represent total wind at 600hPa.*

S in ERA-Interim is associated with less than 3 mm/day compared to climatology (Fig. 10b). MERRA-2 rainfall anomaly values are lower at less than 2 mm/day compared to climatology (Fig.10a). The rainfall pattern is reversed during months of weak AEJ-S (when more rainfall occurs from central to southern CA). In ERA-Interim (Fig.10e) values are more than 3 mm/day compared to climatology and 2 mm/day more than climatology in MERRA-2 (Fig.10d). NCEP-2 does not feature a clear phase opposition between rainfall anomalies and AEJ-S strength. In contrast, the spatial pattern of rainfall anomalies is more complex with positive rainfall anomalies over southern Africa and west Africa while negative anomalies are in evidence over East Africa and the western part of the Congo Basin.

Following recent progress in understanding the dynamics of the region (Pokam et al., 2012) Pokam et al. (2012); Washington et al. (2013); Creese and Washington

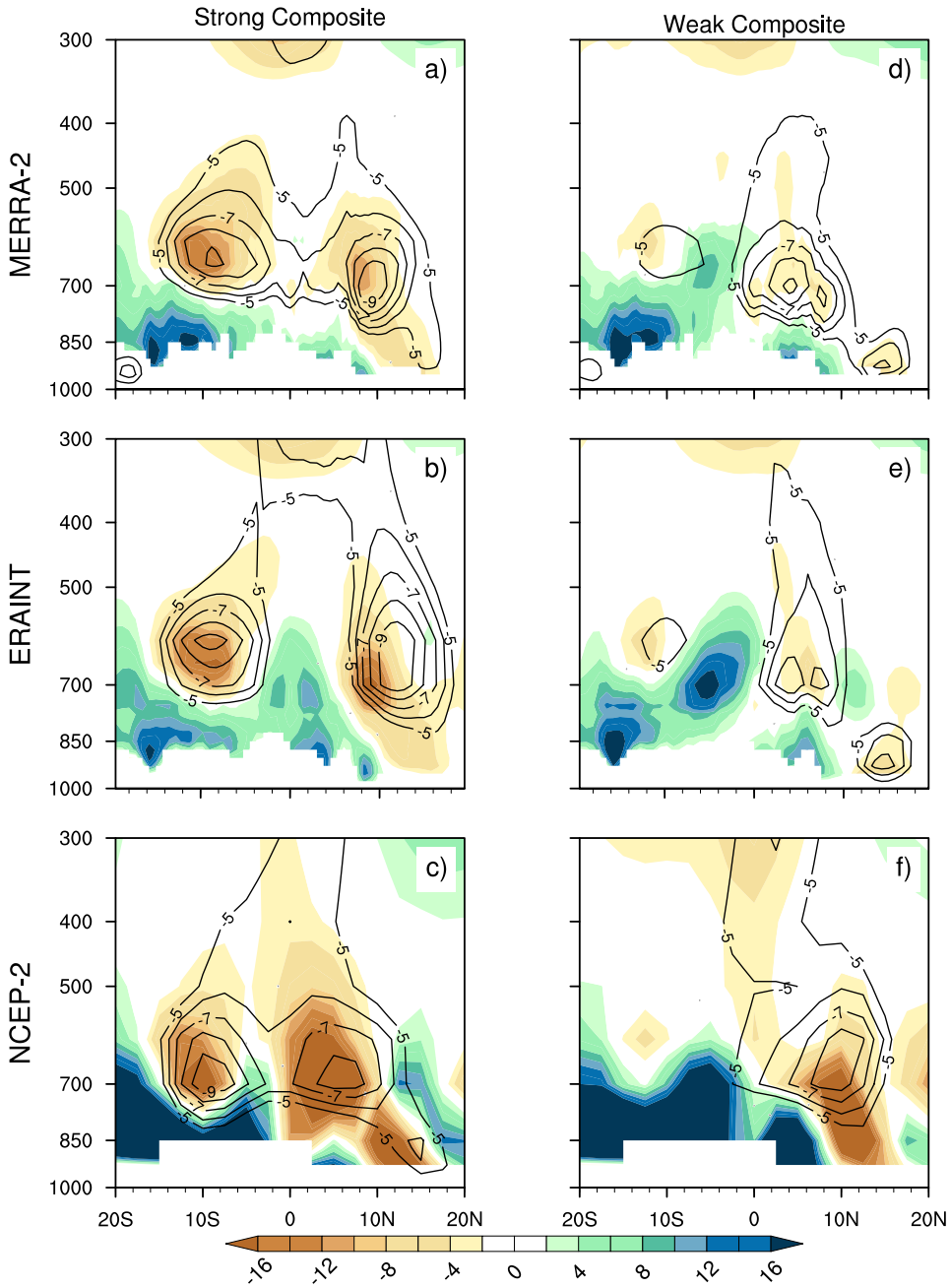

Figure 11: *Latitude/height cross-sections of net zonal moisture flux ($Kg.m^{-1}.s^{-1}$) calculated from West boundary ($10°E$) minus East boundary ($30°E$) for strong (a, b and c) and weak (d, e and f) AEJ-S months. Black solid lines represent AEJ components ($U\ m.s^{-1}$) calculated at $10°E$ for the respectively composites.*

(2016) we examine moisture flux transport over the region extending from 5°N to 20°S. Figure 11 shows net zonal moisture transport, computed as the difference between moisture flux across the western (10°E) and the eastern (30°E) boundary of CA over which the AEJ-S occurs. Positive values indicate moisture flux convergence, negative values moisture flux divergence. During months of strong AEJ-S, strong zonal moisture flux divergence is found at 10°S around 600 hPa in all reanalyzes (Fig. 11a, b, c). This peak of moisture divergence is due to intensification of AEJ-S (Fig.9a, b, c), favoring dry conditions mainly over southern Central Africa (Fig.10a, b).

During months of weak AEJ-S, mid-level zonal moisture divergence induced by the jet decreases substantially (Fig.11d, e, f) contributing to enhanced mid tropospheric moisture convergence between 10°S and the equator over Central Africa, leading to wet conditions over the region (Fig. 10d, e, f). There is a good agreement across reanalyzes (ERA-Interim and MERRA-2) on changes in the strength of AEJ-S and precipitation responses over CA. Our results clearly demonstrate that strong (weak) AEJ-S leads to reduced (enhanced) water vapour convergence at mid-levels over Central Africa leading dry (wet) conditions south of the region.

3.1.3 Control and maintenance mechanisms of African Easterly Jet South

To investigate drivers of AEJ-S, we focus on the formation and maintenance mechanisms. It has been shown that AEJ-S results from thermal contrast between hot and dry subtropical Namib-Kalahari region that is associated with dry convection, and sub-humid region of Congo Basin.

Figure 12 presents AEJ components locations and the 925 hPa meridional temperature gradient for ERA5, ERAINT, MERRA-2 and NCEP-2. AEJ-N (black solid line in the northern hemisphere) is present all year round, whereas AEJ-S (red solid line in the southern hemisphere) is discernible only during SON. AEJ-S is a thermal wind, located slightly equatorward of the lower tropospheric meridional temperature gradient and results from the negative meridional surface temperature gradient. After the AEJ-S is set up, other mechanisms may contribute to its acceleration. We asses these mechanisms based on Chen, (2004) who argued that two main features contribute to AEJ-N acceleration, namely the mid tropospheric meridional divergent circulation and mid tropospheric high located in the vicinity of the jet.

Figure 13 presents August to November meridional-height section of the conversion of divergent kinetic energy into rotational kinetic energy. Chen, (2004) identified a North African divergence center over Chad-Sudan and states that this divergence over West Africa is dominated by v_D because $u_D \ll v_D$ and $v_R \ll u_R$ therefore C is approximated to fu_Rv_D. This divergence center, and the associated strong northerly meridional divergent wind which peaks at 700 hPa and accelerates towards the core of AEJ-N, is well depicted during August (Fig.13a, e, i) and September (Fig. 13b, f, j). Acceleration is accompanied by strong divergent kinetic energy. At the core of

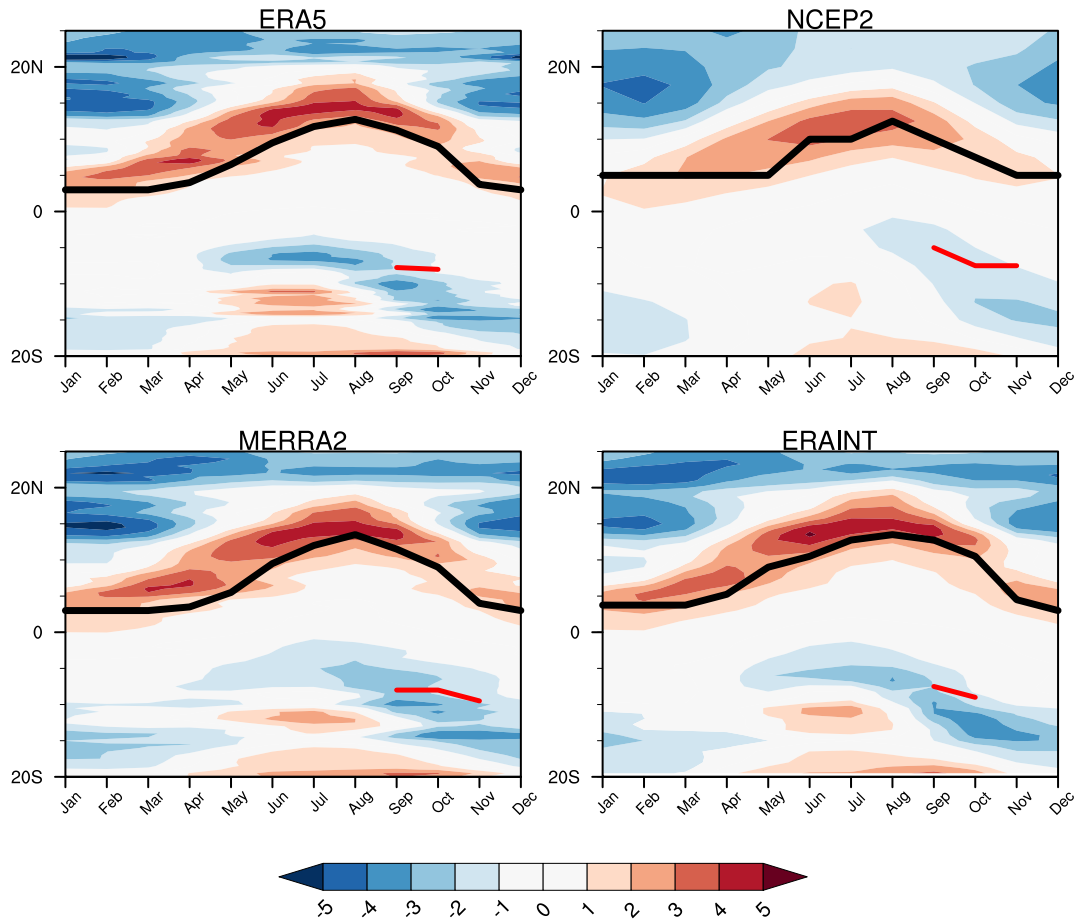

Figure 12: *Latitude/time evolution of the 925 hPa surface temperature gradient (shading) with overlay mean locations of AEJ components core. Black solid line in the north represents AEJ-N and red solid line in the south is the AEJ-S. All variables are averaged between 12-24° E.*

the jet, the meridional divergent circulation under the effect of Coriolis acceleration is deflected westward leading to strong conversion of divergent kinetic energy into rotational kinetic energy, with a peak around 10°N at 700hPa from August to October (Fig. 13). This contributes to the acceleration of the AEJ-N. A recent study (Howard and Washington (2018)) has investigated heat lows dynamic over southern Africa. This study shows that dry convection is evident over the Angola region from September to November and is linked to a peak in mid-level divergence with a core from September to November. Both u_D and v_D contribute to this southern divergent center with $u_D > v_D$. With addition to strong development of u_R over the AEJ-S core ($u_R \gg v_R$), this leads to weak values of C over the AEJ-S core (Fig. 13). The consequence is the very weak contribution of energetic conversion to the strength of AEJ-S during these months in the reanalyses. This mechanism is around five times stronger for AEJ-N in MERRA-2 and ten times in NCEP-2 and ERAINT compared to AEJ-S (Fig. 13e, f, g, j). The divergent circulation which is deflected by the

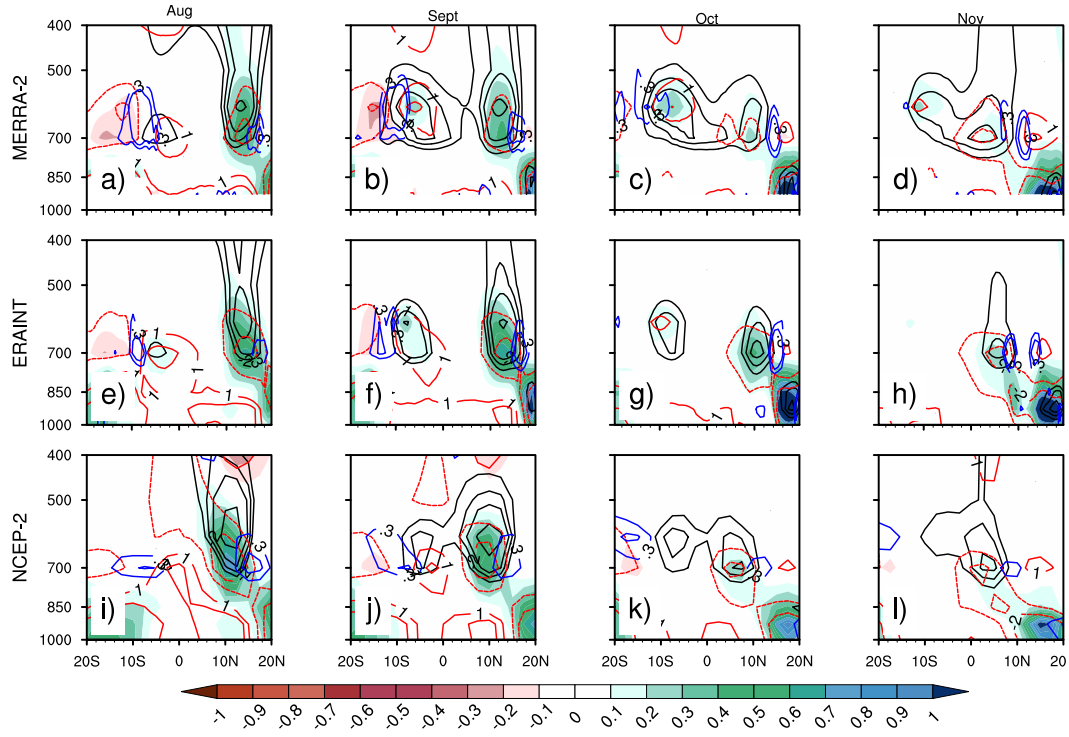

Figure 13: *Latitude/height cross-sections of conversion of divergent kinetic energy into rotational energy (shading in $m^{-2}.s^{-3}$). With overlay AEJ components (black contours in $m.s^{-1}$). Also represented is the meridional component of divergent wind v_D (red contours in $m.s^{-1}$) and total divergence (blue contour in s^{-1}).*

Coriolis acceleration is therefore not well developed over southern Africa compared with the AEJ-N.

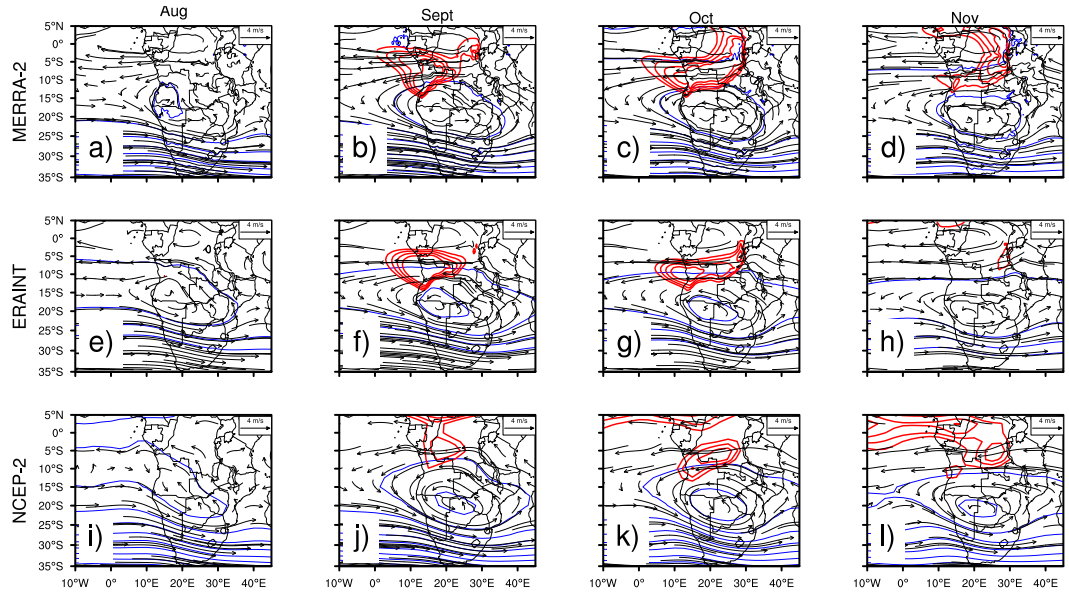

Figure 14: *August to November geopotential heights (blues solid contours) and AEJ-S (red contours) with overlay geostrophic circulation (vectors). All variables are represented at 600 hPa. Geopotential height field is given in meter with an interval of 20 meters.*

The other maintenance process related to the strength of AEJ-S investigated in this work is a mid-level high over Kalahari. Figure 14 shows the August to November,

geopotential height (blue contour) with geostrophic circulation (vectors) and AEJ-S core (red contours). The height field is weak in August (Fig.14a, e, i) showing establishment of mid-level high. It becomes very strong in September (Fig.14 b, f, j) and October (Fig. 6 c, g, k), and weakens in November (Fig.14 d, h, l). Our results provide evidence of the role played by the 600 hPa high in maintaining the strength of AEJ-S. This is depicted in Figure 14 between the latitudes 10°S to 15°S marking the position of AEJ-S (red contours) during September to November. Figure 14 also shows that AEJ-S is dominated by rotational circulation (anticyclonic circulation at the core of the high). The mid-level high maintains the AEJ-S located at the northern flank of the high through anticyclonic circulation that forms at the core of the high. This mechanism is well observed in all reanalyses. Because of the role played by this high pressure system in maintaining to the strength of the AEJ-S, further analysis aimed at understanding how this high develops is required. This is covered next.

From September to November, the mid-level high is located roughly between 15-20°S and 15-25°E (Figure 14) aloft the Angola heat low (Munday and Washington (2017)) suggesting a connection between this heat low and the mid tropospheric high. The dynamics associated with the formation of this mid-level high is presented in Figure 15 which shows the vertical structure of vertical velocity (brown line), divergence circulation calculated using total wind component (green line), total vorticity (blue line) and diabatic heating (red line). The mid-level high over the Kalahari is established in response to local convection from September-November. During these months, the Kalahari heat low is characterized with strong, dry convection associated with surface heating (Adebiyi and Zuidema, (2016); Munday and Washington, (2017); Howard and Washington, (2018)). Surface heating enhances uplift to 600hPa. At upper tropospheric levels, due to evaporative cooling, there is a predominance of subsidence. Updrafts are then blocked by upper level subsidence, leading to a formation of a mid-level high pressure system associated with strong divergence and vorticity. Amplification of vorticity and rotational circulation during September to November is due to the stretching of vortex circulation at mid-tropospheric divergence center and ascent associated with strong sensible heating in the lower troposphere. The Mid-level high induces an anticyclonic circulation at the core of the high represented by positive values of vorticity. We argue, therefore, that

the mechanism controlling this mid-level high pressure system is associated with the dynamics of the heat low described in Howard and Washington (2018). These results put in evidence the link between dynamic of heat low and that of AEJ-S.

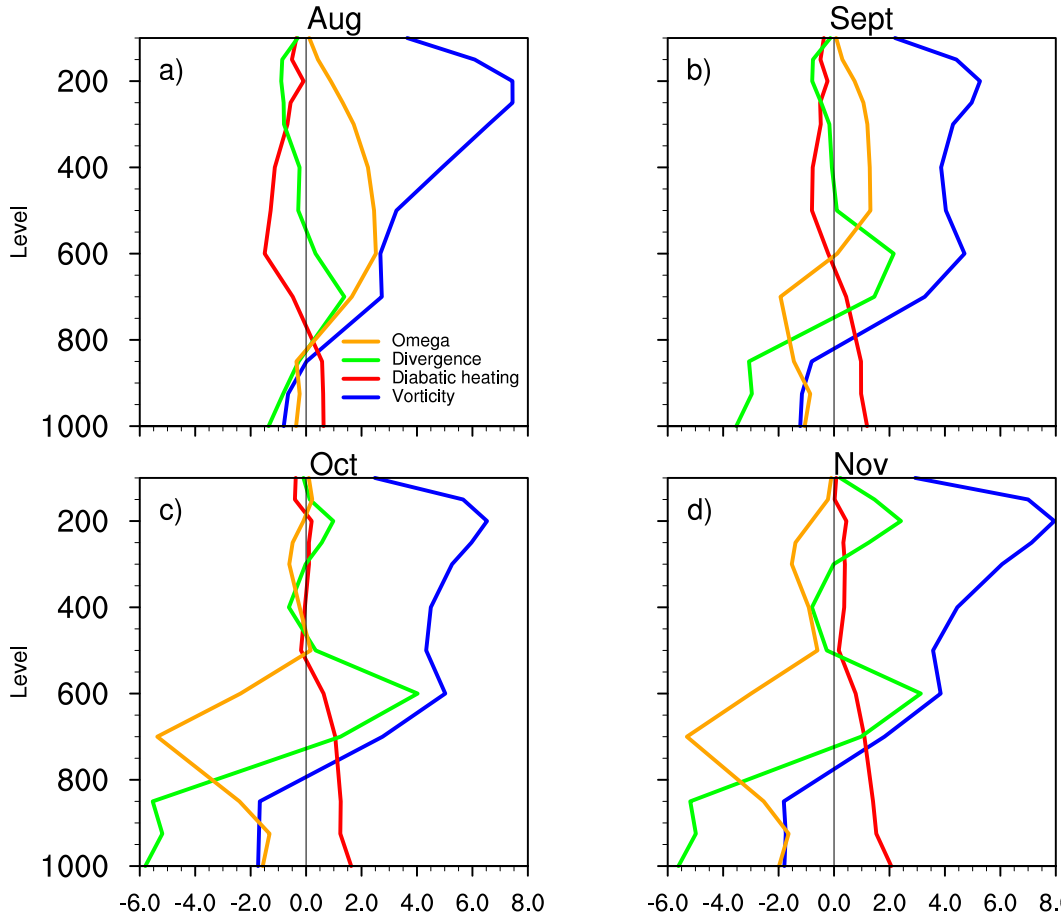

Figure 15: *NCEP-2 Vertical profiles of diabatic heating (red line), vorticity (blue line), divergence (green line) and vertical velocity (brown line) for August to November. All variables are averaged between* $18°S$-$22°S$ *latitude and* $20°E$-$25°E$ *longitude.*

3.2 African Easterly Jet South and Southern subtropical waves

3.2.1 Seasonnal and Interannual Variability

Over southern Africa, subtropical waves may have an impact on cross latitudinal temperature gradient from subtropical regions to equatorial regions; this may act to modify heat low conditions and therefore the AEJ-S strength since the jet is driven by the cross-latitude temperature gradient. It is therefore important to investigate the link between AEJ-S and southern subtropical waves.

Heating over the interior of southern Africa in the Boreal Spring is partly con-

trolled by westerly waves which are responsible for temperature advection such that the ridge system of the waves produces positive temperature anomalies whereas the troughs induce cold air advection. To examine links between the AEJ-S and southern subtropical waves, we evaluate anomalies of geopotential height vertical velocity and temperature using reanalyse data from ERA-Interim, NCEP-2 and MERRA-2 during months of strong and weak AEJ-S. Geopotential height is valuable for locating wave ridges and troughs and wave structure, temperature is used to show how the waves have the potential to modulate the heat low while vertical velocity controls adiabatic heating and cloudiness (Fig.16). Anomalies of these parameters were calculated only during those months when AEJ-S and heat low are strong (September to November).

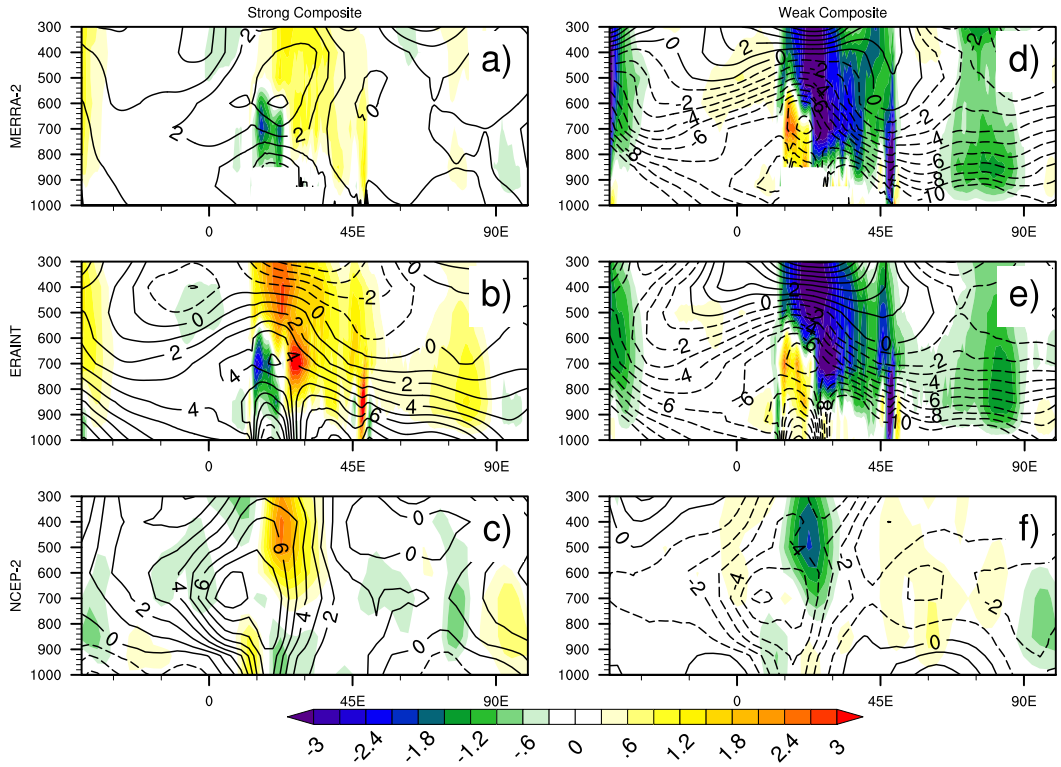

Figure 16: *Longitude-height section of geopotential height (black contours in m) and vertical velocity (shading in $Pa.s^{-1}$) composites anomalies for strong (a, b, c) and weak (d, e, f) AEJ-S months. Variables are averaged in the latitude range of* $12°S$ *to* $20°S$.

Figure 16 present the longitude-height section anomalies of geopotential height and vertical velocity averaged over the latitudinal band 12°S to 20°S. Results show clear differences in terms of opposite anomalies over the heat low region for the strong and weak AEJ-S composites. During months of strong AEJ-S, geopotential height values were higher than climatology (Fig.16 a, b and c) associated with the ridge of a westerly wave with core at mid level between 700 hPa and 500 hPa. But

during months of weak AEJ-S, geopotential height values were lower than climatology leading to negative anomalies associated with an anomalous wave trough (Fig.16 d, e and f). The increase of geopotential height during months of strong AEJ-S in MERRA-2 and NCEP-2 is observed in the entire troposphere from surface (1000 hPa) to 300 hPa, compared to ERA-Interim where positive wave structure is only from surface to 500 hPa. Decrease of geopotential height during months of weak AEJ-S in NCEP-2 is also observed in the entire troposphere while MERRA-2 and ERAINT present same characteristic only between surface and 500 hPa. The wave structure is found in all reanalysis data but is stronger in NCEP-2 (the reanalysis with the largest Jet strength anomalies – see Fig. 1) compared to MERRA-2 and ERA-Interim.

Following this mechanism, efforts were made to understand how troughs and ridges located in the geopotential height fields act to develop or suppress the heat low through vertical velocity. Figure 17 shows 850 hPa temperature anomalies during months of strong and weak AEJ-S. When the warm part or the ridge of the wave overlies southern Africa, it acts to develop the heat low through an increase of surface temperature (Fig.17 a, b, c), radiative heating (not shown) and adiabatic warming associated with subsidence (not shown) consistent with wave theory (Fovell et al. (1992)) leading to a strong cross latitude temperature gradient through equatorial regions and strong AEJ-S, strong AEJ-S, that in turn lead to mid level moisture divergence (Fig. 11a, b and c) favoring dry conditions and therefore less rainfall over southern CA and southern Africa (Figure 10).

But when the cold part of the wave or the trough of wave overlies southern Africa, it suppresses the heat low through a decrease of surface temperature (Figure 9 d, e, f), and also weakens cross latitude temperature gradient through to equatorial regions and therefore is associated to a weak AEJ-S that in turn contributes to enhanced mid level moisture convergence (Fig 11d, e, f), leading to wet conditions and more rainfall over southern CA and south Africa (Figure 10). This mechanism is well observed in all three reanalyses used in this study. Cut Off Lows (COLs) in the southern African region (Taljaard (1985); Favre et al. (2013)) which lead to a cold pool of air extending throughout the troposphere, are baroclinic systems which are an extreme form of the westerly wave pattern. Instead of the trough associated with a westerly wave, a closed, cold pool occurs near the trough axis.

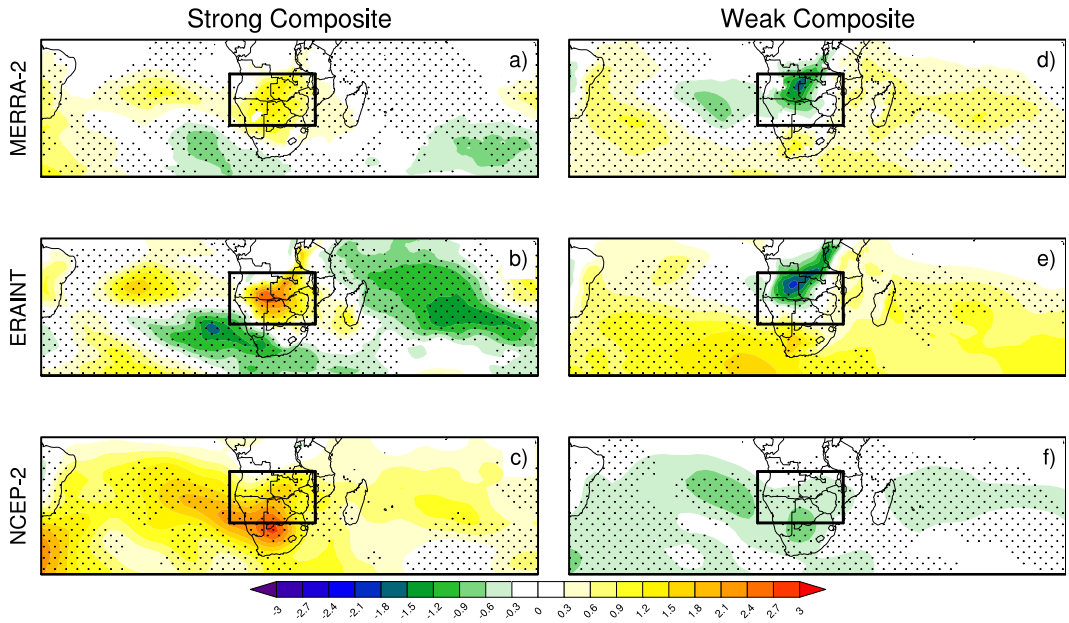

Figure 17: *Composites anomalies of the 850hPa temparature for strong (a, b, c) and weak (d, e, f) AEJ-S months.*

3.2.2 Intraseasonnal Variability

This section aims to describe the meteorological characteristics directly associated with the westerly waves such as wave signature and periodicity. We focus on the daily characteristics of meteorological variables such as geopotential height to describe the wave's existence. The key meteorological impact of the waves on the heat-low and the AEJ-S at daily time-scales will also be presented.

3.2.2.1 Empirical Orthogonal Function Analysis: Wave structure

Analysis of the percentage variance of eigenvalues against the first 10 EOFs factors indicates a Scree term at position 4, showing the possible significance of the first 04 factors. To show wave structure and signal, we highlight the EOF analysis of the first 04 modes of variability of the deseasonalized seasonal anomalies of the 300 Mb geopotential height (Figure 18). The EOF 1 which has the highest percentage of variance (31.9) shows a quasi-stationary signal in the sub-tropical and equatorial region, which may be more associated with the climatology of the pressure field. There is a slight variability in the pressure field in the extra-tropical latitudes of Southern Africa, which may explain the existence of a wave signal in this part, although it is quite weak. The analysis of EOF 2, 3 and 4 with percentage variability of 5.4, 4.8 and 3.8 respectively, shows positive and negative anomalies of the deseasonalized geopotential height in the extra-tropical latitudes. This suggests the possible exis-

tence of a longitudinal wave signal. The low percentage variability of these EOFs could be due to the fact that the passage of the wave over the tropical latitudes of South Africa has a low periodicity. Moreover, as shown in EOF 2, 3 and 4, the structures are coherent and show a large wave signal. This allows us to retain only EOF 2, 3 and 4.

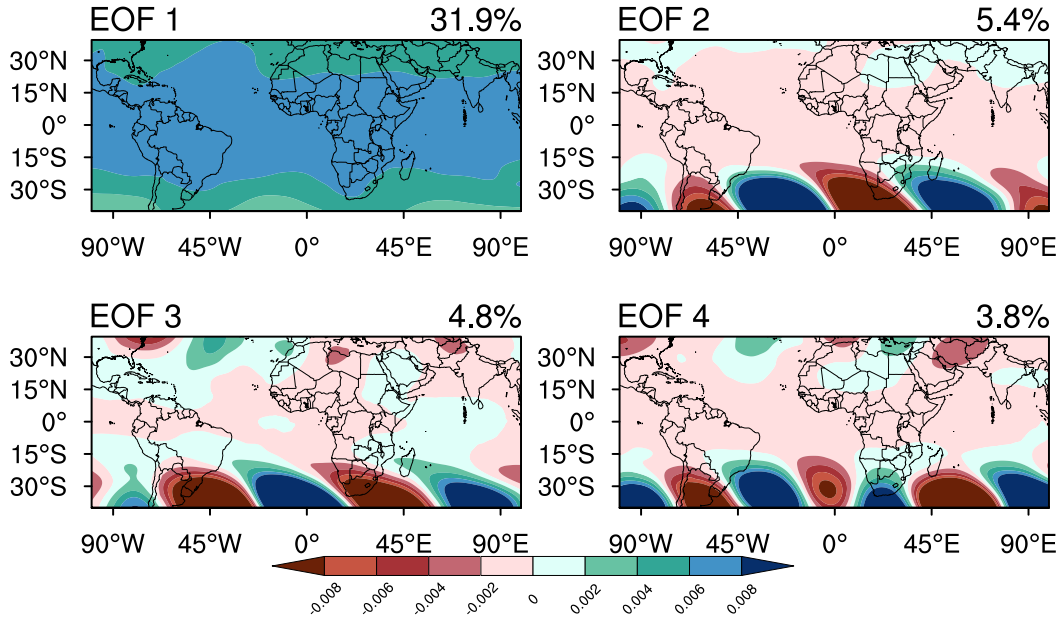

Figure 18: *Spatial patterns of the principal components of the four main modes of the geopotential height at 300 Mb representing the wave signal. The values are calculated from deseasonalised daily data.*

In order to fully describe the different modes of variability and to know which are the most significant and which best represent the wave signal, we have analysed in Figure 19 the offset correlations between the principal components associated with the EOF modes. The PC2 and PC3 appear in phase quadrature, suggesting the probable presence of propagative signals in the extra-tropical region of the Southern Hemisphere. Thus, only EOF 2 and 3 are more significant and will be retained. To better identify and detect the ranges of intraseasonal variability in the wave activity in the selected EOF2 and EOF3, we calculated the variance of the initial field reconstructed from the EOF 2,3 and PC 2,3 in Figure 20. An area of maximum variability can be observed in the South Atlantic since the wave is longitudinal and progressive, so we can say that the wave during one period of the year can originate in this well-defined area (30°S-40°S/10°W-30°W).

It is necessary to construct a regional index of reference in the zone of maximum variability for the analysis of the main intraseasonal variability modes of the wave. To do this, we standardised the deseasonalised anomalies of the geopotential height

field in this box, and we set the anomaly indices greater than 1 as the dates of strong variability and the anomaly indices less than -1 as the dates of weak variability in the box.

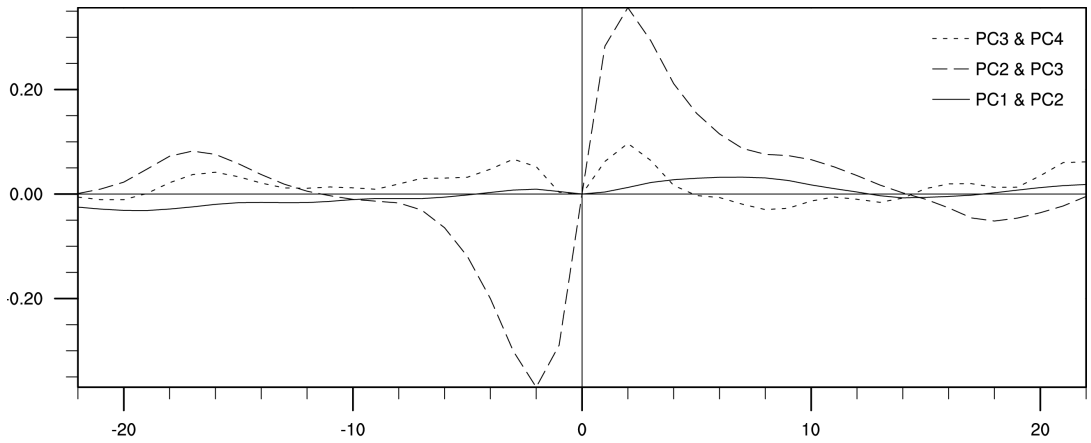

Figure 19: *Cross correlation between principal components associated with EOF modes.*

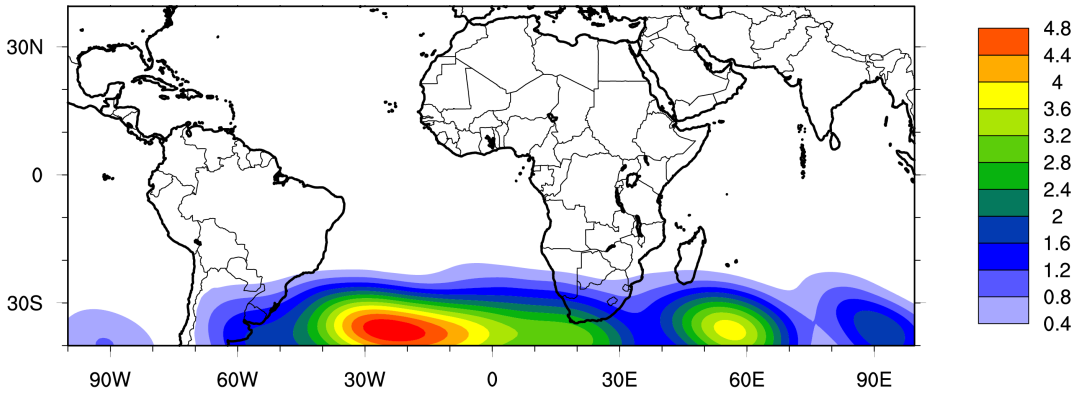

Figure 20: *Variance field of the reconstruction by the second and third principal components.*

These strong and weak temporal indices, which are referred to in the following as strong dates at T0 and weak dates at T0, are constructed during the months of September to October. To better represent the structure and signal of the wave in order to determine its periodicity, we represent the seasonally adjusted anomalies of the geopotential heights between the strong and weak dates from T0 - 10 days to T0 + 10 days. Figure 21 shows the wave signal from T0 - 10 days to T0 + 10 days in the 02-day steps. In the left-hand panel representing the strong date variations, a signal can be seen to originate over the South-West Atlantic Ocean (sky-blue negative peak called the wave trough or negative phase) at T0 -10 and propagate eastwards to reach the west coast of the South African extra-tropical landmass at T0. Similarly, at T0 - 10 days, on the South African coast, a wave ridge (dark red peak representing the

positive phase) propagates eastwards across the extra-tropical region of South Africa to reach the Kalahari thermal heat low region marked by the black dot at T0 before retreating completely. This shows for the strong dates from T0 - 10 days to T0 how a phase of the wave originates and propagates eastward crossing the continent. Similarly, for the right panel, we show the wave signal during the weak dates from T0 - 10 to T0 + 10 days. A strong propagation of the wave signal towards the East with phases opposite to those obtained for the strong dates is well observed. The propagation of the wave peak at T0 - 10 days towards the East reaches the South African coast at T0, replacing the negative phase or wave trough that progressively retreated towards the thermal low region at T0.

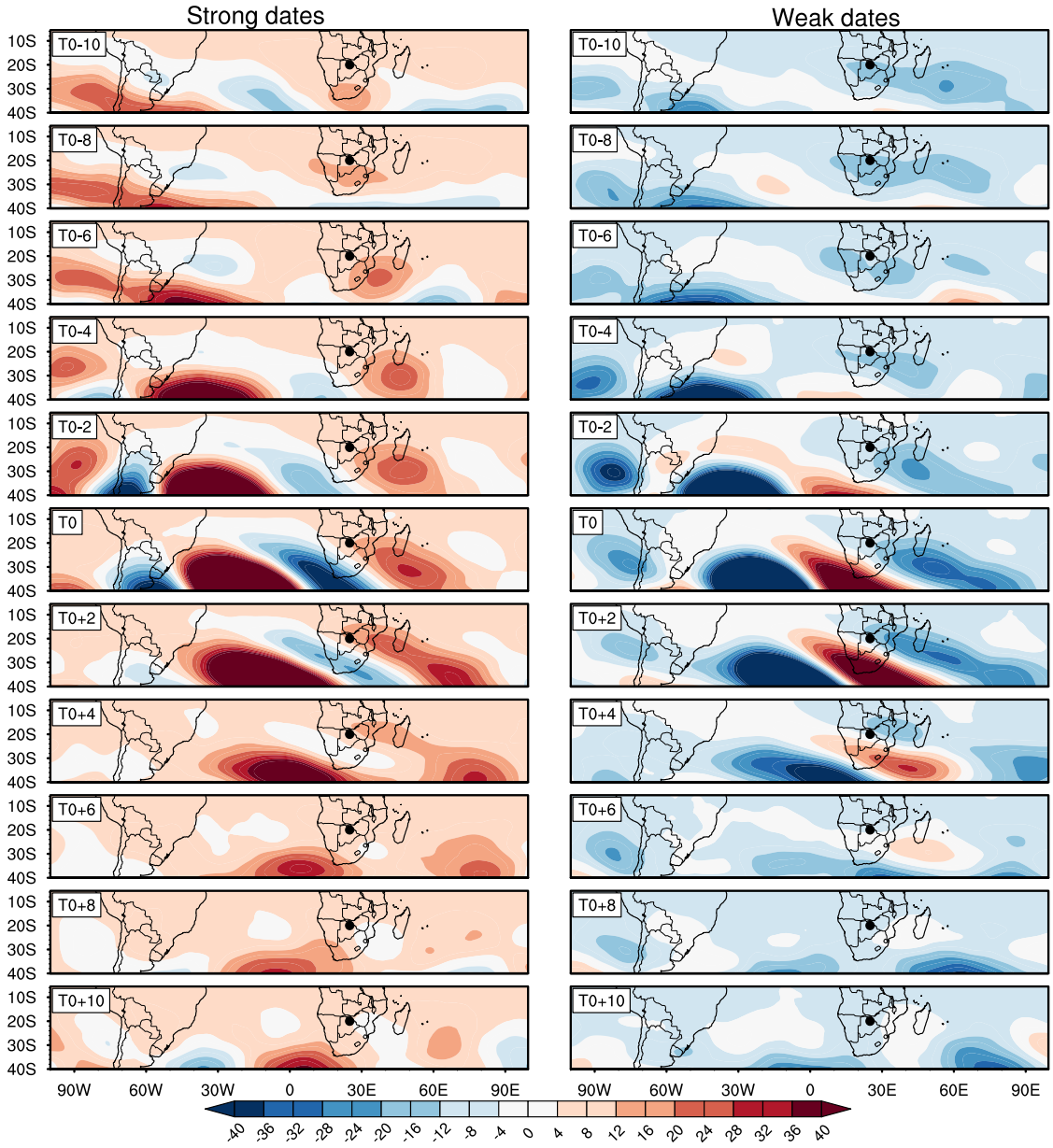

Figure 21: *Composite of the deseasonalised geopotential height anomalies at 300 Mb representing wave signal during strong and weak dates from T0 - 10 days to T0 + 10 days in 02-days steps.*

Wave activity is most important during dates T0 when it crosses the subcontinent. The phases of the wave are opposite and stronger during these dates. Thus, during strong dates, the positive phase or wave ridge is located over the heat low region, while the western coast of the continent is covered by the negative phase of the wave, the 02 forming an East-West dipole in the wave signal during these dates over the continent. Similarly, during weak dates, the heat low region is covered by the negative phase of the wave or wave trough and the western coast of the continent is crossed by the positive phase or wave ridge, creating also an east-west dipole over the continent. After T0, we observe an intensification of the wave signal at T0 + 2 days and at T0 + 04 days, the wave signal decreases to disappear completely at T0 + 06 days. This leads us to conclude that a phase of the wave takes about 10 days to settle on the continent and that after its settlement, its passage on the continent takes about 06 days. This result defines the main structure and periodicity of the wave. The activity of the wave in one phase or another that takes about 06 days after its installation at dates T0 is supported by the results of (Preston-Whyte and Tyson 1973).

3.2.2.2 Wave impact on surface thermal heating and mid-level circulation

To determine the impact of the wave signal and its periodicity on the surface thermal low and the mid-level circulation, we represent the deseasonalised potential temperature anomalies at 850 hPa in Figure 22 between the strong dates from T0-10 and T0+10 days to determine the behaviour of the thermal low during the passage of the wave, and the seasonally adjusted zonal wind anomalies at 600 hPa in Figure 23 to see how the circulation associated with the Botswana and AEJ-S systems behaves during the passage of the wave. Kuete et al. (2019) showed that the passage of the westerlies aloft over land leads to a semi-direct effect of the westerlies on the mid-troposphere circulation, especially over the AEJ-S. Depending on the phase of the wave, this changes the state of the atmosphere and consequently the surface heating. A westerly wave sequence as it crosses the subcontinent brings cold tropospheric conditions and the displacement or elimination of the thermal low in the trough of the wave, while warm conditions favoured by adiabatic heating and strong development of the thermal low are observed as the wave crosses the subcontinent.

We observe in Figure 22, over the continent at T0 -10 days, positive potential

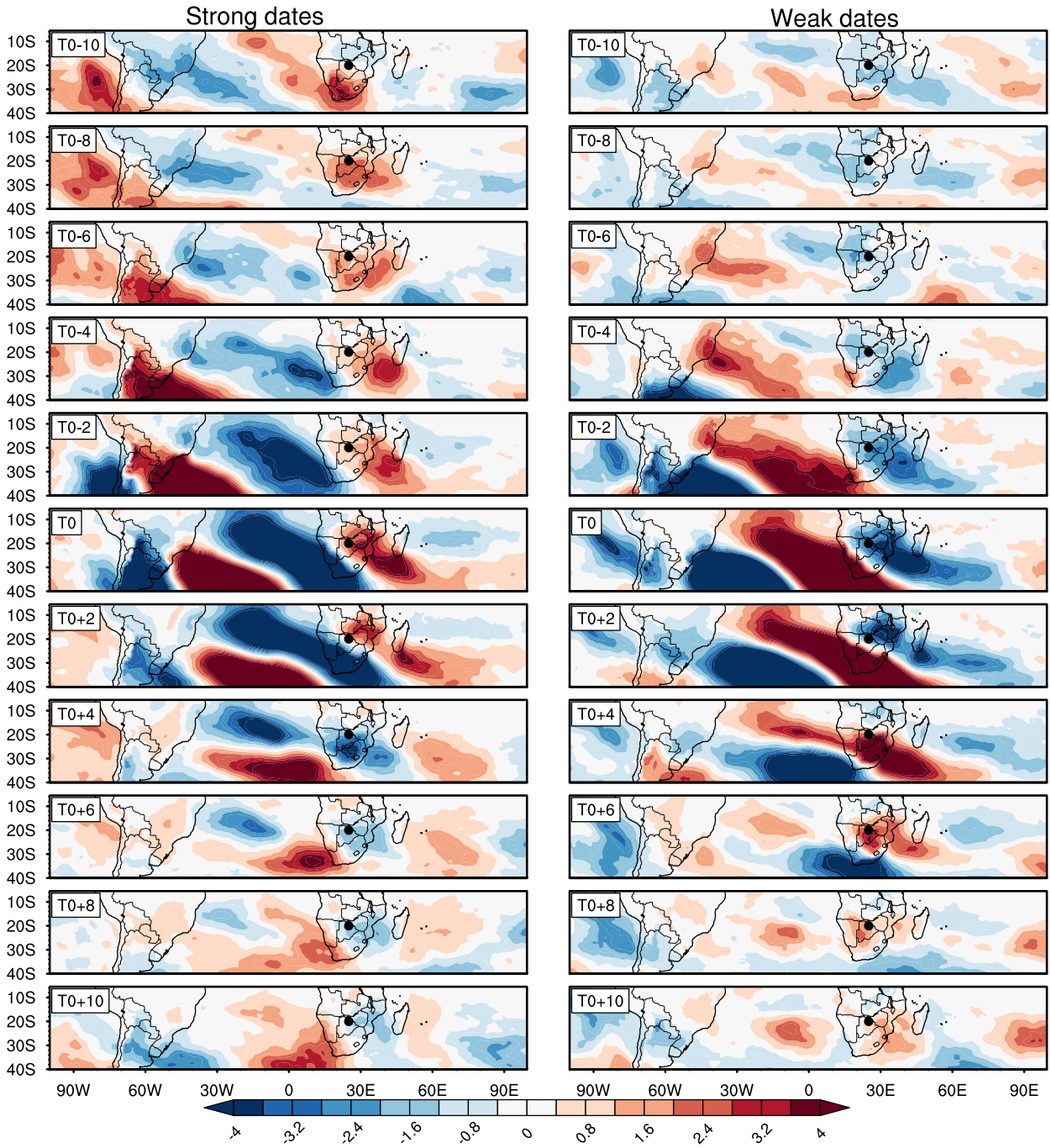

Figure 22: *Composite of the deseasonalised potential temperature anomalies at 850 Mb representing the heat low during strong and weak dates from T0 - 10 days to T0 + 10 days in 02-days steps.*

temperature anomalies for strong dates, and negative anomalies for weak dates, marking warming and cooling respectively. In the western Atlantic Ocean, between 30°W-45°W in tropical latitudes, a negative temperature peak is observed on strong dates. This peak strengthens at T0 -8 days and propagates towards the continent to reach the western coast of the continent at T0, replacing the strong heat low over the continent that gradually recedes and strengthens in the Kalahari region at T0. Contrarily, for the weak dates between T0 -10 days and T0, there is an eastward progression of warming over the Ocean that reaches the western coast of

the continent at T0, and the retreat of the negative temperature anomalies across the Kalahari Thermal heat low region at T0.

After T0, the strengthening of the heat low is maintained at T0 + 2 days and decreases considerably or even disappears at T0 + 6 days. It is replaced by cooling associated with the negative temperature anomalies until T0 + 10 days. Similarly, after T0, for the weak dates, we observe a displacement retreat of the negative temperature anomalies between dates T0 + 2 days and T0 + 4 days which disappears completely at T0 + 6 days and is replaced by the positive temperature anomalies. This is directly associated with the behaviour in the wave signal, as the wave ridge marked by positive geopotential height anomalies favours clear sky, surface heating and an intensification of the heat low, whereas the wave trough associated with negative geopotential height anomalies favours cooling of the atmosphere, leading to the weakening or retreat of the thermal heat low. The characteristic associated with the periodicity of the wave, which is about 6 days, is also associated with the behaviour in the thermal heat low so that when the signal of the wave disappears, its impact on the thermal low is no longer visible.

Figure 23 shows the zonal wind anomalies at 600 hPa between the strong and weak dates. It is important to note that between September and November, the mid-level circulation is dominated by zonal easterly winds. At T0, during the strong dates, there is a weakening of the zonal easterly wind, marked by positive values of the anomalies, due to the cooling in this area associated with wave trough. While over the Kalahari region, where there is a wave ridge and strengthening of the heat, there is a slight increase in the easterly wind, which intensifies between T0 +2 days and T0 +4 days, and decreases or disappears at T0 +06 days. The strengthening of the zonal circulation during this period is associated with an intensification of the AEJ-S, due to an increase of the thermal heat that favoured the surface meridional gradient in temperature. In contrast to the weak dates, there is a decrease in the zonal circulation, associated with the decrease in the intensity of the AEJ-S, due to the weakening or retreat of the thermal heat low during this period. The periodicity of the wave of about 06 days during its passage over the sub-continent is well associated with the behaviour of the thermal low and the mid-level circulation. This shows the importance of the AEJ-S in the intraseasonal variability of precipitation through its modulation by the wave activity and the thermal heat low.

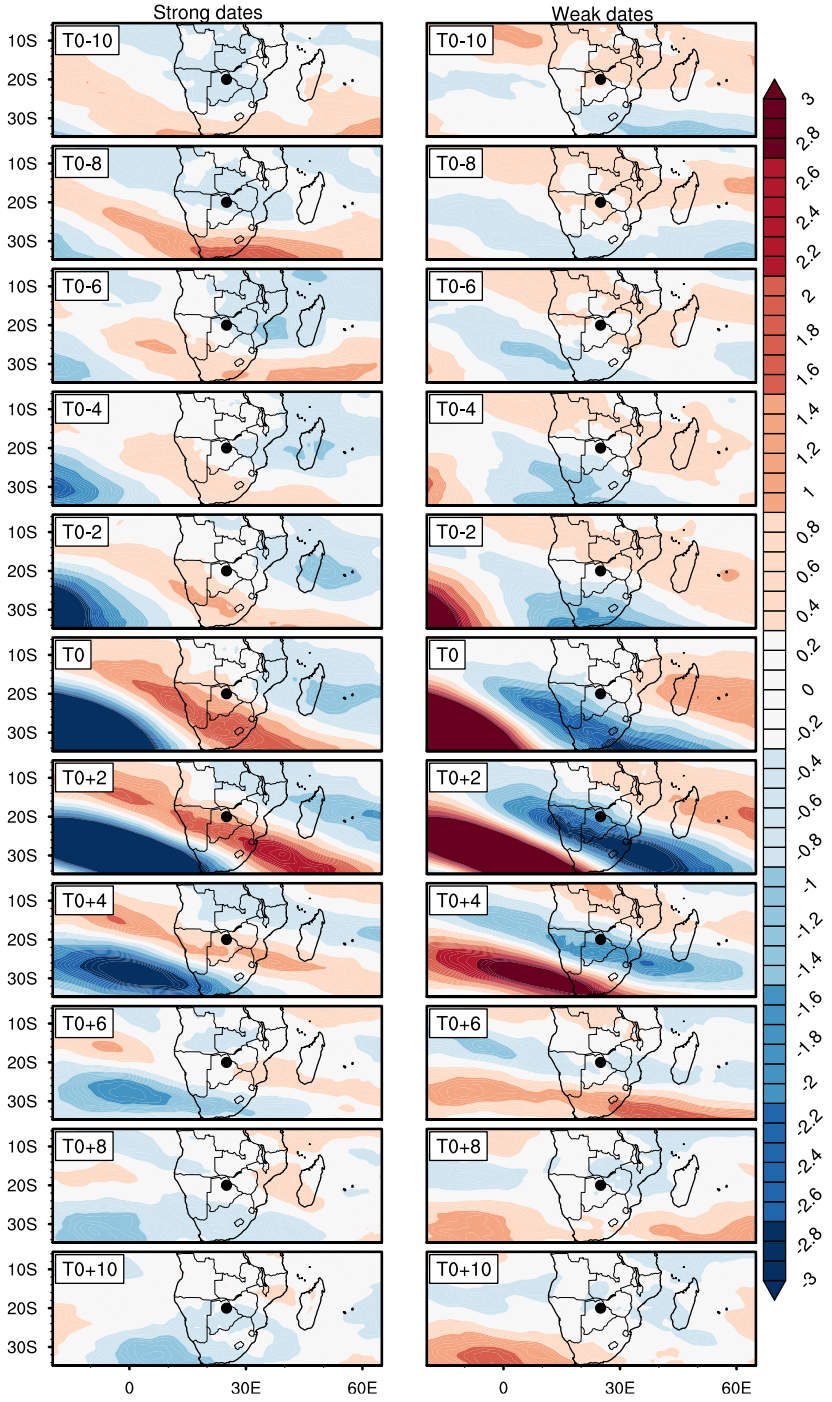

Figure 23: *Composite of the deseasonalised zonal wind anomalies at 600 Mb during strong and weak dates from T0 - 10 days to T0 + 10 days in 02-days steps.*

3.2.3 Conclusion

This first section has examined the formation and maintenance mechanisms of the AEJ-S, and its links with southern subtropical waves. The AEJ-S is a thermal wind and the jet is dominated by the rotational circulation. AEJ-S is maintained by a mid-level high that forms over southern Kalahari/Namibia around 600 hPa. Anticyclonic circulation is associated with positive values of vorticity at 600 mb and strong divergence. Mechanisms associated with this high pressure system are the

Kalahari heat low which is characterized by strong surface heating and associated uplift and dry convection over which there is upper level subsidence. Mid-level divergence results from the dry convection topped by upper level subsidence and with that strong positive vorticity from September to November.

We have also examined atmospheric energetics between the divergent and rotational flow and found that the divergent circulation deflected by the Coriolis forces is not well developed in the case of the AEJ-S. It's contribution to the strength of the AEJ-S is very weak compared to AEJ-N where its contribution is crucial as a result of the well developed North African divergence centers over the Chad-Soudan region. Results have also put in evidence the link between the AEJ-S and subtropical waves (Figure 24). Results highlight that, when subtropical waves overly southern Africa, they act to modify tropospheric heating. A ridge in the westerly wave intensifies the heat low and is associated with a strong AEJ-S and less rainfall, whereas a trough in the westerly wave displaces the heat low and decelerates the jet leading to more rainfall. At the intraseasonal variability, we describe the meteorological characteristics directly associated with the upper wavy flow. Results show that the wave signal takes about 10 days to reach the southern coast, and its activity takes about 06 days over the continent. Its impact on the warming of the atmosphere and on the mid-level circulation is associated with phases, structure and wave periodicity when it crosses the sub-continent.

3.3 African Easterly Jets and their associated dynamics in Models

3.3.1 Foreword

Climate models are vital to the assessment of the impacts of climate change in the Central African regions. Establishing how well models reproduce key processes is important to the confidence we attach to these tools. This second part of the study examines model representation of the September to November characteristics, such as location and intensity, of the African Easterly Jet (AEJ) north and south in a sample of 16 commonly evaluated CMIP5 and CMIP6 models and in two reanalyses (ERA5 and MERRA2). The analysis evolves to assess key drivers of the AEJ from energetic interactions, the characteristics of mid-level highs and thermal lows and

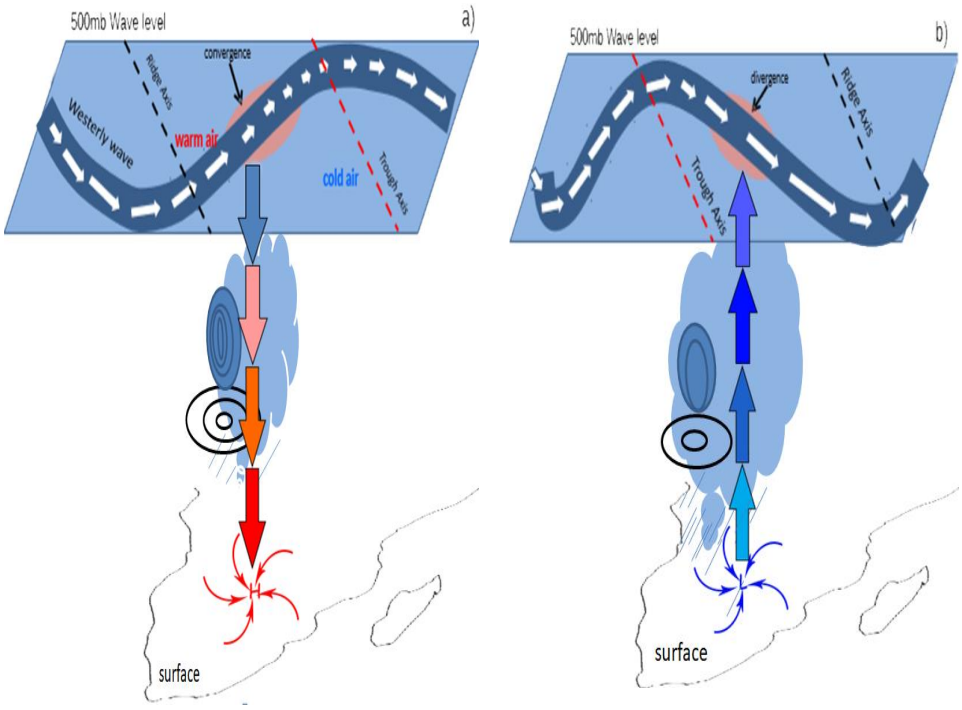

Figure 24: *Conceptual schematic model illustrating the AEJ-S dynamic and link with southern subtropical westerly waves, a for strong AEJ-S months and b for weak AEJ-S months*

the nature of surface thermal heating.

We focus on understanding how the new version of coupled models (CMIP6) represents drivers of AEJ, in order to explain the evolution observed in the previous version of the models (Creese and Washington, (2018)) compared to the new version. Understanding AEJ dynamics in models could help scientists to improve simulations, to understand models' rainfall biases, and temperature biases through assessment of the surface temperature gradient and surface heat fluxes. Our analyses in the current research have shown the importance of understanding surface temperature bias in models, an aspect that is generally neglected in assessment of coupled models, since emphasis is more often on understanding rainfall bias. This is important for the AEJ system, as previous studies showed that the observed amplified warming over the Sahara heat low (Cook and Vizy (2016)) and over the Kalahari heat low (Adebiyi and Zuidema, (2016)) is increasing the meridional temperature gradient and the AEJ is strengthening. Therefore understanding how coupled models represent mechanisms regulating temperature above the Earth's surface will advance understanding of AEJ dynamic in coupled models and improve reliability of future projections.

Model evaluation studies in CA have revealed large differences among CMIP5 models, particularly in their historical rainfall estimates during SON (Creese and

Washington (2018); Crowhurst et al. (2021); Taguela et al. (2022)). This large variation in model rainfall during SON provides an opportunity to further explore the regional circulation elements controlling the models' rainfall climatology. A common feature is the role of the AEJ components which are well developed during SON.

The first aim of this study is to better understand the climatological structure of the AEJ components in the new CMIP6 simulations (Eyring et al. (2016); O'Neill et al. (2016)) and in their CMIP5 predecessors, and we will answer to the following question:

1. What is the climatological structure of the African Easterly Jet during SON in reanalyses and models?

The rest of the study focuses more specifically on the CMIP6 models and will answer the following two questions:

2. What are the drivers responsible for the jet strength variation in models?

3. What are the reasons behind the differences between the drivers in the models and the simulated AEJs?

3.3.2 Jet locations and intensities in models

Figure 25 shows the latitude-longitude mean core locations of the two jets for SON in reanalyses and models. Analyses will focus on the longitudinal band 10°E-30°E encompassing CA. There is a good agreement between reanalyses in the mean SON position of AEJ-N and AEJ-S. Both reanalyses present the same east-west variation with an AEJ-N core starting at about 30°E. The AEJ-N core varies latitudinally between 9°N and 10.5°N in ERA-5 and between 9°N and 10°N in MERRA-2; and the AEJ-S core ranges from 4°S to 11.5°S in ERA-5 and 3°S to 11.5°S in MERRA-2.

Many CMIP5 simulations fail to locate the latitude of the AEJ-N over northern CA. Exceptions are BCC-CSM1-1-m, MIROC5 and HadGEM2-ES, which simulate a jet position close to that of reanalyses, with the best performance for MIROC5. Other CMIP5 models simulate the jet either farther north (CNRM-CM5-2, GFDL-CM3) or farther south (MRI-ESM1, GISS-E2-R, HadGEM2-CC) compared to reanalyses. Over West Africa, several models miss the southeast-northwest orientation of the AEJ-N core, leading to a gap of around 6° in the location of the jet (e.g. BCC-CSM1-1-m, HadGEM2-CC and GISS-E2-R) between 6°N and 12°N. Most CMIP5

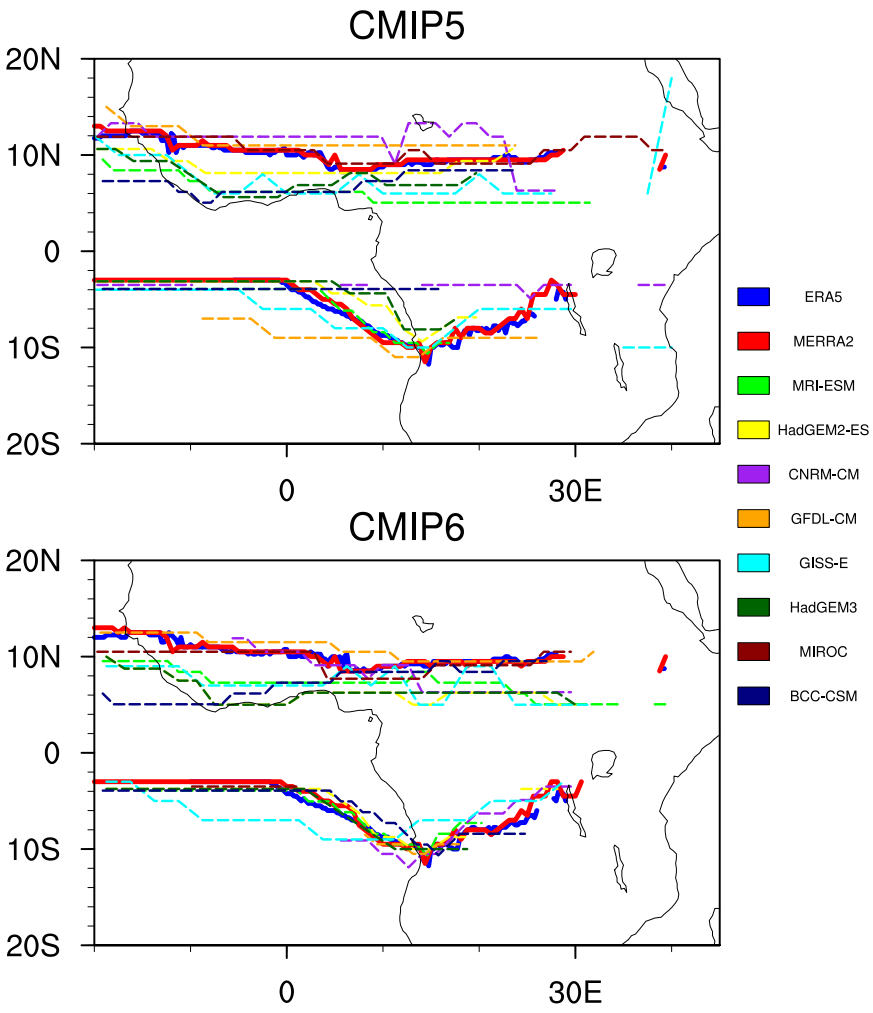

Figure 25: *Long-term mean (1980–2010) September to November latitudinal/longitudinal mean core locations of maximum easterly wind (-6 m.s^{-1}) speed at 700 hPa in region of AEJ-N (northern hemisphere) and at 600 hPa in AEJ-S region (Southern Hemisphere). Models are presented in dashed lines and the reanalyses in thicker continuous lines.*

models also fail to locate AEJ-S over southern CA. Some models (e.g. GISS-E2-R, MRI-ESM1, HadGEM2-ES, GFDL-CM3, HadGEM2-CC) simulate a jet position close to reanalyses only over western CA between 10°E-20°E, and other models (CNRM-CM5-2 and BCC-CSM1-1-m) simulate a jet position farther north (between 10°E-28°E) compared to reanalyses.

In general, the spread of simulated AEJ location around reanalyses is larger for CMIP5 compared to CMIP6 (Fig. 25), indicating improvement from CMIP5 to CMIP6. CNRM shows a very strong improvement in its CMIP6 version by capturing well both AEJ-N and AEJ-S location compared to reanalyses (Fig. 25), GFDL-CM4 and MIROC6 also show improvement in the AEJ-N. Other models (MRI-ESM2-0, GISS-E2-1-G, UKESM1) locate the jet farther south than reanalysis with a strong latitudinal variation of its core. HadGEM3-GC31-LL simulates an almost constant

latitudinal location of the AEJ-N. While CMIP6 models shows an improvement in locating AEJ-N over CA, the spread of the jet locations around reanalyses remain strong over West Africa. The SON climatological AEJ-S is also better simulated by most CMIP6 models compared to CMIP5, but still present some bias relative to reanalyses. For example, GISS-E2-1-G locates the northernmost jet over CA and the southernmost jet over western Equatorial Africa.

Figure 26 illustrates the annual cycle of the AEJs. Improvement of the location of AEJ-N by CMIP6 models spans the SON season, with good representation of north-south annual migration of the jet core (Figure 26a, b), in agreement with reanalyses. Over CA, AEJ-N is discernible throughout the year, but from December to February, the strength of the jet is relatively weak and its core lies between 0 and 3.5°N in ERA-5 and MERRA-2 (Figure 26a, b). A northward migration from March to August is observed when AEJ-N intensity strengthens reaching 8 $m.s^{-1}$ in ERA-5 and MERRA-2 with maximum strength of its core in July through August. During these months, the jet reaches its most northern location, and starts shifting south from September to December, with core speeds reaching almost 10 $m.s^{-1}$ in ERA-5 and MERRA-2 (Figure 26e, f).

AEJ-S is best defined during September to November in MERRA-2 but only present during October and November in ERA-5 (Figure 26c, d). The jet core location is close in the two reanalyses and ranges from 8°S in September to 10°S in November. Its core intensity is less than 7.5 $m.s^{-1}$ in ERA-5 while it reaches 9 $m.s^{-1}$ during October in MERRA-2 (Figure 26g, h).

To quantify the improvement in AEJ-N core location from CMIP5 to CMIP6 (Figure 26a and b), the deviation of the jet core location through the year from reanalysis is computed using the trapezium method. This method consists of calculating a numerical integration based on linear interpolation by intervals between January and December. This determines the area between models and reanalysis curves in the annual cycles of AEJ locations (Fig.26). The area between CMIP6 models and reanalyses curves is small compared to that of CMIP5 and reanalyses. As shown in Figure 26, where the unit of the area is the multiplication of the time axis unit in second by the latitude position in meter, the spread in location (latitude positions in meters) of AEJ-N through the year in CMIP5 compared to reanalysis is 91 s.m (second.meter), about twice that of CMIP6 around reanalysis (42 s.m).

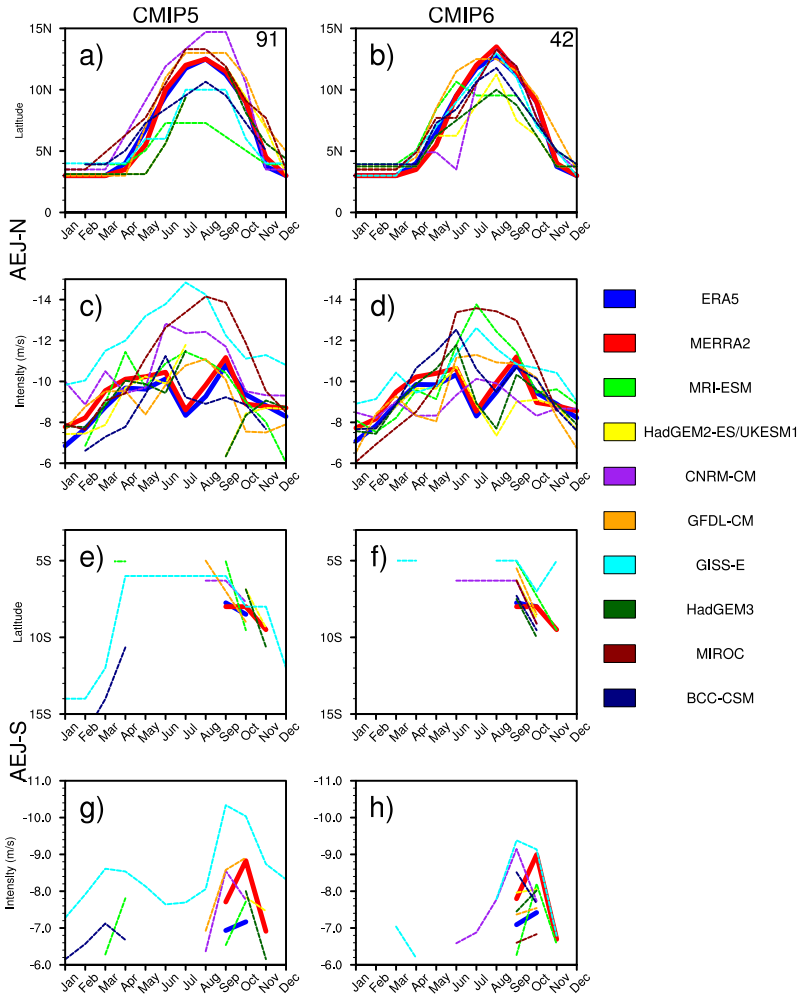

Figure 26: *Mean intensity in ($m.s^{-1}$) and location in (degrees latitudes) of monthly averages of the AEJ-N and AEJ-S jet cores in reanalyses, CMIP5 (a, c,e and g) and CMIP6 (b, d, f and h). Models are presented in dashed lines and the reanalyses in thicker continuous lines.The numbers 91 and 42 at the top of the panels represent the area mesured in (s.m) between the curve of the annual cycle of jet cores locations in models versus reanalyss, in CMIP5 and CMIP6 respectively.*

This result shows that location of AEJ-N in CMIP6 models is closer to reanalyses compared to CMIP5 models.

There are differences in AEJ-S location among CMIP5 models with several models simulating the existence of the AEJ-S over more months than ERA5 (CNRM-CM5-2, GISS-E2-R, MRI-ESM1, GFDL-CM3). The GISS-E2-R model presents a strong bias in the AEJ-S location by simulating the existence of its core over the whole year, but a good improvement is observed in its CMIP6 version with a core well pronounced between August through November. However, the CMIP6 version fails to locate the jet core, which is too far north, ranging between 5°S and 7°S. The BCC-CSM1-1-m model presents an AEJ-S in February through April (Fig. 26c), but the jet is better located in its CMIP6 version (BCC-CSM2-MR), in September and October. Mean

core location of the AEJ-S is generally better simulated in CMIP6 than CMIP5, with some models simulating the existence of AEJ-S over the same months as ERA5 and the spread among models around reanalyses is smaller.

In GISS-E models, AEJ intensities are overestimated in both CMIP5 and CMIP6 versions (Fig. 26e, f, g, h), but with a slight decrease in CMIP6. MIROC models also overestimate AEJ-N intensities in CMIP5 and CMIP6, but MIROC5 presents no AEJ-S and its intensity increases in MIROC6 but remains underestimated. In CMIP6 simulations, some models (GISS-E2-1-G, MRI-ESM2-0 and MIROC6) overestimate AEJ-N annual mean core intensity with peaks during June to August. UKSEM1 and HadGEM3-GC31-LL underestimate AEJ-N intensity from June to September but are close to reanalyses during October and November. CMIP6 models also present differences in AEJ-S intensities compared to reanalyses, this is the case of GISS-E2-1-G and CNRM-CM6-1 models, that fail to locate the jet core, and are the two models with the strongest AEJ-S with their core intensities reaching 9.5 $m.s^{-1}$. MIROC6 features the smallest AEJ-S with core speeds ranging between 6 and 7 $m.s^{-1}$ in September and October.

Analyses of the jet core locations and intensities has revealed improvements from CMIP5 to CMIP6, but some remaining differences between models and reanalyses, with some models (GISS-E2-1-G, MIROC6 and CNRM-CM6-1) depicting a jet core too far north or south and an overestimation in terms of intensity (too strong). These differences will now be investigated by examining meridional temperature gradients in the lower troposphere.

3.3.3 Surface temperature and jet strength in models

AEJs are thermal winds that result from a surface meridional temperature gradient. AEJ-N results from a surface meridional gradient between the hot and dry Sahara and the sub-humid Congo Basin, while AEJ-S results from a meridional thermal gradient between the hot Kalahari and humid Congo Basin. It follows that investigation of the driving meridional temperature gradient is an important step in the analysis of AEJ characteristics.

Before investigating the bias of the temperature gradient in the models compared to the reanalyses, we present in Figure 27 the climatology of the temperature gradient in the reanalyses and the models. We present the annual cycle of the 02 jets here

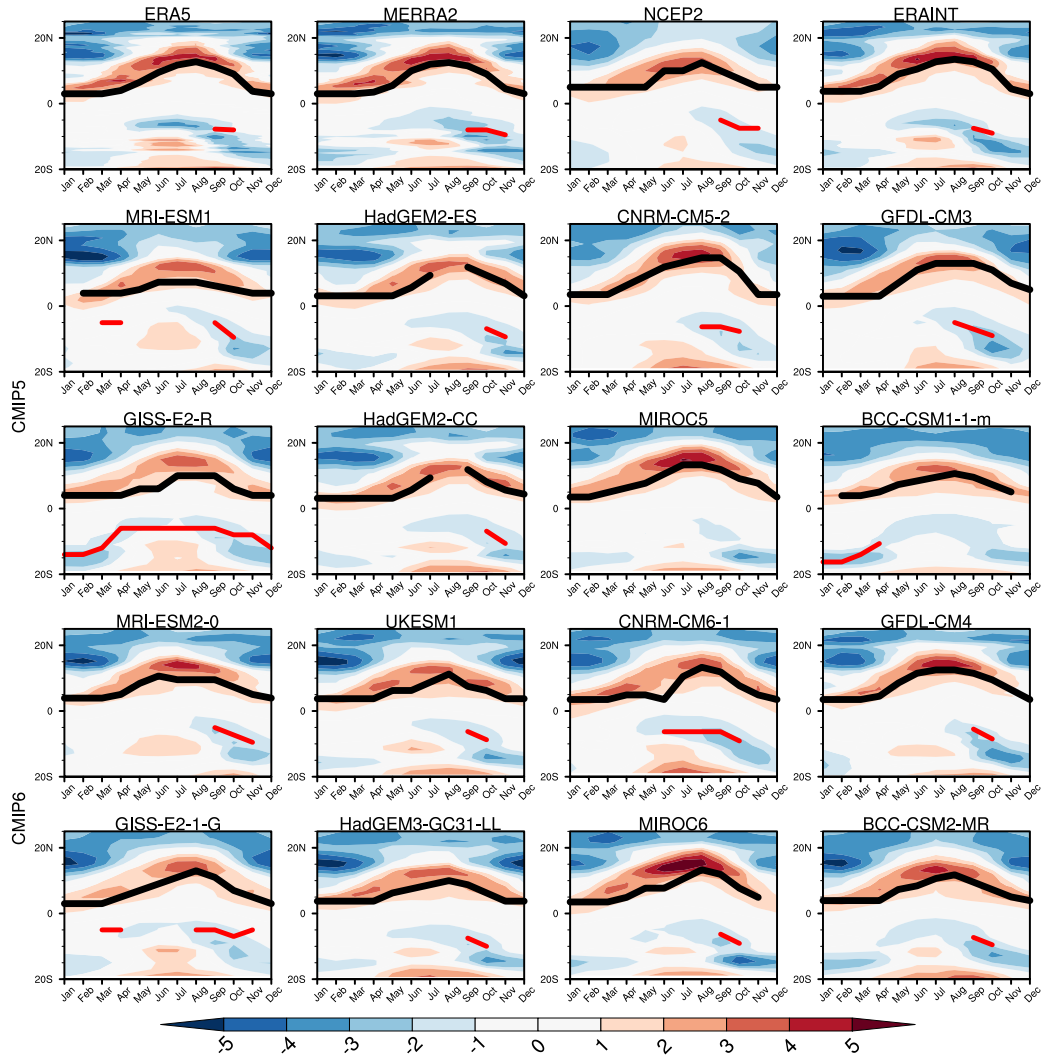

Figure 27: *Latitude/time annual evolution of surface 850hPa temperature gradient ($K.m^{-1}$) climatology in reanalyses (first row only), CMIP5 models (second and third rows) and CMIP6 models (fourth and fifth rows), all averaged in the longitude range of 14°E-24°E. With overlay locations of AEJ-N (black contour in the northern hemisphere) and AEJ-S (red contour in the southern hemisphere).*

to show the annual evolution in the surface temperature gradient and that of the jet. The 04 reanalyses show a similar yearly variation of the surface meridional temperature gradient in the 02 Hemispheres. With the exception of NCEP2 which shows some slight differences (low gradient value), this explains the variation in the annual cycle of AEJ-N. ERA5 explains both a better variation compared to all analyses and at the same time an improvement compared to ERAINT. Thus, we chose ERA5 to calculate the biases in the models.

Figure 28 presents the latitude/time annual evolution of the 850 hPa meridional gradient in temperature in reanalyses, and model biases with reference to ERA-5. The brown solid lines in both hemispheres represent the region (outer contour) of maximum surface temperature gradient in ERA5. The maximum meridional surface

temperature gradient in the northern hemisphere is positive from north to south and located between 3°N and 18°N with the strongest values within the 13°N-15°N band in August, which corresponds to the month when AEJ-N is at its most northern location. AEJ-N (shown by the black line) forms at the southern (equatorward) boundary of the maximum meridional surface temperature gradient and follows its cross-latitude migration through the annual cycle.

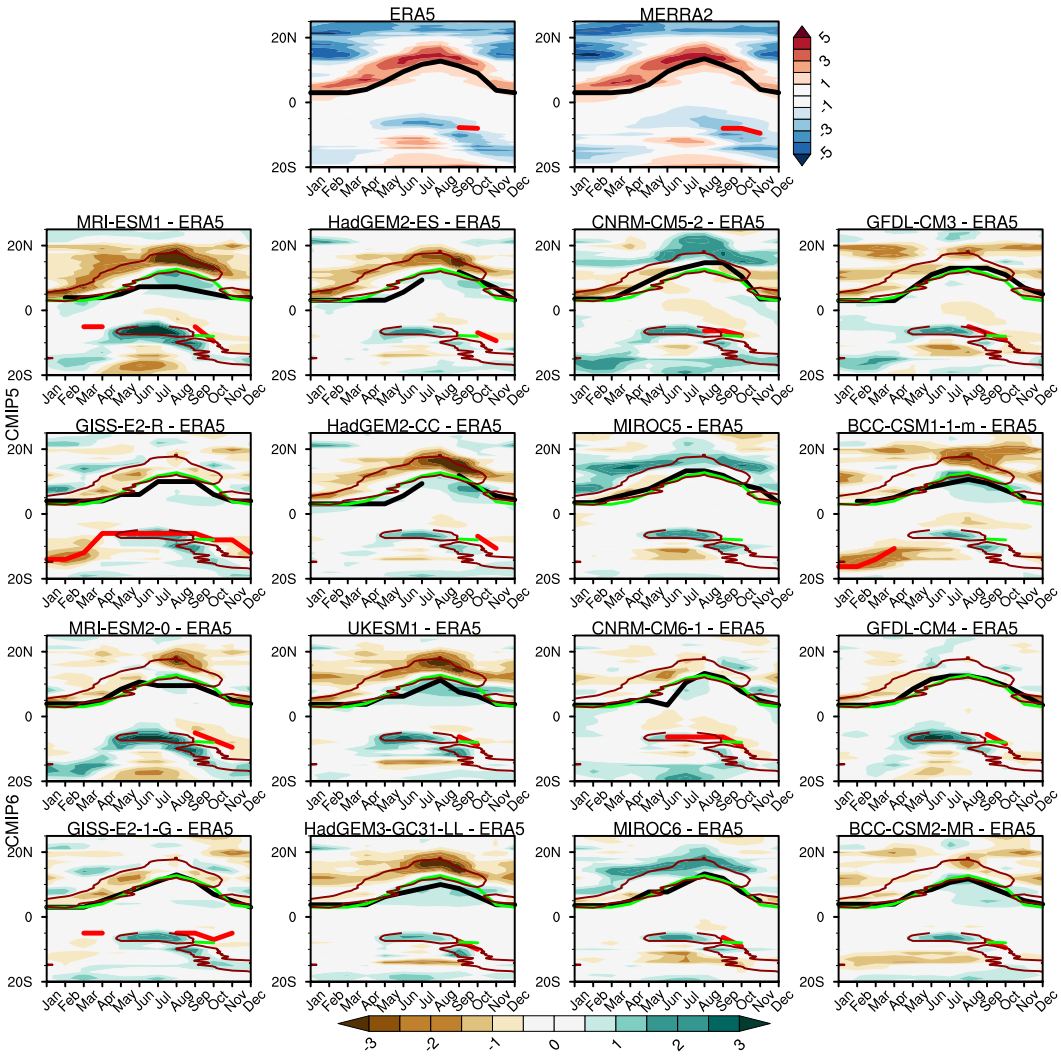

Figure 28: *Latitude/time annual evolution of surface 850hPa temperature gradient ($K.m^{-1}$) climatology in reanalyses (first row), averaged in the longitude range of 14°E-24°E. With overlay locations of AEJ-N (black contour in the northern hemisphere) and AEJ-S (red contour in the southern hemisphere). Bias of temperature gradient in models against ERA-5 is also represented. To show bias in location of the jets in reanalysis compared to models, we represent in green contour line mean climatology of AEJ-N and AEJ-S in ERA5. We also represent the maximum contour of temperature gradient in ERA5 (dark red line).*

The meridional surface temperature gradient in the southern hemisphere is of opposite sign because the gradient is calculated from north to south and, in the case of the southern hemisphere, the warmer temperatures are to the south over

the Namib-Kalahari region. AEJ-S (shown by the red line) forms at the northern (equatorward) boundary of the meridional temperature gradient. The climatological structrure of AEJ-S in ERA-5 appears during two months (September-October).

Most CMIP5 and CMIP6 models underestimate the surface temperature gradient over AEJ-N region with a negative bias (brown shading), except in the MIROC5 and CNRM-CM5-2 models where the bias is positive (turquoise) throughout the annual cycle. In CMIP6 this positive bias persists in MIROC6, but it decreases in CNRM-CM6-1. MIROC therefore has the strongest surface temperature gradient, but with a slight improvement in MIROC6. In most models, the bias is improved from CMIP5 to CMIP6. This could explain why AEJ-N is reasonably well simulated in most CMIP6 models. In the AEJ-S region, MIROC6 and CNRM-CM6-1 presents the strongest temperature gradient (Fig. 28 shown by the negative shadings). The strong temperature gradient in CNRM-CM6-1 explains improvement of its jet's core location from CMIP5 to CMIP6, while in MIROC6, AEJ-S intensity varies oppositely to the surface temperature gradient.

To better understand the relationship between temperature gradients and jet strength/location, we performed long-term seasonal means correlation analyses. If these temperature gradients are responsible for the jets intensity in each model, a strong positive correlation between this thermal contrast and the jets strength is expected. The long-term seasonal means are calculated for AEJ intensity and temperature gradient over the domain 14°E to 28°E of longitude and 5°S to 15°S of latitude for AEJ-S and 3°N to 20°N for AEJ-N in each model.

Figure 29 shows long-term means correlation between 850 hPa maximum surface meridional temperature gradient and AEJs intensities for SON, representing the season when the two jets are strong over CA, and when the relationship between mean AEJs intensities and temperature gradient is most pronounced over the region. Figure 29 highlights that, in the AEJ-S region (Fig. 29a, c and e), the surface temperature gradient is strongly correlated with the jet strength during November in reanalyses ($r = 0.62$ in ERA-5 and $r = 0.56$ in MERRA-2). During September, ERA-5 and MERRA-2 both present weak correlations, but these strengthen in October. Surface temperature gradient and AEJ-S strength are not always well correlated in most coupled models, except for HadGEM3-GC31-LL, which presents a good correlation higher than 0.5 during the months of September to November. CNRM-

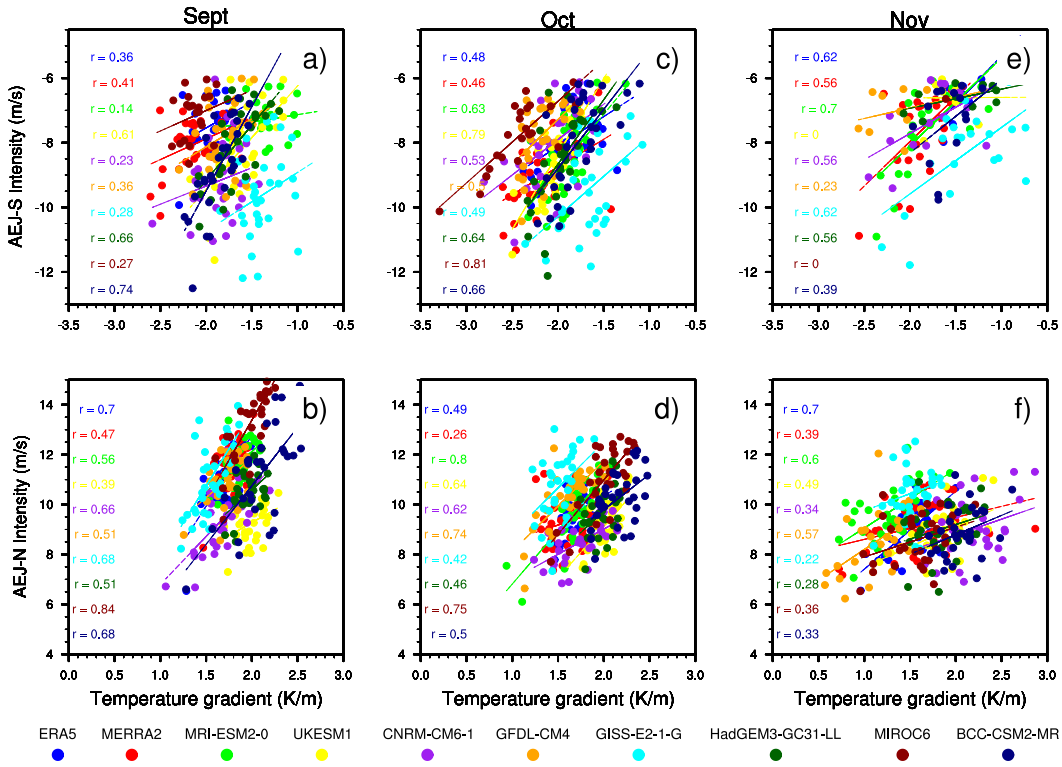

Figure 29: *Scatter Plots showing relationship between September to November long-term mean (1980–2010) 850 hPa surface temperature gradient ($K.m^{-1}$) and AEJs intensities ($m.s^{-1}$) for models and reanalysis. Each dot represents the yearly value in each model.*

CM6-1, GISS-E2-1-G and MRI-ESM2-0 which simulated the existence of AEJ-S during September, October and November, better correlate their jet strength with the surface gradient during October and November but the correlation is weak in September. MIROC6 which locates a maximum jet core intensity over CA during September and October presents a high correlation greater than 0.8 only during October.

For AEJ-N (Fig. 29b, d and f), ERA-5 has higher correlations than MERRA-2. MIROC6 which had the strongest surface temperature gradient, presents strong correlations during September and October. The GISS-E2-1-G model, which simulated the strongest jet from September to November, but had the smallest surface gradient, presents a good correlation only during September. MRI-ESM2-0 and GFDL-CM4 models show good correlations during the three months, while some models (BCC-CSM2-MR,UKESM1 and CNRM-CM6-1) show correlations only during two months. Figure 29 therefore illustrates correlations between surface temperature gradients and jet strength, but in some models the mean strength of the jet intensity do not always relate to the temperature gradient. This suggests that the jets are driven by the surface temperature gradient plus other mechanisms. We will now explore the

contribution of other features to both AEJ-N and AEJ-S maintenance, namely the atmospheric energetics analysis and mid tropospheric high located in the vicinity of the jet.

3.3.4 African Easterly Jet dynamics in models

3.3.4.1 Atmospheric energetic interactions of divergent and rotational flows

Another mechanism known to have a crucial influence in the AEJ maintenance is the energetic interactions of atmospheric divergent and rotational flows, developed by Chen and Wiin-Nielsen (1976) and further assessed by Wiin-Nielsen and Chen (1993). Chen (2004) highlighted that meridional divergent circulation that spills out of the North African divergent center and accelerates towards the AEJ-N core generates divergent kinetic energy. Divergent circulation is deflected westward under the Coriolis effect at the jet core and leads to conversion of divergent kinetic energy into rotational kinetic energy that accelerates the AEJ-N over West Africa during North African summer. Kuete et al. (2019) evaluated the contribution of this mechanism to the maintenance of the AEJ-S, and showed that, due to the dominance of rotational circulation over divergent circulation at mid troposphere in the AEJ-S region during SON, the contribution of conversion of divergent kinetic energy into rotational kinetic energy was ten times less important in the AEJ-S compared to its contribution to the maintenance of the AEJ-N.

Figure 30 shows vertical profiles of the atmospheric energetic interactions as estimated in Kuete et al. (2019). Conversions exhibit centers of positive values at the AEJ-N core around 700 hPa in ERA-5 and MERRA-2. The AEJ-N is located south of the downward branch of the meridional circulation and associated with uplifts below 700 hPa over the Saharan heat low. Saharan meridional northerlies induce Coriolis acceleration that maintains the AEJ-N as indicated by the mid tropospheric positive values of conversion over the AEJ-N core (green shading).

Saharan meridional northerlies induce Coriolis acceleration that maintains the AEJ-N as indicated by the mid tropospheric positive values of conversion over the AEJ-N core (green shading). Dry convection over the Kalahari heat low in the south (Howard and Washington, 2018) is evident from the surface to 600 hPa (shown by vectors) and links to a peak of divergence. Both zonal and meridional divergent wind components contribute to this divergent center but due to the strong development of

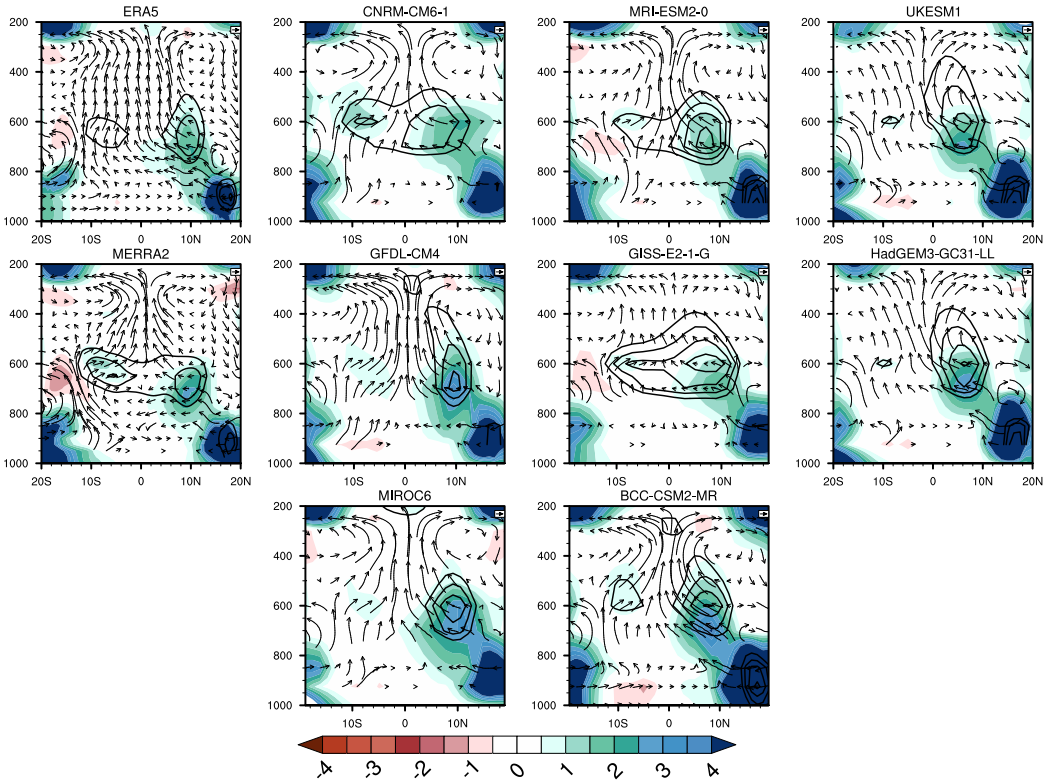

Figure 30: *Latitude/height cross-sections of the atmospheric energetics interaction, representing conversion of divergent kinetic energy into rotational energy (shading in $m^{-2}.s^{-3}$). AEJs components (black contours in $m.s^{-1}$) and meridional divergent circulation in vectors (v_D, w) are overlaid. All variables are averaged over 14°E-28°E representing the longitudinal core of AEJ in this study.*

the zonal rotational wind component, values of conversions are very weak over AEJ-S core (Kuete et al. (2019)), as shown in ERA-5. In MERRA-2, values of conversion are higher over AEJ-S region, due to a stronger acceleration of the divergent flow towards AEJ-S core at 600 hPa. The CNRM-CM6-1 model simulates the energetics well and looks relatively similar to MERRA2 over both AEJ-N and AEJ-S cores. This is generally less consistent in other models which look more like ERA5, with some (e.g. MIROC6, GFDL-CM4 and BCC-CSM2-MR) showing strong positive centers of conversions over the AEJ-N core and very weak peaks over AEJ-S and others (MRI-ESM2-0, GISS-E2-1-G, UKESM1 and HadGEM3-GC31-LL) slightly close to ERA-5 and MERRA-2 over AEJ-N core, but still weak over AEJ-S region.

Weak peaks of this energetic analysis over the AEJ-S's core in MIROC6 can be linked to the very weak acceleration of this jet over CA during SON, compared to CNRM-CM6-1 which overestimates AEJ-S intensity and better simulates its mean core location during SON and presents strong values of conversion over the jet core. As a first order diagnostic of the jet's acceleration, most coupled models better simulate the atmospheric energetic interactions over AEJ-N region that leads to its

strong contribution to AEJ-N maintenance compared to AEJ-S.

3.3.4.2 Mid-Tropospheric highs over Africa

As a second step in understanding the dynamics of the AEJ acceleration mechanisms, we investigate the role of the North African mid-level Saharan high in the maintenance of the AEJ-N and the mid-level Botswana high in the AEJ-S. Their formation and maintenance dynamics are also explored.

A- The Saharan high.

The Saharan high is a conspicuous element of the North African mid tropospheric circulation. The high develops over the land surface and centered at about 200N described briefly by Cook (1999). The AEJ-N is located at the southern rim of this mid-level anticyclone. We use stream function as a diagnostic variable for the anticyclone during SON. At 700 hPa (Figure 31) two high pressure systems are depicted over North Africa, the Saharan high around 20°N, 0-20°E and the Arabian high 25°N, 45°E. To show the rotational flow associated with these high-pressure systems, we use total vorticity at 700 hPa in ERA-5 and MERRA-2. In the Northern Hemisphere, vorticity is strong with negative centers at the two highs cores (brown shading). To the south of the Saharan anticyclone, strong positive meridional pressure gradient increase zonal easterly flow from 28°E, marking the entrance into the AEJ-N region in reanalyses. The spatial quadrature of the Saharan high and its associated anticyclonic circulation is well represented in ERA-5 and MERRA-2, with a more easterly extension of the high in MERRA-2.

We represent in Figure 31 total vorticity bias in models against ERA-5. The spatial formation of the Saharan and Arabian highs are well represented in CMIP6. Most coupled models locate the Sahara high pressure system core further west compared to ERA-5 and MERRA-2, except in CNRM-CM6-1 whose core is located further east. GISS-E2-1-G shows a very strong meridional pressure gradient southeast of the Saharan high core between 10 and 25°E compared to ERA-5 and MERRA-2.

The anticyclonic circulation (represented by vorticity bias relative to ERA-5) is underestimated at the core of the Saharan high in all coupled models, but the vorticity bias increases in GISS-E2-1-G at the outer contour of the high pressure at about 25°E, showing a strong rotational flow at this level in the model. The Arabian

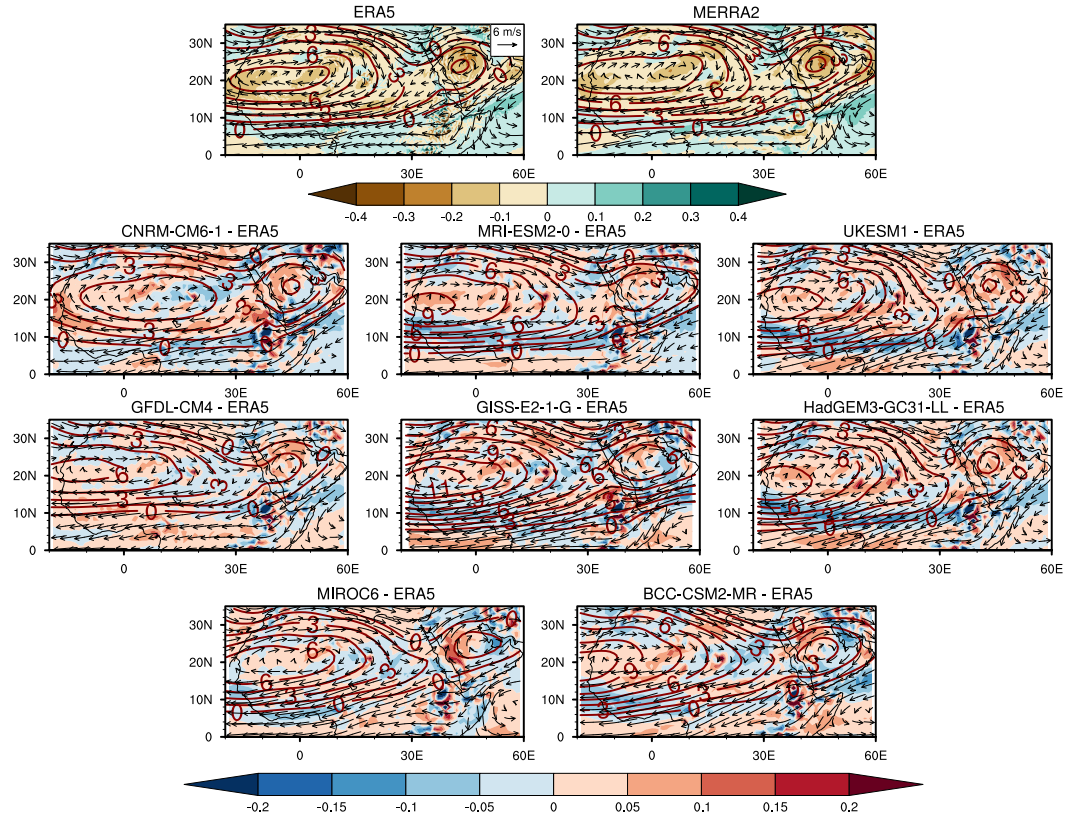

Figure 31: *Saharan mid-level high represented with stream function (brown contours) at 700 mb. The first contour is at 0 and the contour interval is 1.5. Horizontal wind speed at 700 mb is illustrated by vectors (at 6 m.$^{-1}$). Shading shows total vorticity in reanalyses (first row) and vorticity bias in models against ERA5, to show strength of the anticyclonic circulation associated with the mid-level high.*

high pressure also shows a strong meridional pressure gradient west (35°E) of the high pressure marking entrance of the AEJ-N in this model. Thus, AEJ-N acceleration in GISS-E2-1-G is supported by the strong and positive pressure gradient. GFDL-CM4, BCC-CSM2-MR and MIROC6 models present the same circulation as the GISS-E2-1-G model with an increase in total vorticity bias east of the Sahara high pressure system. However, the meridional pressure gradient strong in these models compared to GISS-E2-1-G but close to ERA-5 and MERRA-2. The UKESM1, HadGEM3-GC31-LL and MRI-ESM2-0 models present similar anticyclonic circulation around the Sahara high pressure with a strong meridional gradient south of the high pressure associated with an increase in vorticity bias thus accelerating AEJ-N at its entrance into the jet region at 35°E and maintaining it up to 10°E where the gradient weakens. This mechanism is stronger in MRI-ESM2-0 thus explaining the well simulated and strong AEJ-N (Figure 25 and 26) in this model.

The stream function field associated with the vorticity biases shows rotational flow of the Saharan and Arabian Highs in the models, thus accelerating AEJ-N. On the east side of the Saharan high is the North African divergent center (20°N)

which accelerates northerly flows into lower latitudes that are then converted into rotational flow maintaining AEJ-N (Figure 30). Since this divergent center is formed and maintained in response to heating induced by the Saharan thermal heat low, and the North African divergent center is spatially linked to the Saharan high, this differential heating serves in this study as a formation and maintenance mechanism of the Saharan high. This dynamic process has been described by Chen (2004) and Spinks et al. (2015).

Figure 32 presents a vertical profile of atmospheric parameters describing the dynamic process of formation of the mid-level Saharan high. We use vertical velocity (red line) to show vertical uplifts induced by the Saharan thermal heating. To illustrate the vertical representation of the mid-level high and its circulation, we show the stream function (dark green) and total vorticity (cyan). Saharan thermal heating causes air to be warm at the surface, warm air is lifted into the mid troposphere below 600 hPa, illustrated by negative values of vertical velocity from the surface (925 hPa). The change in vertical velocity sign at 600 hPa is associated with sinking cooler air from the upper troposphere, which converges with uplifts from the surface, forming the mid level anticyclone of the Sahara with its peak located at 700 hPa, illustrated by the vertical structure of the stream function.

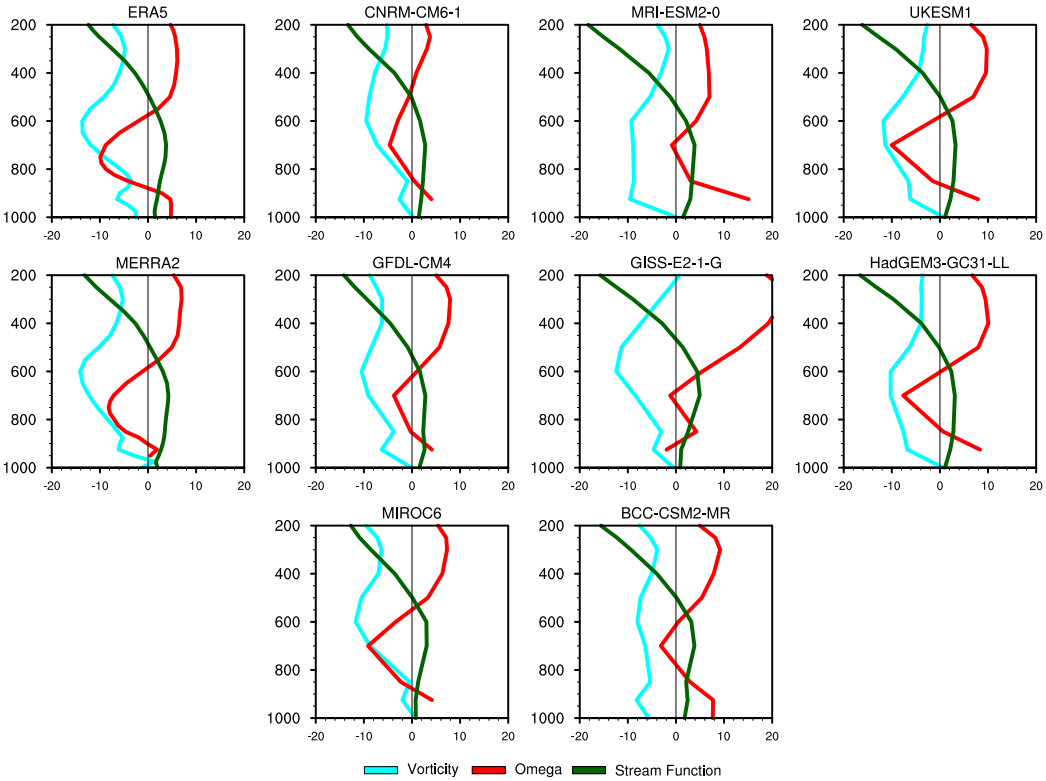

Figure 32: *Vertical profile of total vorticity (cyan), Omega (red) and Stream function (dark green). Variables are for SON and averaged in the core of the Saharan high (18°N-25°N of latitude and 14°E-25°E of longitude).*

The vertical structure of total vorticity shows negative peaks in the mid troposphere between 600 and 700 hPa, indicating the strong anticyclonic circulation at this level associated with the Saharan high. ERA-5 and MERRA-2 present similar vertical structures of these parameters. Most of the coupled models fairly reproduce the vertical structure of the stream function and total vorticity, showing the capability of capturing the horizontal and vertical distribution of the mid-level Saharan high (Figure 31) and the anticyclonic circulation associated to it. MRI-ESM2-0 and GISS-E2-1-G show a similar vertical velocity structure associated with positive values of omega over the entire atmospheric column, thus showing a predominance of subsidence from the top of the troposphere to the surface, but more intense in GISS-E2-1-G. Verifications of this dynamic process was performed using an east-west circulation (Figure 33). We computed the circulation using the magnitude of zonal divergent wind (u_D) and omega (w). The upward motion caused by the Saharan thermal heating is very weak in MRI-ESM2-0 and GISS-E2-1-G, but the east-west circulation is dominated by subsidence in GISS-E2-1-G and associated with strong easterly flow at the surface in MRI-ESM2-0. This analysis indicates that the Saharan high, which accelerates strong AEJ-N in MRI-ESM2-0 and GISS-E2-1-G through the associated meridional pressure gradient and vorticity at the southern rim of the high, forms for the wrong reasons.

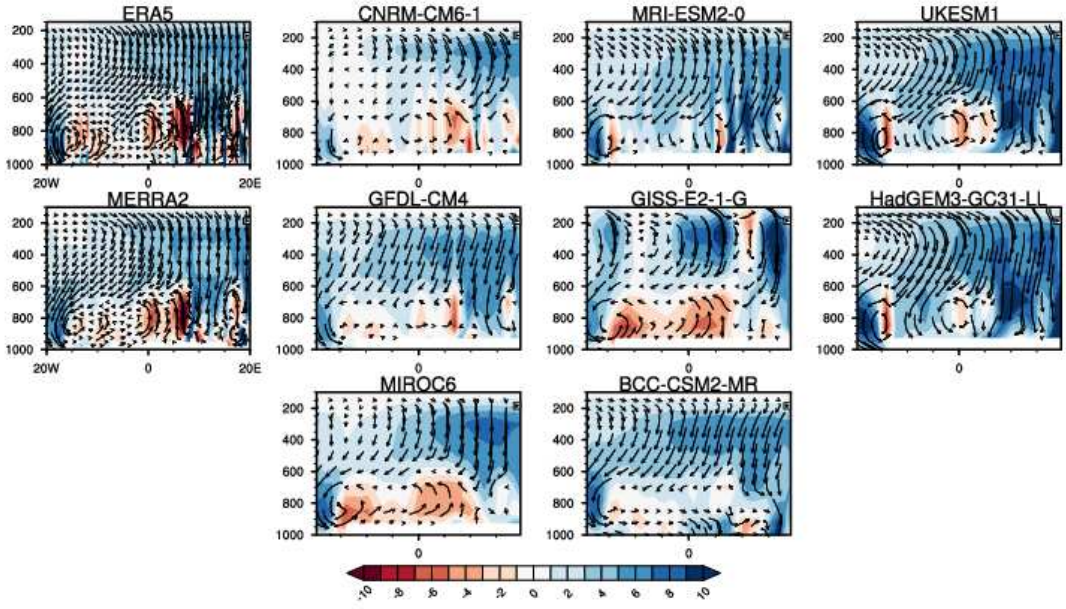

Figure 33: *East-West zonal divergent circulation (u_D, w), superimposed with vertical velocity (shade). Variables are averaged in the longitude range of 18°N-25°N.*

B- The Botswana high.

During SON, the Botswana High is a semi-permanent anticyclone occurring at mid-level (e.g. 600-500 hPa) over Botswana/Namibia. It is formed and maintained in response to heating of the Kalahari heat low, which strengthens upward motion from surface to mid troposphere. Kuete et al. (2019) demonstrated how this high pressure system is connected to the maintenance of AEJ-S. Figure 28 illustrates the 600 hPa stream function field (solid contours) during the SON in reanalyses and models. A ridge of high pressure is shown extending across Botswana/Namibia. ERA-5 and MERRA-2 show similar representations but more intense in MERRA-2. Kuete et al. (2019) suggest that this high pressure forms earlier in the year with an anticyclone becoming evident in August and strengthens through September and October. This is consistent with Kalnay et al. (1996), who identified a high pressure system over the southern landmass of Botswana during August through October, but located slightly higher at 500 hPa, namely the Botswana high. The Botswana high is also formed in response to thermal heating and located southwest of high rainfall regions of Congo (Reason (2016)), this suggests a link between the high pressure identified by Kuete et al. (2019) and the Botswana high in the Southern hemisphere. Very few studies have focused on its dynamics (Driver and Reason (2017)) except regarding rainfall over the Zimbabwe region (Matarira (1990); Unganai and Mason (2002)).

ERA-5 and MERRA-2 show on Figure 34 a strong south-north positive gradient in the stream function field at the northwest rim of the high pressure core, marking the AEJ-S region. The meridional pressure gradient associated with total vorticity which induces anticyclonic circulation at the core of the high pressure accelerates AEJ-S located north of the high. The rotational flow is more intense in MERRA-2 indicating the stronger AEJ-S compared to ERA-5. Model biases in vorticity are shown in Figure 34. Most coupled models capture the location and intensity of the high well, although some models (GISS-E2-1-G, MRI-ESM2-0, BCC-CSM2-MR) have a too intense core. GISS-E2-1-G which has the strongest AEJ-S, underestimates total vorticity at the core of the high pressure system compared to ERA-5. But the vorticity bias is strong and positive north of the high pressure and in the AEJ-S region, indicating strong rotational flows that accelerate the jet north of the high. MIROC6, which had the smallest AEJ-S, underestimates anticyclonic circulation with a negative bias of total vorticity, and a weak pressure gradient, thus explaining

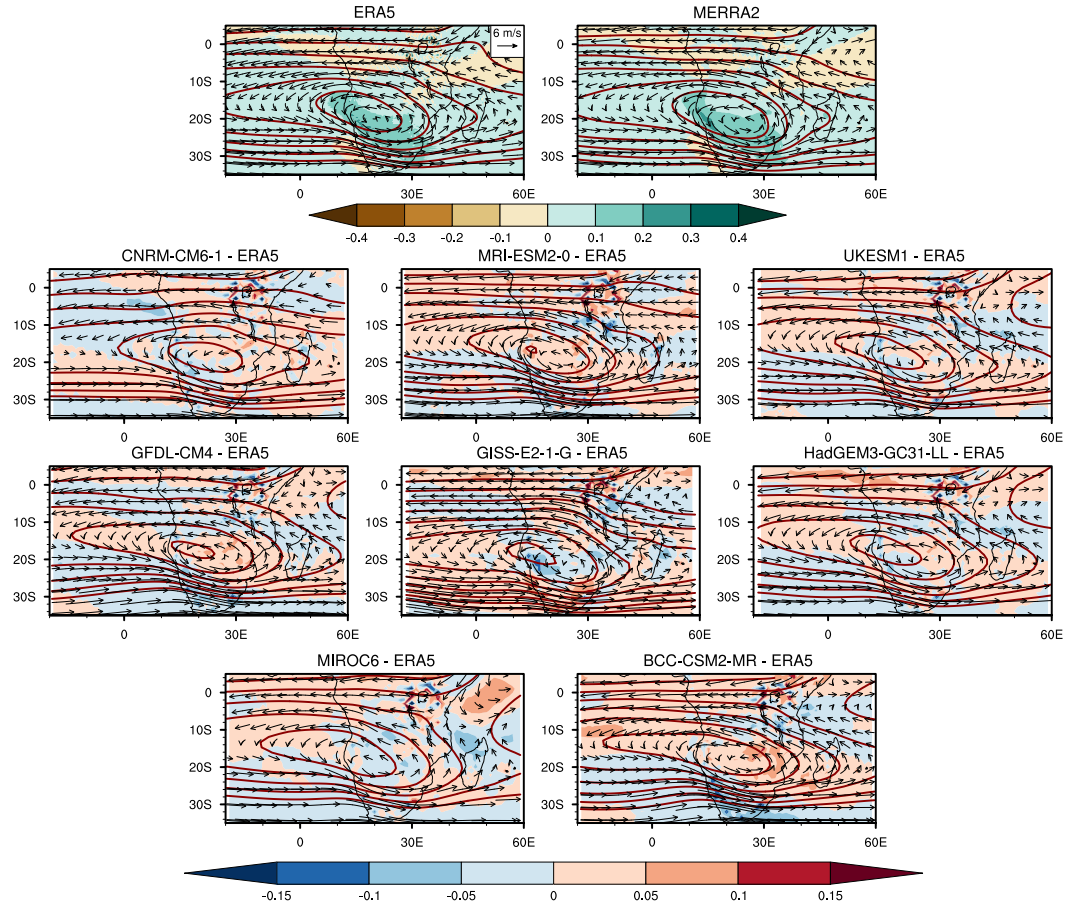

Figure 34: *Botswana mid-level high represented with stream function (brown contours) at 600 mb. The first contour is at 6 and the contour interval is 2. Horizontal wind speed at 600 mb is illustrated by vectors (at 6 m.*$^{-1}$*). Shading shows total vorticity in reanalyses (first row) and vorticity bias in models against ERA5, to show strength of the anticyclonic circulation associated with the mid-level high.*

the very low strength of the jet. GFDL-CM4, MRI-ESM2-0 and BCC-CSM2-MR present a similar circulation with an overestimation of the rotational circulation at the core of the high pressure, which becomes weaker north of the high pressure showing a strong rotation flow in these models at the high's core compared to the circulation in the AEJ-S region. The dynamic associated with the formation of the mid-level high is analyzed in Figure 35 through the vertical structure.

Vertical profiles of omega show variations in uplift from the lower-troposphere that converge with cool upper tropospheric air, forming the high pressure system. During SON, the semi-arid landscapes of the Kalahari region are characterized with strong and dry convection associated with surface heating, which occurs in the form of sensible heat, strengthening updrafts below 500 hPa. This is shown in Figure 35 from the vertical profile of the vertical velocity of ERA-5 and MERRA-2. CMIP6 models represent this mechanism well, detecting peaks of vertical velocity between 800 and 700 hPa, reinforcing updrafts from these levels. The formation of the mid-level high

in coupled models is strongly supported by updrafts, with weaker downward motions at upper levels except for the MIROC6 models where a similar pattern of downward motion to reanalyses is observed.

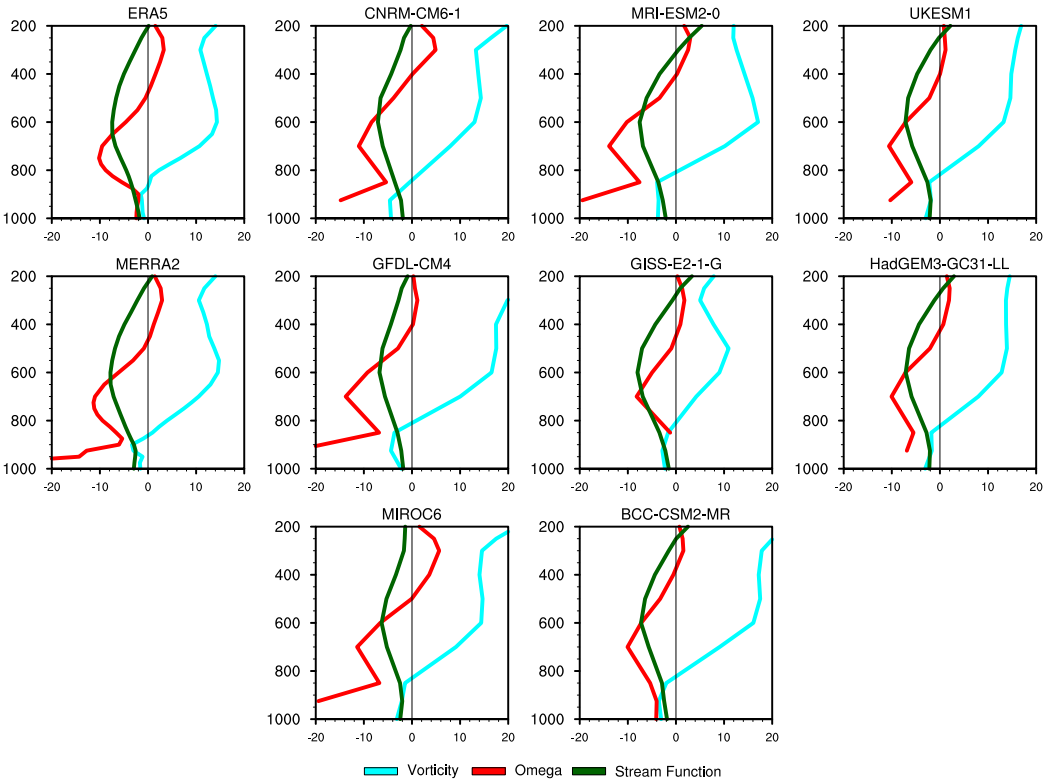

Figure 35: *Vertical profile of total vorticity (cyan), Omega (red) and Stream function (dark green). Variables are for SON and averaged in the core of the Botswana high (16°S-22°S of latitude and 14°E-25°E of longitude).*

To better understand how cool upper-troposphere air converges with lower-troposphere uplifts induced by surface heating, we present in Figure 36 a meridional circulation using divergent meridional wind (v_D) and omega (w), superimposed with vertical velocity (colors).

ERA-5 and MERRA-2 show strong updraft motions from surface to 500 hPa south of 20°S which are then decelerated by the upper tropospheric subsidence associated with the downward branch of the Hadley cell south of 10°S, thus forming the mid level high. This supports findings of the mid tropospheric Botswana high which also forms in response to surface heating. From the vertical structure and dynamics associated with the mid tropospheric high located at 600 hPa that is described in this study, we hypothesized that this mid level high is linked to the Botswana high located at 500 hPa. Most of the models show consistent pattern of the Botswana high with the observed data. Its formation mechanism is well linked to the representation of the high. This indicates that the simulated AEJ-S in models is consistent with the representation of the high and the anticyclonic circulation to which it is

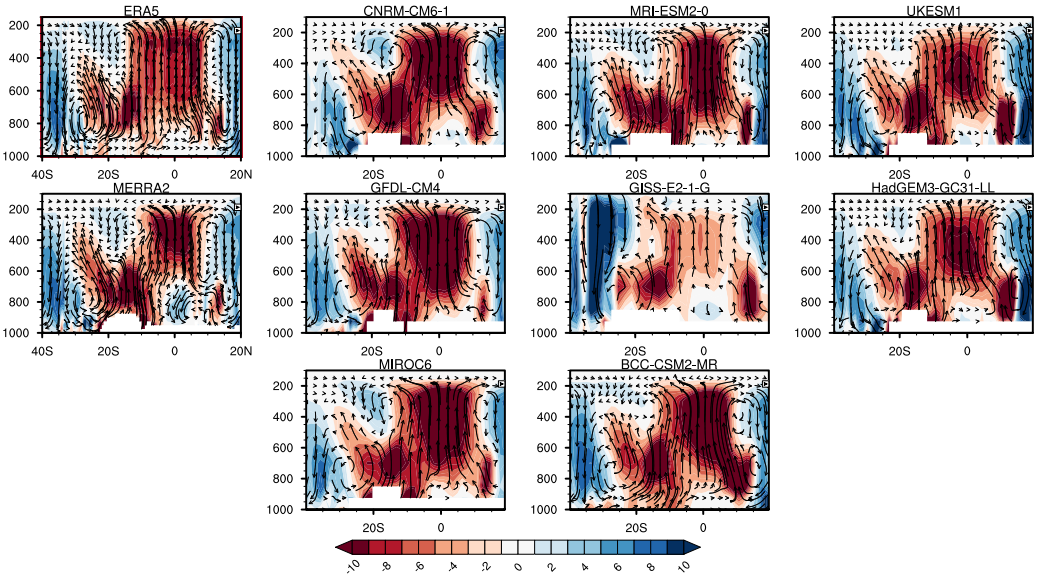

Figure 36: *North–South meridional divergent circulation* (v_D, w)*, superimposed with vertical velocity (shade). Variables are averaged in the longitude range of 15°E-25°E.*

associated. AEJ system is driven a mid-level thermal circulation that is supporter by surface radiative effect. An effort is made in the next section to understand how dry thermal convection over the Namib-Kalahari and Sahara dryland thermal lows supports strong rising motion forming mid-level highs associated with anticyclonic circulation and divergent centres.

3.3.4.3 Heat lows and jets strength in models

The 850 hPa surface temperature is used to analyze the heat lows. This temperature field is closely related to the atmospheric layer of the Kalahari heat low dynamic described in Howard and Washington (2018), and to the low level atmospheric thickness of the Saharan thermal low described in Lavaysse et al. (2009). No criteria was used to track and detect heat low as in these previous studies, but the temperature field used in our study gives a simple definition of the heat low similar to Chauvin et al. (2010) who used it to characterize the Saharan heat low.

Figure 37 presents the SON climatology of 850 hPa temperature in ERA-5 and MERRA-2, and temperature biases in models against ERA-5. Strong heating is observed over the Sahel, Arabia and Kalahari regions in ERA-5 and is more intense in MERRA-2 over the Kalahari region. CNRM-CM6-1 and GFDL-CM4 underestimate temperatures over the Sahel and throughout North Africa and Congo Basin. But, some slight positive temperature bias is observed in the Kalahari region showing an intensification of Kalahari heat low in these models compared to reanalyses.

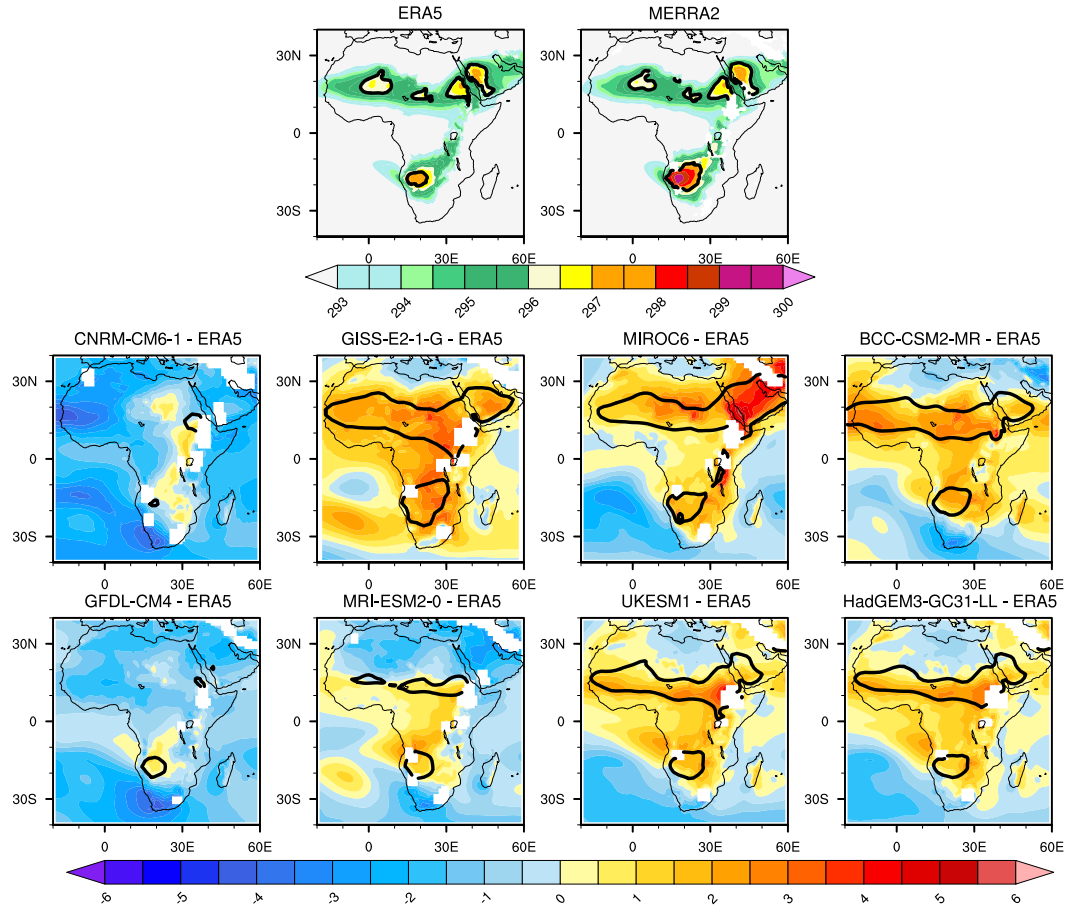

Figure 37: *Sahara and Angola heat lows represented by the mean SON 850 hPa temperature in reanalyses (top panel) and bias in models against ERA-5. The black contour line shows heat low locations in models represented by the 296 Kelvin temperature value in the north and 297 Ke temperature value in the south.*

MRI-ESM2-0 presents a positive temperature bias localized in the region of maximum temperature, but the bias is negative over the northern Sahel. This negative temperature bias over the Sahel reinforces the hypothesis that the acceleration of the AEJ-N is due to an intensification of the Saharan high that is formed for the wrong reasons. GISS-E2-1-G, HadGEM3-GC31-L, MIROC6, BCC-CSM2-MR and UKESM1 models are very hot and show positive temperature bias against ERA-5 over the whole region including the Congo Basin, but the bias is greater in GISS-E2-1-G and MIROC6.

The positive temperature bias over the Congo Basin in GISS-E2-1-G is thought to be responsible for the weak surface temperature gradient. Although the surface temperature gradient is small in GISS-E2-1-G, both jets remained strong and are maintained by high pressure systems in the mid-troposphere, as formation and intensification of these high pressures and their associated circulations are controlled by surface thermal heating due to the reinforcement of the heat low. As surface heating over Sahara and Kalahari regions is important in the generation and maintenance of

the jets, understanding how coupled models represent different behavior of surface heating is an open question for this study. The primary component of insolation that drives surface heating is commonly referred to as surface downward shortwave radiation. We present in Figure 38 the SON climatology of surface solar downward radiation in ERA-5 and MERRA-2, and biases of solar radiation in models against ERA-5. ERA-5 and MERRA-2 show a similar representation of solar radiation, but it is very strong in MERRA-2 in the Southern Hemisphere compared to central Sahel.

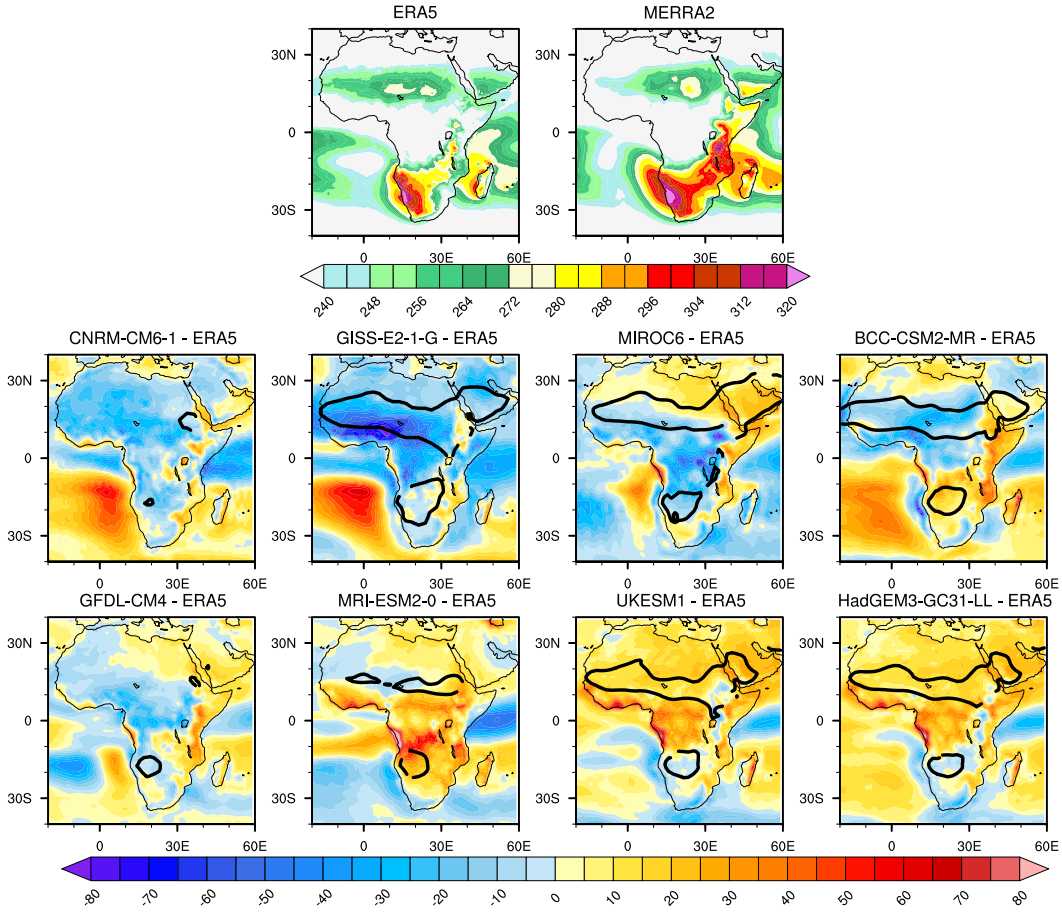

Figure 38: *Mean September to November Surface Solar Downward Radiation in reanalyses (first row only) and bias in models against ERA5 (second and third rows). Values are shown in $W.m^{-2}$. The black contour line shows heat low locations in models represented by the 296 K temperature value in the north and 297 Ke temperature value in the south.*

Solar radiation is strongly overestimated in UKESM1 and HadGEM3-GC31-L over the Sahel, North Africa and Congo Basin, with a slight negative bias at the eastern Congo Basin over the Rift Valley, and over southern Kalahari. In contrast, MRI-ESM2-0 and BCC-CSM2-MR show a strong overestimation of solar insolation over the southern Kalahari, which extends to central Congo Basin in MRI-ESM2-0, and a negative bias in the northern Sahel in BCC-CSM2-MR. GISS-E2-1-G, MIROC6, GFDL-CM4 and CNRM-CM6-1 show a nearly homogeneous negative bias over the

entire heat low region delimited by the black contour. The negative bias is stronger in GISS-E2-1-G but doesn't explain the hot temperature bias in layers above Earth's surface observed in this model or MIROC6.

The Earth's surface exchanges energy with near surface and upper layers through processes such as emission of radiation by the surface, which is associated with an energy flux. Energy heat flux transfer can either occur as sensible heat or latent heat.

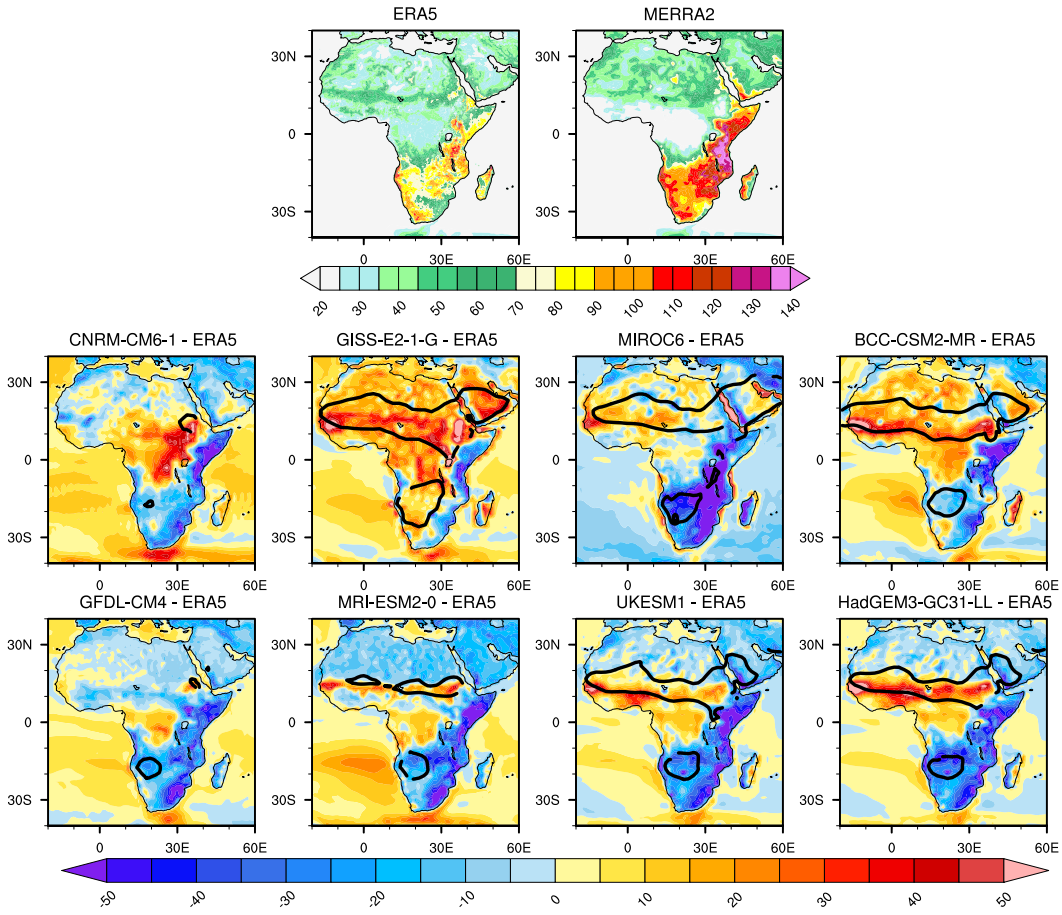

Figure 39: *Mean September to November Surface Upward Sensible Heat Flux in reanalyses (first row only) and bias in models against ERA5 (second and third rows). Values are shown in* $W.m^{-2}$. *The black contour line shows heat low locations in models represented by the 296 Ke temperature value in the north and 297 K temperature value in the south.*

Figure 39 presents the spatial representation of sensible heat flux during SON, and model biases against ERA-5. ERA-5 and MERRA-2 present the same spatial distribution of surface sensible heat flux, but the energy heat flux is stronger over southeast Kalahari in MERRA-2 compared to ERA-5. The Sahel and Congo basin present very weak values of sensible heat flux in reanalyses, indicating that dry soil is not a controlling component of surface heating over these two regions during SON. The model biases show a different spatial structure in the two hemispheres, with the

largest negative biases in the southern hemisphere. An exception is in GISS-E2-1-G, which presents a strong positive bias with a very strong sensible heat compared to other models. Thus enabling the ascent of warm air associated with dry convection which reinforces heating in layers above earth's surface in this model, and therefore intensifies the heat low (Figure 31). MIROC6 and other models show weak negative biases in surface sensible heat flux over southern Kalahari, indicating that the ascent of warm air that strengthens heating above the surface is not associated with dry soil.

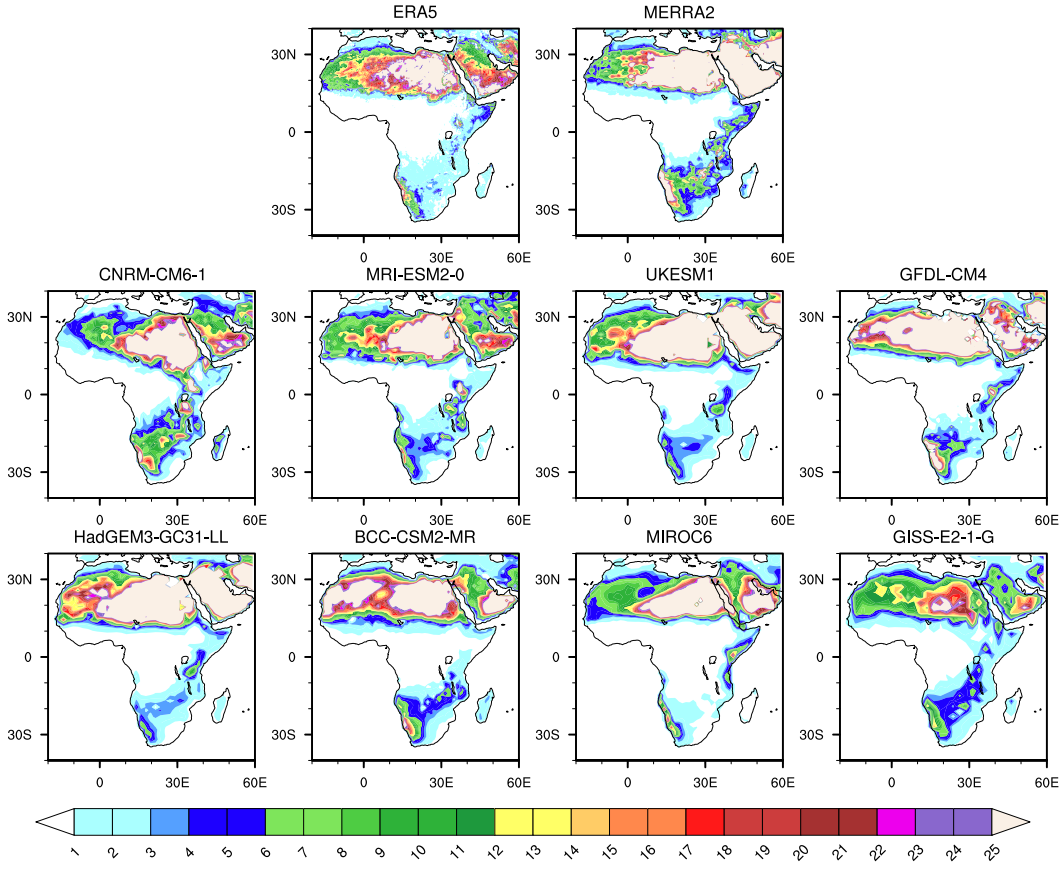

Figure 40: *Mean September to November bowen ratio in models and reanalyses, representing the ratio between surface sensible heat flux and surface latent heat flux.*

To describe the type of heat transfer from the surface in these models, we estimate in Figure 40 the Bowen ratio, representing in models the ratio of the energy heat flux between the sensible heat and the latent heat. The value of the ratio is higher over the northern Sahara arid region in models and reanalyses. This indicates that, more energy is dissipated into the atmosphere as sensible heat rather than latent heat from the surface. Over Southern Kalahari, models also present important values of Bowen ratio. GISS-E2-1G and CNRM-CM6-1 present very strong values of the ratio

greater than 10 over southern Kalahari. This shows that, these models are relatively dry and hot compared to other models. But the ratio is very weak in MIROC6 indicating that the climate is relatively cool and moist. A greater proportion of the available energy at the surface passed into layers above the surface as latent heat (Figure 41) than as sensible heat.

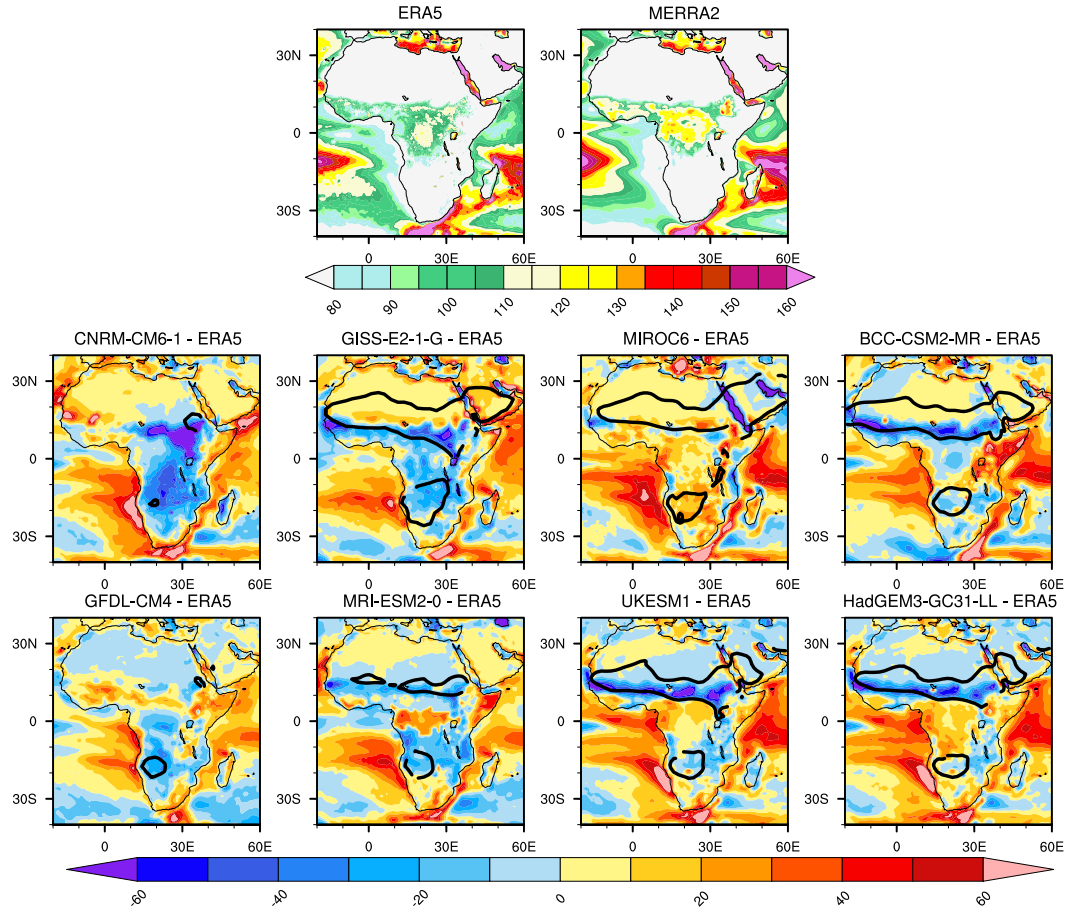

Figure 41: *Mean September to November Surface Upward Latent Heat Flux in reanalyses (first row only) and bias in models against ERA5 (second and third rows). Values are shown in* $W.m^{-2}$. *The black contour line shows heat low locations in models represented by the 296 Kelvin temperature value in the north and 297 Kelvin temperature value in the south.*

We also suggest that heat release above the surface that reinforces the heat low may be supported by long wave thermal radiation. This is shown in Figure 41. The emission of thermal radiation by the surface represents an important mechanism for heat transfer. Understanding the mechanism by which heat radiated away from Earth's surface to the atmosphere and between its surface layers will help to understand how the Earth's energy balance works to regulate our climate. Most coupled models present a positive bias of thermal radiation and this is very strong in MIROC6 compared to reanalyses. Although thermal radiation and surface temperature represent a fundamental characteristic of the Earth's climate, their linear

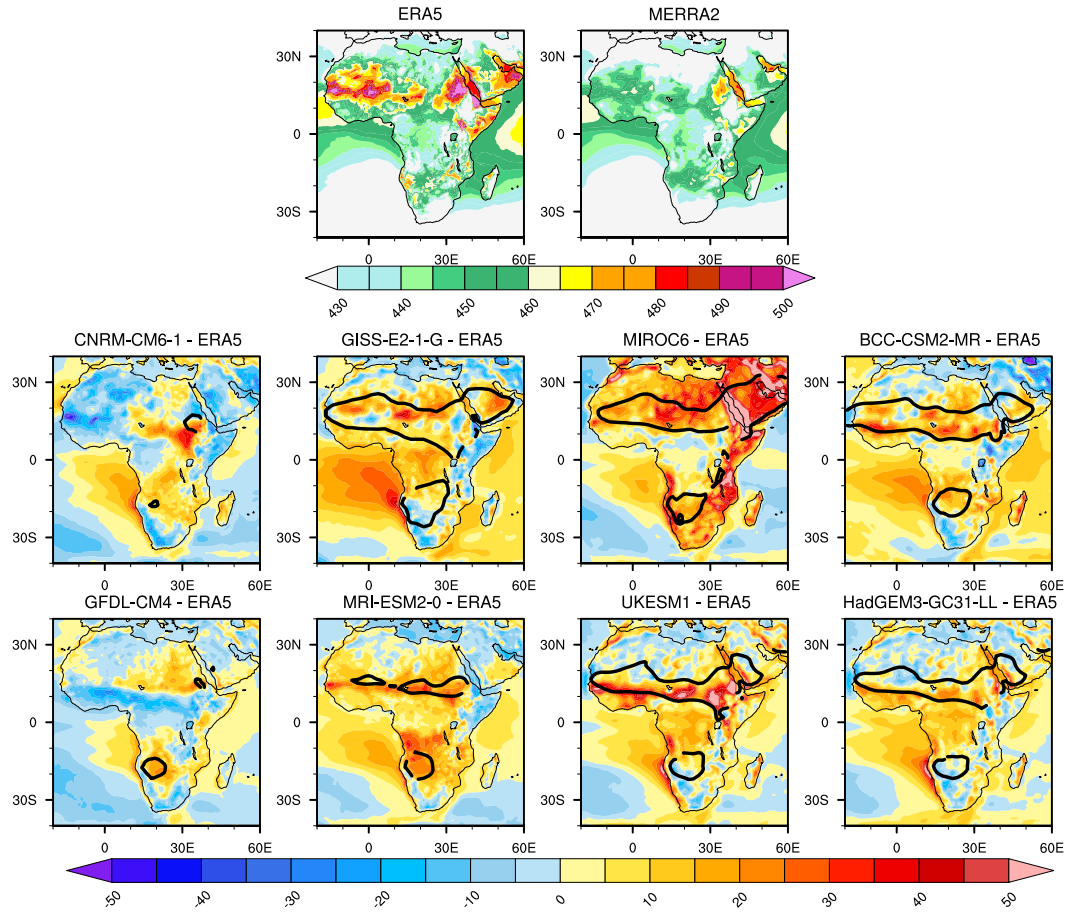

Figure 42: *Mean September to November Upward Longwave Radiation Heat Flux in reanalyses (first row only) and bias in models against ERA5 (second and third rows). Values are shown in* $W.m^{-2}$. *The black contour line shows heat low locations in models represented by the 296 K temperature value in the north and 297 K temperature value in the south.*

relationship is still yet poorly investigated. Our result shows that thermal radiation is a robust feature of surface heat transfer, thus explaining the increasing temperature in MIROC6. This indicates that the higher temperature bias in this model is associated with overestimation of surface thermal radiation that strengthens the heat low intensity and therefore the temperature gradient through Central Africa.

General Conclusion and Avenues for Future Research

1 General conclusion

Central African climate is a key driver of the global tropical circulation although the understanding of that system lags behind that of the other two key regions of diabatic heating, namely over the West Pacific and the Amazon. The African Easterly Jet-North has been shown to be a feature important to the dynamics of Central Africa and the Sahel. Much less is known about the role of the African Easterly Jet–South which forms over the later months of the year during the wetter (September to November) of the two key rainfall seasons in central Africa.

In the first part of the results in this thesis, we have shown how the dynamics of AEJ-S impact on central African climate variability through its impact on rainfall over the region at inter-annual time scales during the SON season. A novel component of this study is the link between Southern Ocean wave dynamics and the AEJ-S. Connections between central and southern African climate dynamics have not been established in the literature though the links shown here between the westerly waves and the AEJ-S are a clear example. If the westerly waves are seen to be independent of the diabatic heating over central Africa, then a case could be made for midlatitude forcing of the African tropical convective system. Theory typically argues for the reverse (Fig. 24).

At the intraseasonal scale, we describe the meteorological characteristics directly associated with the upper wavy flow such as wave signature and periodicity. We focus on the daily characteristics of meteorological variables such as geopotential height to describe the existence of the wave. We also present the key meteorological impact of wave activity on heat low and mid-level circulation. To determine the most important modes of variability that explain the wave signal, we applied the

empirical orthogonal function (EOF) analyses on the deseasonalised geopotential height anomalies. Mode 1, which explains the largest percentage of variance, shows a quasi-stationary signal over the zonal band of extra-tropical latitudes of South Africa. Modes 2, 3 and 4 show a variation of positive and negative alternations, which explains the existence of a wave signal in all three modes.

In order to determine which of the modes is most significant, we applied a time-scale correlation on the principal components (PC) of modes 2, 3 and 4. PC2 and PC3 show a quadrature phase correlation in time, which would better explain the existence of the wave in modes 2 and 3. We therefore retained these modes. We constructed strong and weak variability dates in the variance field reconstructed from modes 02 and 03. Results show that the wave takes about 10 days to settle and its activity takes about 06 days over the continent after its settlement and its impact on the warming of the atmosphere and on the circulation mid-level circulation is associated with phases, structure and wave periodicity when it crosses the sub-continent.

In the second part of this thesis, an assessment based on processes related to the dynamics of the northern and southern components of the African Easterly Jets has been made, to investigate the representation of the mean state climatology of these jets in coupled models. The analysis is focused on the largest rainy season from September to November, defining the period when both jets are present and strong over Central Africa, and play a prominent role in the region's climate variability. A comparison of jet core locations show the AEJ-N is reasonably well located over central Africa in most CMIP6 models compared to AEJ-S with good improvement from CMIP5 to CMIP6.

Analysis of the meridional gradient in 850 hPa temperature in coupled models indicates that, AEJs are thermal winds of the mid troposphere that owe their existence to a low level meridional gradient in temperature and are located slightly equatorward of the region of maximum temperature gradient. In the Northern Hemisphere, CMIP5 models (CNRM-CM5-2 and MIROC5) that locate an AEJ-N core more northward compared to reanalyses feature a stronger and more poleward peak in meridional temperature gradient. This corroborates results found by Creese and Washington (2018) that models that are dry in the east of Congo basin, with equatorward maximum easterly wind speed at mid level, were associated with equatorward

shift in maximum gradient in potential temperature.

However, in this study, results show that improvement in the AEJ strength and core location are not always linked to a better simulation of the maximum meridional gradient in surface temperature. GISS-E2-1-G features the strongest AEJ-N and AEJ-S but weakest meridional gradient in temperature. MIROC6 features a strong AEJ-N associated with a strong gradient, but a weak AEJ-S that is associated to a strong gradient in the southern hemisphere. Since the temperature gradient that is associated with the AEJs does not always explain the jet locations and intensities in models or the change from CMIP5 to CMIP6, other processes were examined. Over the AEJ-N region, models exhibit strong and positive centers of the conversion of divergent kinetic energy into rotational kinetic energy due to Coriolis acceleration. While over the AEJ-S region, most models like GISS-E2-1-G present very weak centers of conversion, around 10 times weaker compared to values of conversion over AEJ-N region. Surface heating is very important in understanding the acceleration mechanism of AEJs, as these jets are thermal winds and are strongly reliant on surface temperature. We find that CMIP models have large biases in temperature. Explanations of surface temperature bias in CMIP6 models are understood by examining the incoming shortwave solar radiation at the surface, and energy heat fluxes that reinforce heat lows strength in layers above the Earth's surface.

Investigations of AEJs dynamics in coupled models is of particular importance to understand mid-level circulation in models over Africa, as AEJs are considered as key Pan-African features (James et al. (2018)), through their interconnection to climate of other regions such as West Africa and Sahel (Chen (2004)), central Africa and South Africa (Kuete et al. (2019); Howard and Washington (2019)). Dynamics of both jets has been assessed in previous studies using reanalysis data (Nicholson and Grist (2003); Adebiyi and Zuidema (2016); Kuete et al. (2019)), global models (Creese and Washington (2018))and regional models (Tamoffo et al. (2019, 2020, 2022)). Despite this progress, our understanding of models representation of AEJ is still limited. We have shown that studies must go beyond analyzing the meridional temperature gradient to diagnose biases in the mean state climatology, location, and core intensity of both jets.

This study has suggested possible causes of the simulated AEJ locations, strength, and their associated dynamics in models (Creese and Washington 2018), and also pos-

sible directions for models assessment and development. In particular, investigations of processes regulating the energy balance that raises the near-surface temperature, rather than focusing only on processes explaining rainfall bias in models in particular over central Africa (Fotso-Nguemo et al. (2017, 2017); Dommo et al. (2018); Fotso-Kamga et al. (2020); Creese and Washington (2018); Tamoffo et al. (2020, 2022)). These surface thermal processes depend strongly on insolation, vegetation cover and albedo. They can also be associated with an energy heat flux such as net surface irradiance, ground heat flux, sensible heat flux, latent heat and long wave radiation. Understanding the energy balance at the Earth's surface is necessary to understand local climate and regional circulation, and arguably to improve simulations of this region.

2 Avenues for Future Research

This thesis characterised the representation of two regional atmospheric climate features, AEJ-N and AEJ-S, in reanalysis data sets and climate model outputs. It has shown that the dynamics of these systems are fundamental to the climate distribution and simulation of rainfall over central Africa.

However, almost all of the characterisation of the basic atmospheric state in this thesis has been based on reanalysis data sets. In Central Africa, the lack of in-situ upper-air observations means that reanalysis products rely heavily on the forecast models that comprise them rather than on assimilated observations. This means that very little of this thesis is based on direct observations of the atmosphere of Central Africa.

Given the influence of the AEJ on rainfall over central Africa, direct measurements of these weather systems would be invaluable. The seasonal cycles and spatial distributions of the AEJ presented in this thesis can be used to inform observational campaigns, with the objective of measuring the vertical profiles of these two systems.

Furthermore, it is known in the literature that the AEJ-N serves as a key energy source for the African Easterly Waves (AEW) and while the detailed characteristics of AEJ-N-AEW interactions have been useful in understanding regional atmospheric disturbances over Africa, no study to our knowledge has attempted to examine the existence of such a link between the southern component of the AEJ (AEJ-S). It

is therefore essential to understand the characteristics of the wave flow in the mid-latitude westerlies over southern Africa and its impact on the thermal low over the Namibia-Kalahari dry land, which is the dominant driver of the AEJ-S.

3 Contributions of this thesis

This thesis has advanced the scientific understanding of the basic state of the mid-level circulation over Central Africa. It characterised the climatology, structure and variability of two important climate features: AEJ-N and AEJ-S. This work clarified their dynamics through interactions with surface thermal heating, atmospheric energy interactions and the mid-level circulation associated with high-pressure systems. This allows the simulation of these processes and their dynamics in climate models to be evaluated, thereby reducing the avoidable uncertainty associated with seasonal forecasts and climate projections. The interannual variability of the AEJ and its link with rainfall over central Africa was also investigated. This thesis applied the process-based model evaluation techniques in Chapter 3 to determine that the AEJ components are well represented in the CMIP5 and CMIP6 models. Based on this analysis, an explanation for the diversity of the individual models was provided.

An additional finding of this work was the research on how the African climate system has historically adopted a regional approach, such as southern Africa studied separately from central Africa which is studied separately from East Africa. Increasingly, we are coming to realize that the regions are connected. For example, we show how the wavy flow high in the mid-latitude westerly winds over southern Africa is able to disrupt strong easterly winds which are closely tied to the rains over central Africa. This result challenges preconceptions regarding the state of the central and southern African Atmospheres. This result should raise awareness of the importance of pan-African evaluation.

References

Adebiyi, A.A., and P. Zuidema, 2016: The role of the southern african easterly jet in modifying the southeast atlantic aerosol and cloud environments. *Quarterly Journal of the Royal Meteorological Society*, **142**, 1574–1589.

Adler, R.F., M.R. Sapiano, G.J. Huffman, J.J. Wang, G. Gu, D. Bolvin, L. Chiu, U. Schneider, A. Becker, E. Nelkin et al., 2018: The global precipitation climatology project (gpcp) monthly analysis (new version 2.3) and a review of 2017 global precipitation. *Atmosphere*, **9**, 138.

Aguilar, E., A. Aziz Barry, M. Brunet, L. Ekang, A. Fernandes, M. Massoukina, J. Mbah, A. Mhanda, D. Do Nascimento, T. Peterson et al., 2009: Changes in temperature and precipitation extremes in western central africa, guinea conakry, and zimbabwe, 1955–2006. *Journal of Geophysical Research: Atmospheres*, **114**.

Alber, K., A. Raghavendra, L. Zhou, Y. Jiang, H.S. Sussman, and S.L. Solimine, 2021: Analyzing intensifying thunderstorms over the congo basin using the gálvez-davison index from 1983–2018. *Climate Dynamics*, **56**, 949–967.

Albrecht, R.I., S.J. Goodman, D.E. Buechler, R.J. Blakeslee, and H.J. Christian, 2016: Where are the lightning hotspots on earth? *Bulletin of the American Meteorological Society*, **97**, 2051–2068.

Aloysius, N.R., J. Sheffield, J.E. Saiers, H. Li, and E.F. Wood, 2016: Evaluation of historical and future simulations of precipitation and temperature in central africa from cmip5 climate models. *Journal of Geophysical Research: Atmospheres*, **121**, 130–152.

Awange, J.L., V.G. Ferreira, E. Forootan, S. Andam-Akorful, N.O. Agutu, and X. He, 2016: Uncertainties in remotely sensed precipitation data over africa. *International Journal of Climatology*, **36**, 303–323.

Bayr, T., D. Dommenget, T. Martin, and S.B. Power, 2014: The eastward shift of the walker circulation in response to global warming and its relationship to enso variability. *Climate dynamics*, **43**, 2747–2763.

Biasutti, M., A.H. Sobel, and S.J. Camargo, 2009: The role of the sahara low in summertime sahel rainfall variability and change in the cmip3 models. *Journal of Climate*, **22**, 5755–5771.

Burpee, R.W., 1972: The origin and structure of easterly waves in the lower troposphere of north africa. *Journal of the Atmospheric Sciences*, **29**, 77–90.

Chauvin, F., R. Roehrig, and J.P. Lafore, 2010: Intraseasonal variability of the saharan heat low and its link with midlatitudes. *Journal of Climate*, **23**, 2544–2561.

Chen, T.C., 2004: Maintenance of the midtropospheric north african summer circulation: Saharan high and african easterly jet. *Journal of climate*, **18**, 2943–2962.

Chen, T.C., and A.C. Wiin-Nielsen, 1976: On the kinetic energy of the divergent and nondivergent

flow in the atmosphere. *Tellus*, **28**, 486–498.

Cook, K.H., 1999: Generation of the african easterly jet and its role in determining west african precipitation. *Journal of climate*, **12**, 1165–1184.

Cook, K.H., and E.K. Vizy, 2006: Coupled model simulations of the west african monsoon system: Twentieth-and twenty-first-century simulations. *Journal of climate*, **19**, 3681–3703.

Cook, K.H., and E.K. Vizy, 2016: The congo basin walker circulation: dynamics and connections to precipitation. *Climate Dynamics*, **47**, 697–717.

Creese, A., and R. Washington, 2016: Using qflux to constrain modeled congo basin rainfall in the cmip5 ensemble. *Journal of Geophysical Research: Atmospheres*, **121**, 13415–13442.

Creese, A., and R. Washington, 2018: A process-based assessment of cmip5 rainfall in the congo basin: the september–november rainy season. *Journal of Climate*, **31**, 7417–7439.

Creese, A., R. Washington, and C. Munday, 2019: The plausibility of september–november congo basin rainfall change in coupled climate models. *Journal of Geophysical Research: Atmospheres*, **124**, 5822–5846.

Crowhurst, D., S. Dadson, J. Peng, and R. Washington, 2021: Contrasting controls on congo basin evaporation at the two rainfall peaks. *Climate Dynamics*, **56**, 1609–1624.

Crowhurst, D.M., S.J. Dadson, and R. Washington, 2020: Evaluation of evaporation climatology for the congo basin wet seasons in 11 global climate models. *Journal of Geophysical Research: Atmospheres*, **125**, e2019JD030619.

Dee, D.P., S. Uppala, A. Simmons, P. Berrisford, P. Poli, S. Kobayashi, U. Andrae, M. Balmaseda, G. Balsamo, d.P. Bauer et al., 2011: The era-interim reanalysis: Configuration and performance of the data assimilation system. *Quarterly Journal of the royal meteorological society*, **137**, 553–597.

Dezfuli, A., 2017: Climate of western and central equatorial africa. In: *Oxford Research Encyclopedia of Climate Science*.

Dezfuli, A.K., and S.E. Nicholson, 2013: The relationship of rainfall variability in western equatorial africa to the tropical oceans and atmospheric circulation. part ii: The boreal autumn. *Journal of Climate*, **26**, 66–84.

Dezfuli, A.K., B.F. Zaitchik, and A. Gnanadesikan, 2015: Regional atmospheric circulation and rainfall variability in south equatorial africa. *Journal of Climate*, **28**, 809–818.

Dieppois, B., M. Rouault, and M. New, 2015: The impact of enso on southern african rainfall in cmip5 ocean atmosphere coupled climate models. *Climate dynamics*, **45**, 2425–2442.

Dommo, A., N. Philippon, D.A. Vondou, G. Sèze, and R. Eastman, 2018: The june–september low cloud cover in western central africa: mean spatial distribution and diurnal evolution, and associated atmospheric dynamics. *Journal of Climate*, **31**, 9585–9603.

Driver, P., and C. Reason, 2017: Variability in the botswana high and its relationships with rainfall and temperature characteristics over southern africa. *International Journal of Climatology*, **37**, 570–581.

Dunning, C.M., E. Black, and R.P. Allan, 2018: Later wet seasons with more intense rainfall over africa under future climate change. *Journal of Climate*, **31**, 9719–9738.

Dunning, C.M., E.C. Black, and R.P. Allan, 2016: The onset and cessation of seasonal rainfall over

africa. *Journal of Geophysical Research: Atmospheres*, **121**, 11–405.

Dyer, E.L., D.B. Jones, J. Nusbaumer, H. Li, O. Collins, G. Vettoretti, and D. Noone, 2017: Congo basin precipitation: Assessing seasonality, regional interactions, and sources of moisture. *Journal of Geophysical Research: Atmospheres*, **122**, 6882–6898.

Eyring, V., S. Bony, G.A. Meehl, C.A. Senior, B. Stevens, R.J. Stouffer, and K.E. Taylor, 2016: Overview of the coupled model intercomparison project phase 6 (cmip6) experimental design and organization. *Geoscientific Model Development*, **9**, 1937–1958.

Favre, A., B. Hewitson, C. Lennard, R. Cerezo-Mota, and M. Tadross, 2013: Cut-off lows in the south africa region and their contribution to precipitation. *Climate dynamics*, **41**, 2331–2351.

Fiolleau, T., and R. Roca, 2013: An algorithm for the detection and tracking of tropical mesoscale convective systems using infrared images from geostationary satellite. *IEEE transactions on Geoscience and Remote Sensing*, **51**, 4302–4315.

Flohn, H., and H. Fleer, 1975: Climatic teleconnections with the equatorial pacific and the role of ocean/atmosphere coupling. *Atmosphere*, **13**, 96–109.

Fontaine, B., and S. Janicot, 1992: Wind-field coherence and its variations over west africa. *Journal of Climate*, **5**, 512–524.

Fotso-Kamga, G., T.C. Fotso-Nguemo, I. Diallo, Z.D. Yepdo, W.M. Pokam, D.A. Vondou, and A. Lenouo, 2020: An evaluation of cosmo-clm regional climate model in simulating precipitation over central africa. *International Journal of Climatology*, **40**, 2891–2912.

Fotso-Nguemo, T.C., R. Chamani, Z.D. Yepdo, D. Sonkoué, C.N. Matsaguim, D.A. Vondou, and R.S. Tanessong, 2018: Projected trends of extreme rainfall events from cmip5 models over central africa. *Atmospheric Science Letters*, **19**, 1–8.

Fotso-Nguemo, T.C., D.A. Vondou, W.M. Pokam, Z.Y. Djomou, I. Diallo, A. Haensler, L.A.D. Tchotchou, P.H. Kamsu-Tamo, A.T. Gaye, and C. Tchawoua, 2017: On the added value of the regional climate model remo in the assessment of climate change signal over central africa. *Climate Dynamics*, **49**, 3813–3838.

Fotso-Nguemo, T.C., D.A. Vondou, C. Tchawoua, and A. Haensler, 2017: Assessment of simulated rainfall and temperature from the regional climate model remo and future changes over central africa. *Climate Dynamics*, **48**, 3685–3705.

Fovell, R., D. Durran, and J. Holton, 1992: Numerical simulations of convectively generated stratospheric gravity waves. *Journal of the atmospheric sciences*, **49**, 1427–1442.

Haensler, A., F. Saeed, and D. Jacob, 2013: Assessing the robustness of projected precipitation changes over central africa on the basis of a multitude of global and regional climate projections. *Climatic Change*, **121**, 349–363.

Harris, I., P.D. Jones, T.J. Osborn, and D.H. Lister, 2014: Updated high-resolution grids of monthly climatic observations–the cru ts3. 10 dataset. *International journal of climatology*, **34**, 623–642.

Heerden, J.v., and J. Taljaard, 1998: Africa and surrounding waters. In: *Meteorology of the southern hemisphere*, pp. 141–174. Springer.

Hersbach, H., B. Bell, P. Berrisford, S. Hirahara, A. Horányi, J. Muñoz-Sabater, J. Nicolas, C. Peubey, R. Radu, D. Schepers et al., 2020: The era5 global reanalysis. *Quarterly Journal of the Royal Meteorological Society*, **146**, 1999–2049.

Hirons, L., and A. Turner, 2018: The impact of indian ocean mean-state biases in climate models on the representation of the east african short rains. *Journal of Climate*, **31**, 6611–6631.

Howard, E., and R. Washington, 2018: Characterizing the synoptic expression of the angola low. *Journal of Climate*, **31**, 7147–7165.

Howard, E., and R. Washington, 2019: Drylines in southern africa: Rediscovering the congo air boundary. *Journal of Climate*, **32**, 8223–8242.

Howard, E., and R. Washington, 2020: Tracing future spring and summer drying in southern africa to tropical lows and the congo air boundary. *Journal of Climate*, **33**, 6205–6228.

Hua, W., L. Zhou, H. Chen, S.E. Nicholson, Y. Jiang, and A. Raghavendra, 2018: Understanding the central equatorial african long-term drought using amip-type simulations. *Climate dynamics*, **50**, 1115–1128.

Hua, W., L. Zhou, S.E. Nicholson, H. Chen, and M. Qin, 2019: Assessing reanalysis data for understanding rainfall climatology and variability over central equatorial africa. *Climate Dynamics*, 1–19.

Jackson, B., S.E. Nicholson, and D. Klotter, 2009: Mesoscale convective systems over western equatorial africa and their relationship to large-scale circulation. *Monthly Weather Review*, **137**, 1272–1294.

James, R., and R. Washington, 2013: Changes in african temperature and precipitation associated with degrees of global warming. *Climatic change*, **117**, 859–872.

James, R., R. Washington, B. Abiodun, G. Kay, J. Mutemi, W. Pokam, N. Hart, G. Artan, and C. Senior, 2018: Evaluating climate models with an african lens. *Bulletin of the American Meteorological Society*, **99**, 313–336.

James, R., R. Washington, and R. Jones, 2015: Process-based assessment of an ensemble of climate projections for west africa. *Journal of Geophysical Research: Atmospheres*, **120**, 1221–1238.

Jiang, Y., L. Zhou, C.J. Tucker, A. Raghavendra, W. Hua, Y.Y. Liu, and J. Joiner, 2019: Widespread increase of boreal summer dry season length over the congo rainforest. *Nature Climate Change*, **9**, 617–622.

Joshi, M., E. Hawkins, R. Sutton, J. Lowe, and D. Frame, 2011: Projections of when temperature change will exceed 2 c above pre-industrial levels. *Nature Climate Change*, **1**, 407–412.

Kalnay, E., M. Kanamitsu, R. Kistler, W. Collins, D. Deaven, L. Gandin, M. Iredell, S. Saha, G. White, J. Woollen et al., 1996: The ncep/ncar 40-year reanalysis project. *Bulletin of the American meteorological Society*, **77**, 437–472.

King, A.D., and L.J. Harrington, 2018: The inequality of climate change from 1.5 to 2 c of global warming. *Geophysical Research Letters*, **45**, 5030–5033.

Krishnamurti, T.N., 1971: Observational study of the tropical upper tropospheric motion field during the northern hemisphere summer. *Journal of Applied Meteorology and Climatology*, **10**, 1066–1096.

Kuete, G., W.P. Mba, and R. Washington, 2019: African easterly jet south: Control, maintenance mechanisms and link with southern subtropical waves. *Climate Dynamics*.

Lavaysse, C., C. Flamant, S. Janicot, D.J. Parker, J.P. Lafore, B. Sultan, and J. Pelon, 2009: Seasonal evolution of the west african heat low: a climatological perspective. *Climate Dynamics*, **33**, 313–

330.

Lazenby, M.J., M.C. Todd, and Y. Wang, 2016: Climate model simulation of the south indian ocean convergence zone: Mean state and variability. *Climate Research*, **68**, 59–71.

Lennard, C., G. Nikulin, A. Dosio, and W. Moufouma-Okia, 2018: On the need for regional climate information over africa under varying levels of global warming. *Environmental Research Letters*, **13**, 060401.

Leroux, M., 2001: *The meteorology and climate of tropical Africa*. Springer Science & Business Media.

Longandjo, G.N.T., and M. Rouault, 2020a: On the structure of the regional-scale circulation over central africa: Seasonal evolution, variability, and mechanisms. *Journal of Climate*, **33**, 145–162.

Longandjo, G.N.T., and M. Rouault, 2020b: On the structure of the regional-scale circulation over central africa: seasonal evolution, variability, and mechanisms. *Journal of Climate*, **33**, 145–162.

Maidment, R.I., R.P. Allan, and E. Black, 2015: Recent observed and simulated changes in precipitation over africa. *Geophysical Research Letters*, **42**, 8155–8164.

Malhi, Y., 2018: Ancient deforestation in the green heart of africa. *Proceedings of the national academy of sciences*, **115**, 3202–3204.

Matarira, C.H., 1990: Drought over zimbabwe in a regional and global context. *International Journal of Climatology*, **10**, 609–625.

Mathon, V., and H. Laurent, 2001: Life cycle of sahelian mesoscale convective cloud systems. *Quarterly Journal of the Royal Meteorological Society*, **127**, 377–406.

McCollum, J.R., A. Gruber, and M.B. Ba, 2000: Discrepancy between gauges and satellite estimates of rainfall in equatorial africa. *Journal of Applied Meteorology*, **39**, 666–679.

Moihamette, F., W.M. Pokam, I. Diallo, and R. Washington, 2022: Extreme indian ocean dipole and rainfall variability over central africa. *International Journal of Climatology*.

Munday, C., and R. Washington, 2017: Circulation controls on southern african precipitation in coupled models: The role of the angola low. *Journal of Geophysical Research: Atmospheres*, **122**, 861–877.

Nesbitt, S.W., and E.J. Zipser, 2003: The diurnal cycle of rainfall and convective intensity according to three years of trmm measurements. *Journal of Climate*, **16**, 1456–1475.

Neupane, N., 2016: The congo basin zonal overturning circulation. *Advances in Atmospheric Sciences*, **33**, 767–782.

Newell, R.E., and J.W. Kidson, 1984: African mean wind changes between sahelian wet and dry periods. *Journal of Climatology*, **4**, 27–33.

Nicholson, S.E., 1986: The spatial coherence of african rainfall anomalies: Interhemispheric teleconnections. *Journal of Applied Meteorology and Climatology*, **25**, 1365–1381.

Nicholson, S.E., 2018: The itcz and the seasonal cycle over equatorial africa. *Bulletin of the American Meteorological Society*, **99**, 337–348.

Nicholson, S.E., and A.K. Dezfuli, 2013: The relationship of rainfall variability in western equatorial africa to the tropical oceans and atmospheric circulation. part i: The boreal spring. *Journal of climate*, **26**, 45–65.

Nicholson, S.E., A.K. Dezfuli, and D. Klotter, 2012: A two-century precipitation dataset for the continent of africa. *Bulletin of the American Meteorological Society*, **93**, 1219–1231.

Nicholson, S.E., and J.P. Grist, 2003: The seasonal evolution of the atmospheric circulation over west africa and equatorial africa. *Journal of climate*, **16**, 1013–1030.

Nicholson, S.E., and D. Klotter, 2021: The tropical easterly jet over africa, its representation in six reanalysis products, and its association with sahel rainfall. *International Journal of Climatology*, **41**, 328–347.

Nicholson, S.E., D. Klotter, A.K. Dezfuli, and L. Zhou, 2018: New rainfall datasets for the congo basin and surrounding regions. *Journal of Hydrometeorology*, **19**, 1379–1396.

Nielsen, A.C.W., and T.C. Chen, 1993: Fundamentals of atmospheric energetics.

O'Neill, B.C., C. Tebaldi, D.P. Van Vuuren, V. Eyring, P. Friedlingstein, G. Hurtt, R. Knutti, E. Kriegler, J.F. Lamarque, J. Lowe et al., 2016: The scenario model intercomparison project (scenariomip) for cmip6. *Geoscientific Model Development*, **9**, 3461–3482.

Parker, D.J., C.D. Thorncroft, R.R. Burton, and A. Diongue-Niang, 2005: Analysis of the african easterly jet, using aircraft observations from the jet2000 experiment. *Quarterly Journal of the Royal Meteorological Society: A journal of the atmospheric sciences, applied meteorology and physical oceanography*, **131**, 1461–1482.

Pereira, L., 2017: Climate change impacts on agriculture across africa. *Oxford research encyclopedia of environmental science*.

Piabuo, S.M., and J.C. Tieguhong, 2020: Health expenditure and economic growth-a review of the literature and an analysis between the economic community for central african states (cemac) and selected african countries. *Health economics review*, **7**, 1–13.

Pokam, W.M., C.L. Bain, R.S. Chadwick, R. Graham, D.J. Sonwa, and F.M. Kamga, 2014: Identification of processes driving low-level westerlies in west equatorial africa. *Journal of Climate*, **27**, 4245–4262.

Pokam, W.M., L.A.T. Djiotang, and F.K. Mkankam, 2012: Atmospheric water vapor transport and recycling in equatorial central africa through ncep/ncar reanalysis data. *Climate dynamics*, **38**, 1715–1729.

Preston-Whyte, R.A., and P.D. Tyson, 1973: Note on pressure oscillations over south africa. *Monthly Weather Review*, **101**, 650–653.

Raghavendra, A., L. Zhou, P.E. Roundy, Y. Jiang, S.M. Milrad, W. Hua, and G. Xia, 2020: The mjo's impact on rainfall trends over the congo rainforest. *Climate Dynamics*, **54**, 2683–2695.

Reason, C., 2016: The bolivian, botswana, and bilybara highs and southern hemisphere drought/floods. *Geophysical Research Letters*, **43**, 1280–1286.

Sonkoué, D., D. Monkam, T.C. Fotso-Nguemo, Z.D. Yepdo, and D.A. Vondou, 2019: Evaluation and projected changes in daily rainfall characteristics over central africa based on a multi-model ensemble mean of cmip5 simulations. *Theoretical and Applied Climatology*, **137**, 2167–2186.

Spinks, J., Y.L. Lin, and A. Mekonnen, 2015: Effects of the subtropical anticyclones over north africa and arabian peninsula on the african easterly jet. *International Journal of Climatology*, **35**, 733–745.

Sultan, B., S. Janicot, and A. Diedhiou, 2003: The west african monsoon dynamics. part i: Documentation of intraseasonal variability. *Journal of Climate*, **16**, 3389–3406.

Taguela, T.N., W.M. Pokam, and R. Washington, 2022: Rainfall in uncoupled and coupled versions of

the met office unified model over central africa: Investigation of processes during the september–november rainy season. *International Journal of Climatology*.

Taljaard, J., 1986: Change of rainfall distribution and circulation patterns over southern africa in summer. *Journal of Climatology*, **6**, 579–592.

Taljaard, J., W. Schmitt, and H. Van Loon, 1961: Frontal analysis with application to the southern hemisphere. *Notos*, **10**, 25–58.

Taljaard, J., and H. Van Loon, 1962: Cyclogenesis, cyclones and anticyclones in the southern hemisphere during the winter and spring of 1957. *Notos*, **11**, 3–20.

Taljaard, J.J., 1972: Synoptic meteorology of the southern hemisphere. In: *Meteorology of the Southern Hemisphere*, pp. 139–213. Springer.

Taljaard, J.J., 1985: *Cut-off lows in the South African region*. Number 14. Weather Bureau, Department of Transport.

Tamoffo, A.T., L.K. Amekudzi, T. Weber, D.A. Vondou, E.I. Yamba, and D. Jacob, 2022: Mechanisms of rainfall biases in two cordex-core regional climate models at rainfall peaks over central equatorial africa. *Journal of Climate*, **35**, 639–668.

Tamoffo, A.T., A. Dosio, D.A. Vondou, and D. Sonkoué, 2020: Process-based analysis of the added value of dynamical downscaling over central africa. *Geophysical Research Letters*, **47**, e2020GL089702.

Tamoffo, A.T., W. Moufouma-Okia, A. Dosio, R. James, W.M. Pokam, D.A. Vondou, T.C. Fotso-Nguemo, G.M. Guenang, P.H. Kamsu-Tamo, G. Nikulin, G.N. Longandjo, C.J. Lennard, J.P. Bell, R.R. Takong, A. Haensler, L.A.D. Tchotchou, and R. Nouayou, 2019: Process-oriented assessment of rca4 regional climate model projections over the congo basin under 1.5°c and 2°c global warming levels: influence of regional moisture fluxes. *Climate Dynamics*, 1911–1935.

Taylor, K.E., R.J. Stouffer, and G.A. Meehl, 2012: An overview of cmip5 and the experiment design. *Bulletin of the American meteorological Society*, **93**, 485–498.

Thorncroft, C., and M. Blackburn, 1999: Maintenance of the african easterly jet. *Quarterly Journal of the Royal Meteorological Society*, **125**, 763–786.

Thorsten, P., and M. Richter, 2014: The atmospheric circulation. *Tropical Forestry Handbook, L. Pancel and M. Köhl, Eds., Springer*, 303–331.

Tierney, J., C. Ummenhofer, and P. DeMenocal, 2015: Past and future rainfall in the horn of africa. sci. adv., 1, e1500682.

Tierney, J.E., J.M. Russell, J.S.S. Damsté, Y. Huang, and D. Verschuren, 2011: Late quaternary behavior of the east african monsoon and the importance of the congo air boundary. *Quaternary Science Reviews*, **30**, 798–807.

Torrance, J., 1979: Upper windflow patterns in relation to rainfall in south-east central africa. *Weather*, **34**, 106–115.

Unganai, L., and S.J. Mason, 2002: Long-range predictability of zimbabwe summer rainfall. *International Journal of Climatology: A Journal of the Royal Meteorological Society*, **22**, 1091–1103.

Van der Ent, R., O. Tuinenburg, H.R. Knoche, H. Kunstmann, and H. Savenije, 2013: Should we use a simple or complex model for moisture recycling and atmospheric moisture tracking? *Hydrology and Earth System Sciences*, **17**, 4869–4884.

Van der Ent, R.J., H.H. Savenije, B. Schaefli, and S.C. Steele-Dunne, 2010: Origin and fate of atmospheric moisture over continents. *Water Resources Research*, **46**.

Vigaud, N., Y. Richard, M. Rouault, and N. Fauchereau, 2009: Moisture transport between the south atlantic ocean and southern africa: relationships with summer rainfall and associated dynamics. *Climate Dynamics*, **32**, 113–123.

Vondou, D.A., A. Nzeukou, and F.M. Kamga, 2010: Diurnal cycle of convective activity over the west of central africa based on meteosat images. *International journal of applied earth observation and geoinformation*, **12**, S58–S62.

Washington, R., R. James, H. Pearce, W.M. Pokam, and W. Moufouma-Okia, 2013: Congo basin rainfall climatology: can we believe the climate models? *Philosophical Transactions of the Royal Society B: Biological Sciences*, **368**, 20120296.

Washington, R., and A. Preston, 2006: Extreme wet years over southern africa: Role of indian ocean sea surface temperatures. *Journal of Geophysical Research: Atmospheres*, **111**.

Webster, J., 1983: Large scale dynamical processes in atmospfjackhere.

Wiin-Nielsen, A., and T.C. Chen, 1993: *Fundamentals of atmospheric energetics*. Oxford University Press, USA.

Williams, C.A., N.P. Hanan, J.C. Neff, R.J. Scholes, J.A. Berry, A.S. Denning, and D.F. Baker, 2007: Africa and the global carbon cycle. *Carbon balance and management*, **2**, 1–13.

Wu, M.L.C., O. Reale, S.D. Schubert, M.J. Suarez, R.D. Koster, and P.J. Pegion, 2009: African easterly jet: structure and maintenance. *Journal of Climate*, **22**, 4459–4480.

Xie, P., J.E. Janowiak, P.A. Arkin, R. Adler, A. Gruber, R. Ferraro, G.J. Huffman, and S. Curtis, 2003: Gpcp pentad precipitation analyses: An experimental dataset based on gauge observations and satellite estimates. *Journal of Climate*, **16**, 2197–2214.

Yang, W., R. Seager, M.A. Cane, and B. Lyon, 2015: The rainfall annual cycle bias over east africa in cmip5 coupled climate models. *Journal of Climate*, **28**, 9789–9802.

Zhou, L., Y. Tian, R.B. Myneni, P. Ciais, S. Saatchi, Y.Y. Liu, S. Piao, H. Chen, E.F. Vermote, C. Song et al., 2014: Widespread decline of congo rainforest greenness in the past decade. *Nature*, **509**, 86–90.

List of publications

1. **Giresse Kuete**, Wilfried M. Pokam, Richard Washington.(2020): **African Easterly Jet South: control, maintenance mechanisms and link with Southern subtropical waves.**. *Climate Dynamics, Springer-Verlag Berlin Heidelberg.* **Vol:54, Pages:1-26**. DOI: 10.1007/s00382-019-05072-w. (*Impact Factor: 5.031*)

2. **Giresse Kuete**, Wilfried M. Pokam, Rachel. James, Ellen. Dyer, Thompson. Annor, Richard Washington.(2022): **How do coupled models represent the African Easterly Jets and their associated dynamics over Central Africa during the September–November rainy season?.** *Climate Dynamics, Springer-Verlag Berlin Heidelberg.* DOI: 10.1007/s00382-022-06467-y (*Impact Factor: 5.031*)

3. Annor Thompson, Ackon Aphia, Rachel. James, Ellen Dyer, Thomas Webb, Wilfried Pokam, **Giresse Kuete**, Richard Washington and Abiodun Babatunde. (2023) : **Heat band, rain band and heat low migration: process-based evaluation of some CMIP6 GCMs over West Africa.** *Climate Dynamics, Springer-Verlag Berlin Heidelberg.* DOI: 10.1007/s00382-023-06930-4 (*Impact Factor: 5.031*)